5 JUNE 1980

(FOUO 9/80)

JPRS L/9127

5 June 1980

USSR Report

ELECTRONICS AND ELECTRICAL ENGINEERING

(FOUO 9/80)

FBIS   FOREIGN BROADCAST INFORMATION SERVICE

NOTE

JPRS publications contain information primarily from foreign
newspapers, periodicals and books, but also from news agency
transmissions and broadcasts. Materials from foreign-language
sources are translated; those from English-language sources
are transcribed or reprinted, with the original phrasing and
other characteristics retained.

Headlines, editorial reports, and material enclosed in brackets
[] are supplied by JPRS. Processing indicators such as [Text]
or [Excerpt] in the first line of each item, or following the
last line of a brief, indicate how the original information was
processed. Where no processing indicator is given, the infor-
mation was summarized or extracted.

Unfamiliar names rendered phonetically or transliterated are
enclosed in parentheses. Words or names preceded by a ques-
tion mark and enclosed in parentheses were not clear in the
original but have been supplied as appropriate in context.
Other unattributed parenthetical notes within the body of an
item originate with the source. Times within items are as
given by source.

The contents of this publication in no way represent the poli-
cies, views or attitudes of the U.S. Government.

For further information on report content
call (703) 351-2938 (economic); 3468
(political, sociological, military); 2726
(life sciences); 2725 (physical sciences).

FOR OFFICIAL USE ONLY

JPRS L/9127

5 June 1980

USSR REPORT

ELECTRONICS AND ELECTRICAL ENGINEERING

(FOUO 9/80)

CONTENTS

ANTENNAS

COMMUNICATIONS; COMMUNICATIONS EQUIPMENT INCLUDING RECEIVERS AND
TRANSMITTERS; NETWORKS; RADIO PHYSICS; DATA TRANSMISSION AND
PROCESSING; INFORMATION THEORY

ELECTROMAGNETIC WAVE PROPAGATION; ELECTRODYNAMICS

- a -   [III - USSR - 21E S&T FOUO]

FOR OFFICIAL USE ONLY

FOR OFFICIAL USE ONLY

CONTENTS (Continued)

FOR OFFICIAL USE ONLY

FOR OFFICIAL USE ONLY

ANTENNAS

STATISTICAL CHARACTERISTICS OF ADAPTIVE ANTENNA SYSTEMS MAXIMIZING SIGNAL
TO NOISE RATIO

[Article by I. Ye. Pozumentov, Gor'kiy State University]

[Text] The basic statistical characteristics of adaptive
antenna systems that maximize the signal to noise ratio are
determined: the mean and correlation matrix of the vector
of weight coefficients, powers of interference and of the
useful signal, output signal to noise ratio and spectral
correlation characteristics of a system. The analysis is
presented in consideration of the finite correlation time
of input Gaussian interference.

1. Adaptive antenna systems are being used more and more widely today in
connection with the problem of extracting a useful signal from a mixture
with noise (interference). Systems of this kind are used for the contin-
uous optimization of the radiation pattern by aiming the nulls in the
directions of arrival of interference. The most widely used criteria of
the functioning of adaptive systems are the minimum mean square error [1]
and the maximum output signal to noise ratio [2]. The statistical charac-
teristics of adaptive systems that maximize the signal to noise ratio, used
both in radar [3-5], and for selecting weak acoustical signals [6, 7], are
analyzed in this article. It is important to note that the assumption that
the envelopes of the input interference are not correlated with the vector
of the weight coefficients, was used in the cited works for analyzing the
efficiency of systems. This approximation, as will be shown below, is
valid in the case of δ-correlated input interference. Exact methods of
analysis, used in [8, 9], for finding the statistical characteristics of a
single-channel automatic corrector are not applicable here because of the
high order of the differential stochastic equation system that describes
the behavior of a system. Therefore an approximate method of analysis,
which leads to correct results in the first order of smallness in terms of
the parameter $\alpha = \tau_c/\tau$, where τ_c is the correlation time of the interfer-
ence envelopes, and τ is the time constant of the filters of the correlation

1

feedback circuits, is used in this article for determining the statistical characteristics of an adaptive system. We should like to mention that some of the statistical characteristics of such systems were determined differently in the literature [10].

2. A functional diagram of an adaptive antenna system that maximizes the signal to noise ratio is presented in Figure 1. Here $V^t = (v_1, v_2, \ldots,$ $\ldots, v_N)$, where v_i is the complex envelope of the noise in the i-th element of the array, and the superscript "t" denotes transposition; W is the vector of the weight coefficients; $W^t V$ is the output signal of the adaptive system. Vector S is the vector of phases of the useful signal, the angle of incidence of which is assumed to be known:

$$S^\tau = \left(e^{j\varphi_1}, e^{j\varphi_2}, \ldots, e^{j\varphi_N} \right). \tag{1}$$

We will assume below that the useful signal is substantially weaker than the interference and its influence on the vector of the weight coefficients is negligible. Then the stochastic differential equation that describes the behavior of W(t) acquires the form

$$\tau \frac{d}{dt} W(t) + (I + \gamma M) \dot{W}(t) = \gamma S^*, \tag{2}$$

where I is the unit matrix, $M = V^* V^t$, and the superscript "*" denotes complex conjugation. The envelope vector V(t) is assumed to be a complex Gaussian process, which satisfies the equation

$$\frac{d}{dt} V(t) + \nu V(t) = \xi(t), \tag{3}$$

where $\xi(t)$ is a complex δ-correlated random process with $\langle \xi \rangle = 0$ and $\langle \xi \xi_\tau^t \rangle = D\delta(\tau)$. Then V(t) is a complex Gaussian process with finite correlation time $\tau_c = 1/\nu$ and correlation matrix $\langle V^* V^t \rangle = (1/2\nu)D$. To determine the mean vector $\langle W(t) \rangle$ of the weight coefficients we derive from (2) and (3) the following equation for the vector of moments $\langle MW \rangle$:

$$\left(\frac{d}{dt} + \frac{1}{\tau} + 2\nu \right) \langle MW \rangle = 2\nu \langle M \rangle \langle W \rangle + \frac{\gamma}{\tau} \langle M \rangle S^* - \frac{\gamma}{\tau} \langle M^2 W \rangle. \tag{4}$$

If we restrict the analysis of the statistical characteristics of a system to the first order of smallness in terms of the parameter $\alpha = \tau_c/\tau$, we may then use for approximation the assumption that random matrix M(t) and vector W(t) in equation (4) are uncorrelated, i.e., [11]

$$\langle M^2 W \rangle \approx \langle M \rangle (\langle M \rangle + PI) \langle W \rangle,$$

2

where $P = Sp<M>$ is the summary power of the interference processes entering the array. For convenience we convert to the Q-matrix notation that diagonalizes the covariation matrix of input interference processes $Q^t<M>Q = \Lambda$ and find as a result an equation system for determining the stationary mean vector of the weight coefficients $\Omega = Q^t<W>_{st}$:

$$\Omega + \gamma R = \gamma F^*,$$

$$\left(1 + \frac{\alpha}{2}\right) R = \Lambda \Omega + \frac{\alpha}{2} \gamma \Lambda F^* - \frac{\alpha}{2} \gamma \Lambda [\Lambda + PI] \Omega, \qquad (5)$$

where $R = Q^t<MW>_{st}$, $F^* = Q^t S^*$. Hence it is easy to derive expressions for the elements of vector Ω:

$$\omega_i = \frac{\gamma f_i^*}{1 + \gamma \lambda_i - \frac{\alpha}{2} \gamma \lambda_i \gamma P}. \qquad (6)$$
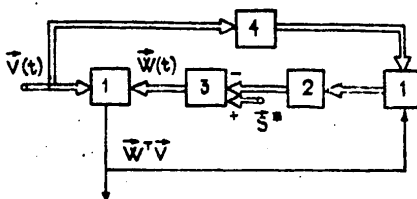
Figure 1. Functional diagram of adaptive antenna system that maximizes signal to noise ratio: 1 -- multipliers; 2 -- low-pass filter; 3 -- amplifier-integrator with gain γ; 4 -- complex conjugation unit. Double lines denote vector connections.

We can be shown (see also [12-14]) that the conditions under which the examined approximation are applicable are

$$\alpha, \alpha \gamma P \ll 1. \qquad (7)$$

The difference between (6) and its optimum value $\omega_{i\ opt} = f_i^*/\lambda_i$ is extremely small within the frameworks of (7). Consequently we may use, for the purpose of determining the mean vector of the weight coefficients, the approximation whereby $M(t)$ and $W(t)$ in original equation (2) are uncorrelated, which corresponds to $\alpha = 0$ or $\tau_c = 0$. However, as will be shown

3

FOR OFFICIAL USE ONLY

below, this approximation is completely unacceptable for finding the covariation matrix of the vector of the weight coefficients.

3. From (2) we derive an equation for the correlation matrix $\langle WW^+\rangle$:

$$\left(\tau\frac{d}{dt}+2I\right)\langle WW^+\rangle = \gamma S^*\langle W^+\rangle + \gamma\langle W\rangle S^\tau - $$
$$- \gamma\langle MWW^+\rangle - \gamma\langle WW^+M\rangle. \tag{8}$$

We note that $\langle WW^+M\rangle^+ = \langle MWW^+\rangle$ (the superscript "+" denotes Hermitian conjugation).

Writing the equation for $\langle MWW^+\rangle$, analogous to (4), and using in it the assumption that M(t) is not correlated with W(t), we find in Q-matrix representation a system for determining elements K_{ij} of matrix $Q^t\langle WW^+\rangle_{st}Q$:

$$2K_{ij} = \gamma f_i^*\omega_j^* + \gamma\omega_i f_j - \gamma\varphi_{ij} - \gamma\varphi_{ji}^*,$$

[ycr=st]

$$(1+\alpha)\varphi_{ij} = \lambda_i K_{ij} + \frac{\alpha}{2}\gamma\lambda_i f_i^*\omega_j^* + \frac{\alpha}{2}\gamma\lambda_i\omega_i f_j - $$

$$- \frac{\alpha}{2}\gamma\lambda_i(\lambda_i + P)\omega_i\omega_j^* - \frac{\alpha}{2}\gamma\lambda_i[\lambda_j\dot\omega_i\omega_j^* + \tag{9}$$

$$+ Sp(\langle M\rangle\langle W\rangle_{ycr}\langle W^+\rangle_{ycr})\delta_{ij}],$$

where δ_{ij} is Kronecker's symbol. Hence we obtain

$$K_{ij} = \frac{\gamma^2 f_i^* f_j}{(1+\gamma\lambda_i)(1+\gamma\lambda_j)} + \frac{\alpha}{2}\gamma P\frac{\gamma^2 f_i^* f_j[\gamma\lambda_j(1+\gamma\lambda_i)+\gamma\lambda_i(1+\gamma\lambda_j)]}{(1+\gamma\lambda_i)^2(1+\gamma\lambda_j)^2} + $$

$$+ \frac{\alpha}{2}\frac{\gamma\lambda_i}{1+\gamma\lambda_i}\delta_{ij}\gamma Sp(\langle M\rangle\langle W\rangle_{ycr}\langle W^+\rangle_{ycr}). \tag{10}$$

From (10) and (6) it is easy to find covariation matrix Σ of the vector of the weight coefficients:

$$\sigma_{ij} = \frac{\alpha}{2}\frac{\gamma\lambda_i}{1+\gamma\lambda_i}\delta_{ij}\gamma Sp(\langle M\rangle\langle W\rangle_{ycr}\langle W^+\rangle_{ycr}). \tag{11}$$

We note that covariation matrix Σ is diagonal in Q-matrix representation, i.e., fluctuations of vector W(t) are completely defined by covariation matrix $\langle M\rangle$ of input interference. When $\gamma\lambda_i \gg 1$ the imperfection of the filters of the correlation coupling circuits may be ignored; then we have from (11)

4

FOR OFFICIAL USE ONLY

$$\Sigma = \frac{\alpha}{2} \gamma \, \mathrm{Sp}\left(\langle M \rangle \langle W \rangle_{yc\tau} \langle W^{+} \rangle_{yc\tau}\right) I \equiv \sigma I ,\qquad (11a)$$

i.e., in this case the covariation matrix of vector W(t) will also be diagonal in the original notation. We also note that the fluctuations of vector W increase as the effective power of interference $\gamma\lambda_i$ increases.

The requirement that these fluctuations be limited conflicts with the requirement of the shortest possible tuning time of the system, which is determined by (5) and is inversely proportional to $\gamma\lambda_i$. Therefore, to choose gain γ it is necessary to seek a compromise solution that best satisfies the requirements imposed on a system.

4. Let us determine the transformation characteristics of a system in terms of noise and useful signal. The steady state output interference power $P_{v} = \langle |W^{\tau}V|^{2} \rangle_{st}$ is expressed as

$$P_V = S + \langle W^{*} \rangle - \frac{1}{\gamma} \langle W^{\tau} W^{*} \rangle$$

and in the examined approximation it acquires the form

$$P_V = P_{V0} + \sigma P, \qquad P_{V0} = \sum_{i=1}^{N} \frac{|f_i|^2}{\lambda_i} \quad (\gamma\lambda_i \gg 1), \qquad (12)$$

i.e., the increase of the output interference power in comparison with the minimum is determined entirely by fluctuations of the vector of the weight coefficients.

We derive in like manner the expression for the power of the useful output system of an adaptive array:

[вх=in] $$P_s = \left(1 + \frac{\alpha}{2} \gamma P\right) P_{s0} + \sigma P_{s \, вх} \qquad (\gamma\lambda_i \gg 1), \qquad (13)$$

where S_i is the amplitude of the signal in the i-th element of the array;

$$P_{s \, in} = \sum_{i=1}^{N} S_i^2, \qquad P_{s0} = \sum_{i, j=1}^{N} S_i S_j \frac{|f_i| \, |f_j|}{\lambda_i \lambda_j}.$$ Hence we find μ, the signal to noise ratio:

$$\mu = \frac{P_s}{P_V} = \frac{P_{s0}}{P_{V0}} \left[1 + \frac{\alpha}{2} \gamma P - \sigma \frac{P}{P_{V0}} \right] + \sigma \frac{P}{P_{V0}} \frac{P_{s \, вх}}{P}. \qquad (14)$$

5

FOR OFFICIAL USE ONLY

Thus the output signal to noise ratio of the system is determined by the given amount of suppression of interference P/P_{vn} and by the input signal to noise ratio $P_{s\ in}/P$ of the array, and it depends on fluctuations σ of the vector of the weight coefficients.

5. In conclusion we will determine the spectral correlation characteristics of the examined adaptive antenna system. The equation for the correlation matrix of control voltages acquires the form

$$\left(\tau \frac{d}{d\theta} + I\right) \langle W_\theta\ W^+ \rangle = \gamma S^* \langle W^+ \rangle - \gamma \langle M_\theta\ W_\theta\ W^+ \rangle,$$

(15)

$$f_\theta = f(t + \theta),$$

with the initial condition $\langle W_\theta\ W^+ \rangle |_{\theta=0} = \langle W W^+ \rangle_{ycr}$. Hence, to the accuracy of terms of the first order of smallness in terms of the parameter α, we find in matrix notation

$$\sigma_{ij}(\theta) = \sigma_{ij} \exp\left[-\frac{1}{\tau}(1 + \gamma\lambda_i) | \theta |\right],$$

(16)

i.e., the band of the power spectrum of fluctuations W(t) gets wider as the power of interference $\gamma\lambda_i$ increases. Thus, the power of the interference and useful output system [see (12), (13)] increases as a result of parasitic modulation by fluctuations of the vector of the weight coefficients. The bandwidths of the power spectra of the output signal and interference increase, i.e., they become faster.

BIBLIOGRAPHY

1. Woodrow, B., et al, TIIER, Vol 55, No 12, p 78, 1967.

2. Applebaum, S. P., IEEE TRANS., AP-24, No 5, p 585, 1976.

3. Special Issue on Active and Adaptive Antennas, IEEE TRANS., AP-12, March 1964.

4. "Teoreticheskiye Osnovy Radiolokatsii" (Theoretical Principles of Radar), edited by Ya. D. Shirman, izd. Sov. radio, Moscow, 1970.

5. Ponomareva, V. D. and V. M. Komarov, ZARUBEZHNAYA RADIOELEKTRONIKA (Foreign Radio Electronics), No 8, p 33, 1977.

6. Special Issue on Nuclear Test Detection, PROC. IEEE, Vol 53, December, 1965.

6

FOR OFFICIAL USE ONLY

FOR OFFICIAL USE ONLY

7. Edelblute, D. J., J. M. Fisk and G. L. Kinnison, J. ACOUST. SOC. AM., Vol 41, No 1, p 199, 1967.

8. Mal'tsev, A. A. and A. I. Saichev, RADIOTEKHNIKA I ELEKTRONIKA (Radio Engineering and Electronics], Vol 23, No 12, p 2543, 1978.

9. Dubkov, A. A. and A. A. Mal'tsev, IZV. VUZOV -- RADIOFIZIKA (News of Higher Educational Institutions -- Radio Physics), Vol 22, No 3, p 353, 1979.

10. Brennan, L. E., E. L. Pugh and I. S. Reed, IEEE TRANS., AES-7, No 2, p 254, 1971.

11. Reed, I.S., IEEE TRANS., IT-8, p 194, 1962.

12. Mal'tsev, A. A., O. V. Muzychuk and I. Ye. Pozumentov, RADIOTEKHNIKA I ELEKTRONIKA, Vol 23, No 7, p 1401, 1978.

13. Mal'tsev, A. A. and I. Ye. Pozumentov, IZV. VUZOV -- RADIOFIZIKA, Vol 22, No 2, p 150, 1979.

14. Arzamasov, S. N., A. N. Malakhov, O. V. Muzychuk and I. Ye. Pozumentov, RADIOTEKHNIKA I ELEKTRONIKA, Vol 24, No 3, p 545, 1979.

7872
CSO: 1860

FOR OFFICIAL USE ONLY

UDC 621.396.67

ACOUSTIC-OPTICAL PROCESSING OF SPACE-TIME SIGNALS IN THE FRESNEL ZONE

[Article by N. A. Potapov]

[Text] There is presently considerable interest in application of
optical methods to processing space-time signals of antenna arrays.
This interest stems from a number of properties that optical and elec-
tronic systems have in common [Ref. 1-4]. In Ref. 1-3, an examination
was made of optical processing of signals in the far wave zone of linear
antenna arrays (LAR) when the wave fronts of the received signals are
planar. However, the methods described in Ref. 1-3 cannot be directly
used for processing signals with spherical wave fronts. To realize
signal processing in the Fresnel zone we need a processing system that
"focuses" the LAR on different ranges, i. e. a system that is multi-
channel not only with respect to direction, but also with respect to
range [Ref. 5]. In this connection it is of interest to synthesize
optical systems that realize processing of signals with spherical wave
fronts, and to analyze their characteristics.

Let us consider the case of active location of a small-sized ("point")
target situated in the Fresnel zone of the LAR at point C with coordinates
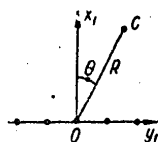(θ, R) that are to be measured (Fig. 1). An N-element (N = 2m + 1) equidis-
tant LAR is oriented along axis Oy_1 with center at the
coordinate origin O. The aperture of the LAR L = 2md,
where d is the distance between its adjacent elements.
To simplify the computations, just as in Ref. 1, 2, we
will consider the LAR to consist of weakly directional
elements, i. e. we will assume that the radiation pattern
of an individual element of the LAR changes but little
within the limits of the angles that are of interest.
In studying the probing signal from point O, in the ab-
sence of signal distortions during reflection and propagation, the
signal received by the k-th element of the LAR can be represented as in
Ref. 5:

Fig. 1

8

$$s_k(t) = Re\{\dot{U}(t - \tau + \mu k d - v k^2 d^2)\exp[j\omega_0(t - \tau + \mu k d - v k^2 d^2) + j\varphi_0]\}, \qquad (1)$$

where

$$\mu = \sin\Theta/c, \quad v = \cos^2\Theta/2Rc, \quad \tau = 2R/c, \qquad (2)$$

ϕ_0 is the unknown initial phase, c is the speed of light, $\dot{U}(t)$ is the complex envelope of the signal.

In the case of a "narrow-band" signal where the signal correlation time is much greater than the maximum value of the difference of signal propagation times to different elements of the LAR, the complex signal envelope (2) can be considered identical in all reception elements [Ref. 5] and the signal from the k-th element can be written as

$$s_k(t) = Re\{\dot{U}(t - \tau)\exp[j\omega_0 t + j\psi_k + j(\varphi_0 - \omega_0\tau)]\}, \qquad (3)$$

where

$$\psi_k = \omega_0(\mu d k - v d^2 k^2) \qquad (4)$$

is the difference in phases of the signals of the k-th and 0-th elements of the LAR.

A diagram of an acoustic-optical processor for LAR signals is shown in Fig. 2. Spatial-multichannel light modulator 1 is located in the focal plane of spherical lens 2 with focal length f.
The output plane 3 of the acoustic-optical processor is located in the rear focal plane of the lens. The light modulator is made in the form of a system of N identical ultrasonic light modulators (ULM) that operate in the Bragg diffraction mode and are located on a parabola in rectangular apertures in an optically opaque transparency. The k-th ULM has dimensions D along the Ox axis, W along the Oy axis, H along the Oz axis, and is removed from the central ULM (k = 0) by a distance $l_x k^2$ along the Ox axis, and $l_y k$ along the Oy axis.

Fig. 2

The signal from the k-th element of the LAR goes to the k-th ULM, exciting ultrasonic vibrations with wavelength $\Lambda = 2\pi V/\omega_0$, where V is the speed of ultrasound propagating along the Ox axis. The multichannel ULM is exposed to a collimated beam of coherent light with wavelength λ_0, the angle of incidence of the ULM being equal to the Bragg angle $\lambda_0/2\Lambda$.

Let us first consider diffraction of the light only by the "zero" ULM in the case where its center is located on the optical axis of the lens. The distribution of the light field in the rear focal plane of a spherical lens in the diffraction spectrum of first order is defined by the expression [Ref. 3]

9

FOR OFFICIAL USE ONLY

$$\dot{F}_0(u, v, t) = E_n \sin(\beta/2) \dot{M}(u, v, t) \dot{F}(u, t), \tag{5}$$

where E_n is the intensity of the incident light beam, β is the modulation index

$$\dot{M}(u, v, t) = \text{sinc}\left[(\lambda_0 H/2n_0)(u^2 - 1/4\Lambda^2)\right] \text{sinc } Wv e^{j(\omega_0 - \omega_{CB})t} e^{j(\varphi_0 - \omega_0 \eta)}, \tag{6}$$

where n_0 is the index of refraction of the sound-conducting medium, ω_{CB} is the frequency of light vibrations,

$$\text{sinc } x = \sin \pi x / \pi x;$$

$u = x_2/\lambda_0 f$, $v = y_2/\lambda_0 f$ are spatial frequencies, i. e. the normalized coordinates (x_2, y_2) in the output plane of the acoustic-optical processor.

For a harmonic signal the function $\dot{F}(u, t)$ is described by the formula [Ref. 3]

$$\dot{F}(u, t) = \dot{F}_0(u) = e^{-j\pi(u - 1/2\Lambda)D} \text{sinc}\left[(u - 1/2\Lambda)D\right].$$

It can be shown that in the case of a radio pulse of duration τ_H the function $\dot{F}(u, t)$ takes the form

$$\dot{F}(u, t) = \frac{1}{D} \int_{a(t)}^{b(t)} \dot{U}(t - \tau - x/V) e^{-j2\pi(u - 1/2\Lambda)x} dx, \tag{7}$$

where the limits $a(t)$ and $b(t)$ of integral (7) define the region occupied by the signal of the ULM at time t

$$a(t) = \max\{V(t - \tau - \tau_H), 0\}, \quad b(t) = \min\{V(t - \tau), D\},$$

$$0 \leqslant a(t) \leqslant b(t) \leqslant D.$$

For a simple pulse signal with square envelope of duration $\tau_H = D/V$, calculations by formula (7) give

$$\dot{F}(u, t) = \frac{b(t) - a(t)}{D} e^{-j\pi(u - 1/2\Lambda)[b(t) + a(t)]} \text{sinc}\{(u - 1/2\Lambda)[b(t) - a(t)]\}. \tag{8}$$

The function $|\dot{F}(u, t)|$ reaches a maximum at time

$$t_m = \tau + \tau_H, \tag{9}$$

i. e. when the ULM is completely filled with the signal.

Let us now find the distribution of the light field $\dot{E}_k(u, v, t)$ that is diffracted by the k-th ULM. According to transport theory [Ref. 4] the displacement of the k-th ULM relative to the 0-th by distances $-l_x k^2$ along the Ox axis, and $l_y k$ along the Oy axis in the input plane causes an additional factor $\exp\{j2\pi(l_x k^2 u - l_y kv)\}$ to show up in the expression for the diffraction spectrum in the output plane. Therefore

$$\dot{E}_k(u, v, t) = \dot{E}_0(u, v, t) \exp\{j2\pi(l_x k^2 u - l_y kv) + j\psi_k\}, \tag{10}$$

10

FOR OFFICIAL USE ONLY

where the phase difference ψ_k is defined by formula (4).

By using the principle of superposition, we get the following distribution of light intensity diffracted by all N ULM's

$$I(u, v, t) = C \mid \dot{M}(u, v, t) \mid^2 \mid \dot{F}(u, t) \mid^2 \Phi(u, v),\tag{11}$$

where

$$\Phi(u, v) = \frac{1}{N^2} \left| \sum_{k=-m}^{m} \exp\{j2\pi[(l_x u - f_0 v d^2) k^2 - (l_y v - f_0 \mu d) k]\} \right|^2,\tag{12}$$

$$C = N^2 E_n^2 \sin^2(\beta/2), \quad f_0 = \omega_0/2\pi.$$

Let us note that in the case where the center of the "zero" ULM is removed from the axis of the lens by a distance x_0 along the Ox axis, and y_0 along the Oy axis, the right member of formula (10) must (in accord with the transport theorem of Ref. 4) be multiplied by the expression $\exp\{j2\pi(x_0 u + y_0 v)\}$. Nonetheless, the distribution of light intensity as before will be described by formula (11), since $\mid \exp\{j2\pi(x_0 u + y_0 v)\} \mid^2 = 1$.

As implied by formulas (6) and (8), if $l_x \geqslant D$, $l_y \geqslant W$ and $H \leqslant n_0 \Lambda D/\lambda_0$, the product of functions $\mid \dot{M}(u,v,t) \mid$ and $\mid \dot{F}(u,t) \mid$ at fixed time $\tau < t < \tau + 2\tau_H$ reaches the maximum value at the point of the output plane with coordinates $(u = 1/2\Lambda, v = 0)$ and changes smoothly in the region of values (u,v)

$$\left. \begin{array}{l} 1/2\Lambda - 1/2 l_x \leqslant u \leqslant 1/2\Lambda + 1/2 l_x \\ -1/2 l_y \leqslant v \leqslant 1/2 l_y \end{array} \right\},\tag{13}$$

acting as a slowly changing "constant." Consequently, all information on the angular position and range of a target as coded in parameters μ and ν of the received signal, is contained in the last cofactor of expression (11).

Function (12) is periodic with respect to axes Ou and Ov with periods $\Delta u = 1/l_x$ and $\Delta v = 1/l_y$ respectively, and reaches maximum values at points with coordinates

$$\left. \begin{array}{l} u_s = f_0 v d^2/l_x + s/l_x \\ v_k = f_0 \mu d/l_y + k/l_y \end{array} \right\},$$

where s, k = 0, ±1, ±2,...

Conditions (13) will be satisfied by a point with coordinates (u_i, v_0), where

$$1/2\Lambda - 1/2 l_x \leqslant u_i \leqslant 1/2\Lambda + 1/2 l_x,\tag{14}$$

and i takes on one of the values i = 1, 2, 3... At this point function (11) will reach its maximum value. The selection of a point with coordinates (u_i, v_0) is illustrated in Fig. 3, where curve 1 is a graph of
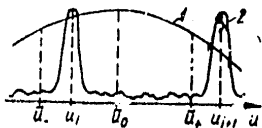
11

Fig. 3

the function $|\dot{M}(u, v_0, t_m)| \, |F(u, t_m)|$, curve 2 is a graph of the function $\Phi(u, v_0)$, and $\tilde{u}_- = 1/2\,\Lambda - 1/2\,l_x$, $\tilde{u}_0 = 1/2\,\Lambda$, $\tilde{u}_+ = 1/2\,\Lambda + 1/2\,l_x$. If the target is in the far zone of the LAR, then $\nu = 0$, and inequality (14) becomes

$$1/2\Lambda - 1/2l_x \leqslant i/l_x \leqslant 1/2\Lambda + 1/2l_x. \tag{15}$$

Taking the equal sign in the left member of (15), we get $l_x = (2i+1)\Lambda$. Thus in order for the maximum of function (12) to be located at a point with coordinates $(1/2\Lambda - 1/2l_x, v_0)$ when the target is located in the far zone of the LAR, the parameter l_x must be equal to an odd number of wavelengths of the ultrasonic vibrations. With such a choice of the parameter l_x, the maximum of the distribution of light intensity (11) in the region of values (u,v) as described by formulas (13) will be observed at time $t_m = \tau + \tau_H$ at a point of the output plane with coordinates

$$\left. \begin{array}{l} u_i = f_0 v d^2/l_x + 1/2\Lambda - 1/2l_x \\ v_0 = f_0 \mu d/l_y \end{array} \right\}. \tag{16}$$

Substituting expressions (2) in (9) and (16), we find the polar coordinates of the target expressed in terms of the coordinates of the maximum of light intensity in plane u0v and the time when the light intensity reaches the maximum

$$R = c(t_m - \tau_n)/2 \tag{17}$$

$$\theta = \arcsin(l_y \lambda v_0/d) \tag{18}$$

$$R = \frac{d^2 - l_y^2 \lambda^2 v_0^2}{2l_x \Lambda (u_i - 1/2\Lambda + 1/2l_x)} \tag{19}$$

In the case where echo signals are arriving at the antenna aperture from several targets located at different angles and ranges of the zone of coverage, each of them has a corresponding light spot in the output plane of the acoustic-optical processor with time of appearance proportional to the distance to the target [Ref. 1, 2]. To determine the resolution of the acoustic-optical processor with respect to angle and range, we will use the same approach as in Ref. 1, 2. As a measure of the resolution of the acoustic-optical processor with respect to angle and range as measured from the phase front of the signal (by formulas (18) and (19)) we will take the distances with respect to angle $\delta\theta$ and range δR in the Fresnel zone for which the maxima of the light spots in the output plane of the acoustic-optical processor are removed by amounts δv and δu equal to the width of the principal maximum of the light spot with respect to some fixed level in the direction of axes 0v and 0u respectively.

12

Resolution δR_τ with respect to the range measured from signal delay time (by formula (17)) we will determine on the 0.5 level of function $|\dot{F}(u,t)|$. As implied by expressions (8) and (17), in the case of a simple pulse signal of duration $\tau_\mu = D/V$

$$\delta R_\tau = c\tau_\mu/2.$$

The resolution of the acoustic-optical processor with respect to angle and range as measured from the phase front of the signal is determined by the properties of function (12) that describes the image of a point target formed in the output plane of the acoustic-optical processor. Substituting expressions (2) in formula (12) and introducing the normalized variables $\xi = l_x u$, $\eta = l_y v$, we get

$$\Phi(\xi, \eta) = \frac{1}{N^2} \left| \sum_{k=-m}^{m} \exp\left\{ j2\pi \left[\left(\xi - \frac{d^2 \cos^2\Theta}{2\lambda R} \right) k^2 - \left(\eta - \frac{d\sin\Theta}{\lambda} \right) k \right] \right\} \right|^2. \quad (20)$$

To elucidate the lobe structure of formula (20), let us consider its behavior at a fixed value of one of the arguments. Setting $\xi = \xi_1 = l_x u_1$, we get

$$\Phi(\xi_1, \eta) = \frac{\sin^2 \pi N (\eta - d\sin\Theta/\lambda)}{N^2 \sin^2 \pi (\eta - d\sin\Theta/\lambda)}. \quad (21)$$

Thus along an axis parallel to 0η and passing through point $(\xi_1, 0)$ the side lobes are determined by a function that describes the square of the radiation pattern of the LAR. As implied by expression (21), the width of the main lobe on level $[N \sin(\pi/2N]^{-2} \doteq 4/\pi^2 \doteq 0.405$ is equal to $\delta\eta = l_y \delta v = 1/N$. Since

$$\delta\eta = \eta_2 - \eta_1 = \frac{d}{\lambda}(\sin\Theta_2 - \sin\Theta_1) \doteq \frac{d}{\lambda}\cos\Theta\,\delta\Theta,$$

where $\delta\Theta = \Theta_2 - \Theta_1 \ll 1$, $\Theta = \Theta_1 + \delta\Theta/2 \doteq \Theta_1$, an element of resolution with respect to angle is

$$\delta\Theta = \lambda/Nd\cos\Theta. \quad (22)$$

In virtue of the periodicity of formula (21), unambiguous measurement of the angle is possible only in the range of angles

$$|\Theta| \leqslant \arcsin(\lambda/2d).$$

The number of elements of resolution with respect to angle within the limits of this interval is

Along the axis parallel to axis 0ξ and passing through the point $(0, \eta_0 = l_y v_0)$, the lobe nature of function (20) is determined by the expression

$$\Phi(\xi, \eta_0) = \frac{1}{N^2} \left| \sum_{k=-m}^{m} \exp\left\{ j2\pi \left(\xi - \frac{d^2 \cos^2\Theta}{2\lambda R} \right) k^2 \right\} \right|^2. \quad (23)$$
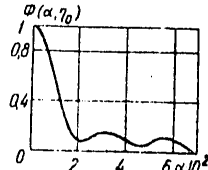
13

Fig. 4

Shown in Fig. 4 is a graph of the function

$$\Phi(\alpha, \eta_0) = \frac{1}{N^2} \left| \sum_{k=-m}^{m} \exp\{j2\pi\alpha k^2\} \right|^2, \qquad (24)$$

where $\alpha = \xi - \xi_1$ is the difference between coordinate ξ and the value of ξ_1 at which function (23) reaches a maximum for the case when $m = 6$.

Computer calculations by formula (24) for different values of m have shown that when $m \geqslant 5$, the width of the main lobe of function (23) at the 0.25 level is equal to $\delta\xi = l_x\delta u = 1/m^2$. Since

$$\delta\xi = \xi_2 - \xi_1 = \frac{d^2\cos^2\Theta}{2\lambda}\left(\frac{1}{R_2} - \frac{1}{R_1}\right) = \frac{d^2\cos^2\Theta}{2\lambda}\frac{\delta R}{R^2},$$

where $R^2 = R_1 R_2$, $\delta R = R_1 - R_2$, an element of resolution with respect to range is equal to

$$\delta R = \frac{2\lambda R^2}{m^2 d^2 \cos^2\Theta} = \frac{8\lambda R^2}{L^2 \cos^2\Theta}. \qquad (25)$$

Formulas (22) and (25) imply that the resolution of an acoustic-optical processor with respect to range and angle as measured from the phase front of the signal is independent of the parameters of the processor, and coincides with the resolution of the LAR.

In virtue of the periodicity of function (23), unambiguous measurement of range from the curvature of the wave front of a signal is possible only at ranges of

$$R \geqslant d^2\cos^2\Theta/2\lambda.$$

REFERENCES

1. L. Lambert, M. Arm, A. Aymet, "Electron-Optical Signal Processing in Phased Antenna Arrays," ZARUBEZHNAYA RADIOELEKTRONIKA, No 8, 1968, p 3.

2. L. D. Bakhrakh, A. P. Kurochkin, S. G. Rudneva, "Using an Ultrasonic Light Modulator for Parallel Processing of Signals of an Antenna Array" VOPROSY RADIOELEKTRONIKI, SERIYA OBSHCHETEKHNICHESKAYA, No 1, 1972, p 36.

3. Ye. T. Aksenov, V. Ya. Grigor'yev et al., "A Multichannel Ultrasonic Light Modulator that Operates in the Bragg Diffraction Mode for an Optical Signal Processing System," VOPROSY RADIOELEKTRONIKI, SERIYA OBSHCHETEKHNICHESKAYA, No 5, 1972, p 8.

4. A. Papulis, "Teoriya sistem i preobrazovaniy v optike" [Theory of Systems and Transformations in Optics], Moscow, Mir, 1971.

FOR OFFICIAL USE ONLY

5. I. Ya. Kremer, V. A. Pon'kin, "Space-Time Signal Processing in the
   Fresnel Zone," RADIOTEKHNIKA I ELEKTRONIKA, Vol 22, No 1, 1977 p 72.

[184-6610]

COPYRIGHT: "Izvestiya vuzov SSSR - Radioelektronika", 1980

6610
CSO: 1860

FOR OFFICIAL USE ONLY

INFLUENCE THAT A COHERENT-OPTICS PROCESSOR HAS ON THE DIAGRAM FORMING
PROPERTIES OF RADIO-OPTICAL ANTENNA ARRAYS

[Article by A. Yu. Grinev and Ye. N. Voronin]

[Text] A radio-optical antenna array [ROAR] consists of an active recep-
tion antenna array (radiators and reception modules), input devices in
the form of a multichannel space-time light modulator controlled by the
signals of the antenna array, a coherent-optics processor that reproduces
the space-time spectrum of the received radio emission, and an extraction
system (photorecorder, interface, computer) [Ref. 1].

A number of papers have examined both planar [Ref. 2, 3] and non-planar
[ref. 4, 5] ROAR's. In these works, the coherent-optics processors (con-
sisting of a laser, collimator, lens system, transparencies and so on)
were taken as ideal: nondistorting and non-noisy.

However, as a precision computing device of analog type, the coherent-
optics processor is quite critical to all kinds of deviations from
ideality (wavelength of light of the order of 0.633 μm or even shorter)
[Ref. 6].

This paper evaluates appreciable factors of nonideality of coherent-
optics processors that are detrimental to the diagram forming properties
of ROAR's, and that determine their competitiveness as compared for
example with phased antenna arrays, multibeam antenna arrays and other
systems.

The paper systematizes both known results (found without reference to
the problem under consideration), and presents a number of new results
that are necessary for the most complete consideration of the studied
effects.

16

Gain of the ROAR, dynamic range and defocusing of the coherent-optics processor. We define the reception gain of the ROAR as the ratio of its responses to a plane wave I_q and the isotropic emission I_M energetically equivalent to this wave with consideration of defocusing $Д\Phi$ of the directional diagram (radiation pattern) of the coherent-optics processor ($Д\Phi \leqslant 1$ characterizes a reduction in the maximum of the directional diagram) and parasitic background illumination I_3, which are caused by the nonideality of the coherent-optics processor

$$KY_{ROAR} = \frac{Д\Phi I_q}{I_{u} + I_{3}} = Д\Phi(KY_{AP}^{-1} + ДД^{-1})^{-1},\qquad(1)$$

where $KY_{AP} = I_q/I_M$ is the gain of an antenna array with an ideal coherent-optics processor, $ДД = I_q/I_3$ is the dynamic range of the coherent-optics processor [Ref. 7, p 117].

Let us note that the given definition of reception gain of the ROAR stems from the definition of the transmission gain of the antenna.

Relation (1) implies that $KY_{ROAR} \to ДД$ as $KY_{AP} \to \infty$, and therefore the dynamic range of an optical processor in essence determines the limiting gain of the ROAR (ROAR's with gain of the antenna array proper exceeding the dynamic range of the coherent-optics processor are energetically unfeasible).

Distortions of the directional diagram (defocusing – $Д\Phi$) and parasitic background illumination at the output may be caused by the following set of statistically independent factors:

1) pupil effects and mutual interference of the channels of the space-time light modulator [Ref. 8, 9];
2) aberrations of the optical system of the coherent-optics processor;
3) misalignment of the optical system;
4) spatial incoherence of the readout light;
5) time incoherence of the laser;
6) Fresnel re-reflections in the optical system;
7) light scattering on inhomogeneities;
8) the presence of a conjugate image with two-band input [Ref. 2, 3, 8, 9];
9) nonlinearity of the space-time light modulator;
10) zero order of diffraction.*

The statistically independent factors make the following contribution to the resultant defocusing of the coherent-optics processor:

$$Д\Phi = \prod_{n=1}^{10} Д\Phi_n \qquad(2a)$$

---

*Distorting factors that arise on the level of the antenna array and reception modules (errors of element excitation, non-identity of channels and so on) are not explicitly enumerated since they are unavoidable in other systems as well (phased antenna arrays, multibeam antenna arrays) and can be accounted for by other methods [Ref. 10].

17

($Д\Phi_n$ is defocusing of the directional diagram by the n-th distorting factor), and the resultant dynamic range of the coherent-optics processor is

$$ДД = I_q/I_s = I_q/\sum_{n=1}^{10} I_n = \left[\sum_{n=1}^{10} ДД_n^{-1}\right]^{-1} \qquad (2b)$$

($ДД_n = I_q/I_n$ is the dynamic range of the coherent-optics processor in the presence of the n-th factor alone).

The enumerated factors are different in nature, and may lead to defocusing ($Д\Phi_n < 1$, $ДД_n = \infty$), to background illumination ($Д\Phi_n = 1$, $ДД_n < \infty$) and to mixed effects ($Д\Phi_n < 1$, $ДД_n < \infty$). Let us take these up in detail.

Pupil effects and interference of channels of the space-time light modulator. In Ref. 3, 5, 8, 9 it is shown that the given effect leads only to distortion of the directional diagram; these papers also give an estimate of defocusing and point out ways to compensate for it (we will assume hereafter that such compensation has been carried out). However, multichannel space-time light modulators have a discrete structure that reduces the diffraction efficiency of the coherent-optics processor $ДЭ$ [Ref. 3, 8] (the ratio of the useful energy of the luminous flux that falls in the region of radio visibility to the total energy in the region of optical visibility is $ДЭ < 0.5$) as compared with the coherent-optics processor that has a continuous-wave space-time light modulator. As a result, the response of the system to a planar wave is reduced by a factor of $ДЭ$, and the background illumination due to the finite dynamic range of the coherent-optics processor remains practically unchanged; therefore we have the estimate

$$ДД \cong ДЭ \cdot \tilde{ДД}, \qquad (3)$$

where $\tilde{ДД}$ is the dynamic range of a coherent-optics processor with a cw space-time light modulator.

Expression (3) enables us to use the more convenient model of a cw space-time light modulator hereafter in evaluating the other factors.

Aberrations of the optical system of the coherent-optics processor. To evaluate defocusing of the directional diagram due to aberrations of the optical system, we use the expression [Ref. 11 p 502] that applies to small aberrations of arbitrary form:

$$Д\Phi_s \cong 1 - \alpha, \qquad (4)$$

where $\sqrt{\alpha}/k$ is the mean square aberration of the wave front at the input to the coherent-optics processor, $k = 2\pi/\lambda$ is the wave number.

18

Aberrational optimization of objective lenses for Fourier processors has shown [Ref. 6, p 70] that for dimensions of the space-time light modulator aperture $\Delta x \times \Delta y < 40 \times 40$ mm (f $\sim$1 mm), the mean square aberration is determined only by the spatial bandwidth ПШП of transmission of the optical system.

$$\text{ПШП} = \frac{1}{2\pi_j}\,\Delta\omega_x \Delta x = \frac{1}{2\pi_j}\,m_x \Delta\Omega_x\,\frac{\Delta X}{m_x} \leqslant \frac{1}{2\pi}\,2K\Delta X = \frac{X}{0{,}5\lambda},$$

where $\Delta\omega_x$, $\Delta\Omega_x \leqslant 2K$ are the bands of spatial frequencies of the optical wave and the radio wave ($K = 2\pi/\Lambda$ is the wave number of the radio wave); $m_x = \Delta X/\Delta x$ is the scale of modeling [Ref. 2]; Δx, ΔX are the respective sizes of the space-time light modulator and the antenna array. Considering that $K\!\mathcal{Y}_{AP} \sim 2\pi\Delta X\Delta Y/\Lambda^2 \sim (\text{ПШП})^2 < \text{ДД}(< 10^6$, [Ref. 6]), we have ПШП $< 10^3$.
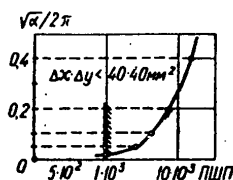

Fig. 1

Fig. 1 shows a curve for the maximum attainable mean square aberration as a function of ПШП, plotted from data of Ref. 6, p 70. As we can see, values of $\sqrt{\alpha}/k < 0.01$ correspond to values of ПШП $< 10^3$. The only lenses that have characteristics like this are long-focus (f $\sim$1 m) astronomical objectives with eliminated aberrations at an infinitely remote point on the optical axis. According to (4), defocusing $\Delta\Phi_2 \geqslant 0.996$ corresponds to aberrations of such a magnitude. As a rule, the actual coherent-optics processor in the ROAR contains two or three sequential Fourier processors [Ref. 8, 9]. Since small aberrations of such processors are practically uncorrelated, and the initial ПШП-parameter in this case does not change (just as there is no change in the analogous parameter of a time signal with linear transformations), in this case the resultant defocusing of the directional diagram of the ROAR will be

$$\Delta\Phi_3 \cong (1-\alpha)^{2\div3} \geqslant (0{,}996)^{2\div3} \cong 0{,}99. \qquad (5)$$

In essence the resultant estimate characterizes the potential precision ($\sim$1%) of reproduction of the directional diagram of the ROAR, and will subsequently be useful as a rough criterion of the perfection of a coherent-optics processor.

Misalignment of the elements of the coherent-optics processor. Longitudinal and transverse (relative to the axis of the coherent-optics processor) displacements of the elements (lenses, transparencies and so forth) defocus the directional diagram of the ROAR.

To evaluate the influence of longitudinal displacements, we use the known relation for the distribution of light intensity in the focal spot along the axis of the processor [Ref. 11, p 477]

19

$$\text{Д}\Phi_3 = \text{sinc}^2\left(\frac{\Delta x^2 \delta z}{2\lambda f^2}\right),\tag{6}$$

where f is the focal length of the lens (~1 m), δz is longitudinal displacement out of the focal plane, $\Delta x/f \approx 4\cdot10^{-2}$ m.

Let us estimate the influence of transverse displacements of elements of the optical system. Obviously such displacements in a Fourier processor do not lead to distortions, but merely cause corresponding displacements of the output diffraction pattern, or weighting by a linear phase multiplier. Transverse displacements lead to distortions in more complex processors that produce convolution transformation [Ref. 4, 5, 9]. For example, assume that the transparency T in Fig. 4 of Ref. 4 is displaced along axis ω_y by $\delta\omega_y = m_y\delta\Omega_\phi$. Then instead of the necessary transformation $\hat{L}$ of (16) in Ref. 4, the coherent-optics processor will perform a transformation of the form

$$R_0\hat{F}_\phi^{-1}\{\hat{F}\{\ldots J_z(Z)\}\}\hat{T}(\Omega_\phi + \delta\Omega_\phi, \Omega_z)\} = \hat{L}\{\ldots \exp(-i\delta\Omega_\phi\phi)\}.$$

The phase multiplier $\exp(-i\delta\Omega_\phi\phi) = \exp(-i\delta\omega_y y)$ is a variety of transverse Seidel aberration [Ref. 11], and therefore the defocusing effect of transverse displacements of elements of the optical system can be estimated by formula (4), the quantity α appearing in this formula being equal to

$$\alpha = \frac{1}{\Delta y}\int_{-0.5\Delta y}^{0.5\Delta y}|\delta\omega_y y|^2\,dy = \frac{(\delta\omega_y\Delta y)^2}{12} = \frac{\left(\frac{k}{f}\delta y\Delta y\right)^2}{12}.\tag{7}$$

Spatial incoherence of light. It is convenient to evaluate the space-time coherence of light by a normalized function of mutual coherence reduced to the coordinate system of the antenna array

$$\gamma(\vec{R}_1, \vec{R}_2; t_1, t_2) = \gamma_{12}(\vec{R}_1, \vec{R}_2)\gamma_{11}(t_2 - t_1)^*,\tag{8}$$

where R is a surface point of the antenna array, $\gamma_{12}(\vec{R}_1, \vec{R}_2) = \dot{E}(\vec{R}_1)\dot{E}(\vec{R}_2)/|\dot{E}(\vec{R}_1)\dot{E}(\vec{R}_2)|$ is the degree of space coherence; $\gamma_{11}(t_2 - t_1) = \dot{E}(\vec{R}_1, t_1)\dot{E}(\vec{R}_1, t_2)/|\dot{E}(\vec{R}_1)|^2$ is the degree of time coherence of the light $\dot{E}(\vec{R}, t) = \dot{E}(\vec{R})\exp i[2\pi\nu t + \varphi(t)]$ at the collimator output (ν is the frequency of the light).

The reduction in directionality of the ROAR with processing algorithm $\hat{L}$ [Ref. 9] due to partial coherence of the collimated beam in the general case can be estimated by an expression in which the numerator is represented by analogy with Ref. 13, p 267

*Light at the output of the laser-collimator system as a rule is "spectrally pure" [Ref. 12 (p 383), 13], and therefore it permits factorization of the function of mutual coherence (8).

$$\text{ДФ}_4 = \frac{\hat{L}_1\{\dot{E}(\vec{K}_q, \vec{R}_1)\,\hat{L}_2\{\dot{E}(\vec{K}_q, \vec{R}_2)\,\gamma_{12}(\vec{R}_1, \vec{R}_2)\}\}}{|\hat{L}\{\dot{E}(\vec{K}_q, \vec{R})\}|^2}\Bigg|_{\vec{K}'=\vec{K}_q}, \qquad (9)$$

where $\hat{L}_1$, $\hat{L}_2$ are the processing algorithms $\hat{L}$ on sets $\vec{R}_1$ and $\vec{R}_2$ respectively, $E(\vec{K}_q,\vec{R})$ is the aperture response of the antenna array to a plane wave with wave vector $\vec{K}_q$; $\vec{K}'$ is the direction of the maximum of the antenna array.

In the general case, calculation of (9) is difficult (the corresponding result will be given below only for a planar ROAR). We will get around this difficulty by using an estimate found in Ref. 10,

$$\text{ДФ}_4 \geqslant \exp(-\alpha), \qquad (10)$$

where α is the dispersion of the amplitude-phase distribution, valid for errors with correlation coefficient $R_\alpha \geqslant \Lambda$ (in the given case this condition is patently guaranteed by the smooth nature of the function γ_{12}). Let us find the correspondence between the dispersion α and the degree of spatial coherence (8) by using the known model of partly coherent light in the form of a superposition of a coherent wave and weakly correlated spatial noise

$$\gamma_{12}(\vec{R}_1, \vec{R}_2) = \overline{\exp i[\Phi(\vec{R}_1) - \Phi(\vec{R}_2)]} \simeq 1 + \overline{i[\Phi(\vec{R}_1) - \Phi(\vec{R}_2)]} -$$

$$\text{whence} \qquad -\frac{1}{2}\overline{[\Phi(\vec{R}_1) - \Phi(\vec{R}_2)]^2} = 1 - 0{,}5\alpha, \qquad (11a)$$

$$\alpha \leqslant 2 - 2\gamma_{12_{\text{мин}}}, \qquad (11b)$$

where $\gamma_{12\text{мин}}$ is the minimum value of the degree of spatial coherence within the limits of the space-time light modulator, $\Phi = \arg[\dot{E}(\vec{R})]$.

Thus

$$\text{ДФ}_4 \geqslant \exp(2\gamma_{12_{\text{мин}}} - 2) \geqslant 2\gamma_{12_{\text{мин}}} - 1. \qquad (12)$$

It is useful to compare the resultant large estimate with the value of ДФ₄ (9) calculated for a specific ROAR (for example a planar one). Setting specific values for the quantities in (9) and considering the steady-state nature of the degree of time coherence $\gamma_{12}(\vec{R}_1, \vec{R}_2) = \gamma_{12}(\vec{R}_{\perp_1} - \vec{R}_{\perp_2})$, we get

$$\text{ДФ}_4 = \frac{\hat{F}\{\gamma_{12}(\vec{R}_\perp)\} \otimes \otimes F^2(\vec{K}'_\perp - \vec{K}_{\perp_q})}{4\pi^2 F^2(\vec{K}'_\perp)}\Bigg|_{\vec{K}'_\perp = \vec{K}_{\perp_{q'}}} = \gamma_{12_{\text{ор}}}, \qquad (13)$$

where $\hat{F}(...)$ is the operator of Fourier transformation (the processing algorithm of the aperture response of a planar ROAR), $\vec{R}_\perp$ is the radius vector in the plane of the antenna array, $\vec{K}_\perp$ is the projection of the vector K on the plane of the array, $F(\vec{K}_\perp) = \hat{F}^{-1}\{J(\vec{R}_\perp)\}$ is the directional

21

diagram of the antenna array, $J(\vec{R}_\perp)$ is the amplitude-phase distribution,

$$\gamma_{12_{cp}} = \frac{\sum \iint \gamma_{12}(\vec{R}_\perp)\, d^2\vec{R}_\perp}{\Sigma} \quad \text{is the mean value of the degree of spatial coherence}$$

within the limits of the space-time light modulator, Σ is the area of the antenna array.

As we can see, the specific estimate (13) does not contradict (12): $\gamma_{12cp} > 2\gamma_{12MHH} - 1$ (since $\gamma_{12MHH} < \gamma_{12cp} < 1$), and is less severe.

Time incoherence of the collimator beam. The weak time coherence of the readout light $\vec{E}(\vec{R},t)$ at the output of the collimator distorts the directional diagram of the ROAR for two reasons: in the first place due to the dispersion of spatial frequencies of the optical signal, and in the second place due to chromatic aberration of the optical system. The former effect can be evaluated in the general case by reducing it to the preceding effect (spatial incoherence). Actually, the coherent-optics processor compensates phase delays of the radio wave in the aperture of the antenna array by corresponding delays of the light wave $\vec{E}(\vec{R},t)$:

$$\vec{K}'(\vec{R}_2 - \vec{R}_1) = (2\pi\nu + \Omega)(t_2 - t_1) = \omega(t_2 - t_1),$$

where Ω is the circular frequency of the radio wave. Considering this, as well as the quasi-monochromatic nature of the light wave, we represent the time coherence γ_{11} as [Ref. 12]

$$\gamma_{11}(t_2 - t_1) = \gamma_0(t_2 - t_1)\exp[i2\pi\nu(t_2 - t_1)] = \gamma_0[\vec{K}'(\vec{R}_2 - \vec{R}_1)/\omega] \times$$

$$\times \exp[i2\pi\nu(t_2 - t_1)], \quad \text{where} \quad \gamma_0(t_2 - t_1) = \overline{\exp i[\varphi(t_2) - \varphi(t_1)]}$$

(the line above indicates averaging).

The resultant representation coincides in form with the function of mutual coherence (8). The first cofactor ($\gamma_0[\dots]$) plays the role of the degree of spatial coherence γ_{12}, and the second ($\exp[\dots]$) plays the role of time coherence γ_{11} of an ideally monochormatic wave [Ref. 12]. Thus defocusing of the directional diagram due to time incoherence can be estimated from formula (9) with the substitution of $\gamma_0(\dots)$ for $\gamma_{12}(\dots)$. However, in virtue of the circumstances previously pointed out, an estimate of type (12) should be used instead of (9), with the corresponding substitution

$$\text{Д}\Phi_6 > 2\gamma_{0_{MHH}} - 1, \tag{14}$$

where $\gamma_{0MHH} = \min\{\gamma_0[\vec{K}'(\vec{R}_2 - \vec{R}_1)/\omega]\} = \gamma_0(K\Delta D/\omega)$ (ΔD is the diameter of the antenna array).

Since for practical purposes [Ref. 7] $\gamma_0(t_2 - t_1) = |\gamma_{11}(t_2 - t_1)| \simeq \exp - [(t_2 - t_1)/\tau_\kappa]^2$ (τ_κ is coherence time), we have $\gamma_{0MHH} \simeq \exp - [K\Delta D/\omega\tau_\kappa]^2 > 1 - \left(\frac{\lambda}{\Lambda}\frac{\Delta D}{l_\kappa}\right)^2$ ($l_\kappa = c\tau_\kappa$ is coherence length). Substituting γ_{0MHH} in (14),

we get

$$\text{ДФ}_{\text{в}} \geqslant 1 - \left(\frac{\lambda}{\Lambda}\frac{\Delta D}{l_{\text{к}}}\right)^2,\tag{15}$$

Defocusing (15) depends on the parameters of both the coherent-optics processor and the antenna array. If we assume that partial time coherence does not distort the directional diagram, but causes parasitic background illumination, then instead of (15), in accordance with (1) and (2a), (2b), we get

$$\text{ДД}_3 = \frac{\text{ДФ}_{\text{в}} \cdot \text{КУ}_{\text{AP}}}{1 - \text{ДФ}_{\text{в}}} \simeq \frac{4\pi\,(\Delta D/\Lambda)^2}{\left(\dfrac{\lambda}{l_{\text{к}}}\dfrac{\Delta D}{\Lambda}\right)^2} = 2\pi\,(l_{\text{к}}/\lambda)^2,\tag{16}$$

which is independent of the parameters of the antenna array, and consequently more objectively characterizes the contribution of the given factor to the general nonideality of the coherent-optics processor.

To evaluate chromatic aberration, we use formula (4), which is valid for small aberrations of arbitrary form.

The relative error of the focal length $\Delta f/f$ as a consequence of change in wavelength $\Delta\lambda$ [m] is

$$\Delta f/f \cong \frac{\Delta}{0.2 \cdot 10^{-6}}\,\Delta\lambda,$$

where Δ is the relative dispersion of the lens ($\leqslant 1/30$).

Thus for one lens of a coherent-optics processor the dispersion of the phase error α is

$$\alpha \cong \overline{\left[\Delta f \cdot d\left(\frac{k}{2f}\,r^2\right)/df\right]^2} < \left(\frac{k d_{\text{л}}^2 \Delta f}{8 f^2}\right),$$

where $r \leqslant \frac{1}{2}$, $d_{\text{л}}$ is the diameter of the lens.

On the average, there are 3-5 lenses in a coherent-optics processor, and therefore in accordance with (4) we have

$$\text{ДФ}_S \cong (1-\alpha)^{3 \div 5} \geqslant 1 - \frac{10^{-12}}{l_{\text{к}}^2},\tag{17}$$

where $l_{\text{к}}$ is the coherence length [m].

Re-reflection in the optical system of the coherent-optics processor. A reduction in the ДД of the coherent-optics processor as a result of re-reflections of light in the optical system ($\text{ДД}_6 < \infty$, $\text{ДФ}_6 = 1$) takes place for two reasons: in virtue of attenuation of the physical luminosity of the coherent-optics processor, and manifestation of a background of false

23

images ("ghosts"). The first factor can be accounted for by a coefficient of light transmission [Ref. 11] $t_{OC} = (1 - r_{yT})^{2N_{yT}} \cdot (1 - r_\pi)^{2N_\pi} \cdot (1 - r_T)^{2N_T} \sim 0,15 \div 0,80$, where $N_{yT} = 1 \div 2$, $N_\pi = 3 \div 5$, $N_T = 1$ is the number of controllable transparencies (of the space-time light modulator), the number of lenses and the number of uncontrolled transparencies with coefficients of reflection $r_{yT} = 0,03 \div 0,185$; $r_\pi = 0,03 \div 0,08$; $r_T = 0,04$, respectively.

"Ghosts" arise due to multiple re-reflections inside and between elements, the major part being played by double re-reflections since single, triple and quintuple re-reflections go to the input of the optical system, while quadruple and sextuple re-reflections are two or three orders of magnitude weaker than double re-reflections. Actually, the relative level of the latter is $r^2 = r_\pi^2 + r_\pi \cdot r_{yT} = 0,00688 \div 0,015$. With double re-transformation of the light inside a lens, its focal length becomes equal to [Ref. 6] $f' = f \dfrac{n_\pi - 1}{3n_\pi - 1}$ ($n_\pi \leqslant 1,8$ is the index of refraction of the glass of the lens). The relative intensity of a "ghost" in this case can be estimated as the square of the normed integral of the phase error over a Gauss comparison sphere [Ref. 11]

$$\left| \int_0^{d_\pi/2} \int_0^{2\pi} \exp\left[\frac{ik\rho^2}{2} \left(\frac{1}{f'} - \frac{1}{f} \right) \right] \rho \, d\rho \, d\varphi \Big/ \frac{\pi d_\pi^2}{4} \right|^2 = \left| \frac{8f(n_\pi - 1)}{kd_\pi^2 n_\pi} \right|^2 \sim 10^{-5}; \qquad (18)$$

ρ is the distance from a point of the lens to the axis.

To account for reflections between elements it is advisable to restrict ourselves to examination of only the unfavorable situation where they are not attenuated by vignetting on the lens holders [Ref. 6]: in the case of re-reflections between closely spaced elements (the collimator and the space-time light modulator, lenses and objectives). As can be seen from Fig. 2, depending on the kinds of re-reflections (a, b, c, d) the optical path in this case is elongated (shortened) by:
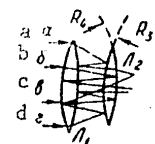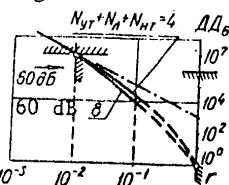

Fig. 2

Fig. 3

a) $\dfrac{k\rho^2}{2} 2\left(\dfrac{1}{R_2} - \dfrac{1}{R_3} \right) \sim \dfrac{k\rho^2}{f(n_\pi - 1)}$;

b) $\dfrac{k\rho^2}{2} 2\left(-\dfrac{1}{f_1} - \dfrac{1}{R_1} - \dfrac{1}{f_2} - \dfrac{1}{R_4} \right) \sim -\dfrac{k\rho^2}{f} \dfrac{2n_\pi - 1}{n_\pi - 1}$;

c) $\dfrac{k\rho^2}{2} 2\left(\dfrac{1}{R_2} - \dfrac{1}{f_2} - \dfrac{1}{R_4} \right) \sim -\dfrac{k\rho^2}{f}$;

d) $\dfrac{k\rho^2}{2} 2\left(-\dfrac{1}{f} - \dfrac{1}{R_1} + \dfrac{1}{R_3} \right) \sim -\dfrac{k\rho^2}{f}$,

24

where $\dfrac{1}{f_{1,2}} = (n_\pi - 1)\left(\dfrac{1}{R_{1,3}} - \dfrac{1}{R_{2,4}}\right)$ is the focal length of lens $\mathit{Л}_{1,2}$ with

radii of curvature of $R_{1,3}$ on the forward and $R_{2,4}$ on the rear surface. Corresponding to retransformations a, b, c and d are the following relative intensities of "ghosts":

$$\text{a)} \quad \left[\frac{8f\,(n_\pi - 1)}{kd_\pi^2}\right]^2 \sim 10^{-5}; \qquad \text{b)} \quad \left[\frac{8f\,(n_\pi - 1)}{kd_\pi^2\,(2n_\pi - 1)}\right]^2 \sim 10^{-6};$$

$$\text{c)} \quad \left[\frac{8f}{kd_\pi^2}\right]^2 \sim 5\cdot 10^{-5}, \quad \text{d)}\left[\frac{8f}{kd_{x\pi}^2}\right]^2 \sim 5\cdot 10^{-5},$$

which come to a total of $\sim 10^{-4}$.

Thus (see Fig. 3)

$$\mathit{ДД}_6 > t_{\text{OC}}/r^2 [N_\pi \cdot 10^{-5} + (N_{\text{УТ}} + N_\pi + N_{\text{Т}}) \cdot 10^{-4}] > \frac{t_{\text{OC}}}{r^2} \cdot 10^3. \tag{19}$$

Since $t_{\text{OC}}/r^2 \approx \dfrac{1}{r^2} - 2\,(N_{\text{УТ}} + N_\pi + N_{\text{Т}})/r \sim 10 \div 100$, we have $\mathit{ДД} \sim 10^4 - 10^5$, which corresponds to data of Ref. 6.

Light scattering on inhomogeneities of the optical system. High-quality processors are characterized by inhomogeneities with dimensions that do not exceed $r_\alpha \leqslant 10$ μm [Ref. 6]. The errors of amplitude-phase distribution caused by such inhomogeneities are characterized by a correlation coefficient of $R_\alpha \sim m_x r_\alpha \sim 10^2 \cdot 10$ μm $= 1$ mm$\ll \Lambda \sim 1$ cm.

This means that we can use an estimate [Ref. 10] that is more accurate than (10)

$$\mathit{ДФ}_7 \geqslant 1 - 3\pi^2 \alpha R_\alpha^2 / 4\Lambda^2. \tag{20}$$

Since (20) depends on the parameters of the antenna array, by analogy with (16) we have

$$\mathit{ДД}_7 = \frac{\mathit{ДФ}_7 \cdot \mathit{КУ}_{\text{АР}}}{1 - \mathit{ДФ}_7} \simeq \frac{4\Lambda^2}{3\pi^3 \alpha m_x^2 r_\alpha^2} \frac{4\pi \Sigma}{\Lambda^2} = \frac{1{,}7\sigma_{\text{УТ}}}{\alpha r_\alpha^2}, \tag{21}$$

where $\Sigma = m^2 \sigma_{\text{УТ}}$ is the area of the surface of the antenna array (of the space-time light modulator).

Let us note that simultaneous attenuation of retransformations and light scattering on inhomogeneities of the optical system of the coherent-optics processor is difficult: an increase in the number of reflection-reducing coatings increases scattering. In the best case [Ref. 6]

$$[\mathit{ДД}_6^{-1} + \mathit{ДД}_7^{-1}]^{-1}_{\max} \simeq 10^6. \tag{22}$$

25

Estimate (22) should be taken as the limiting dynamic range of the coherent-optics processor since other factors are subject to greater attenuation. The last three factors (conjugate image, nonlinearity of the space-time light modulator and zero order of diffraction) are completely dictated by the working conditions and the parameters of the space-time light modulator (are not determined by the coherent-optics processor), and are evaluated in a separate paper.

The table summarizes the requirements for parameters of the coherent-optics processor and space-time light modulator, guaranteeing potential accuracy of the ROAR of 1% in a maximum dynamic range of the coherent-optics processor of 60 dB.

Table 1

A) Система допусков КОП произвольной РОАР.

п.п	Искажающий фактор п		Оценка вклада		Требования, ограничения, допуски
			ΔФп, отн.ед	ΔДп, дб	
1	Эффекты зрачка и взаимовлияния ПВМС		1	∞	При наличии КО-компенсации X)
			ΔДкоп≥0,5(ΣΔДп)		КИП ПВМС ≥ 0,5 Y)
2	Аберрации волнового фронта светового пучка		≥0,99	∞	Для длиннофокусных астрономических объективов с Δx/f≤4·10⁻⁴ и ПШП≤10³ z)
3	Деюстировка элементов ОС	продольная F	≥0,999	∞	если любой из элементов ОС установлен с точностью |δz|≤100 мкм 1)
		поперечная G	≥0,999	∞	|δy|≤1 мкм 2)
4	П-некогерентность	считывающего пучка	≥0,999	∞	γ12мин≥0,9995 в пределах ПВМС 3)
5	В-некогерентность	хроматическая аберрация	≥0,999	∞	lк≥0,03 мм (длина когерентности) lк≥1 мм 4)
		дисперсия П-частот	1	≥70	lк≥1,0 мм
6	Переотражения	от оптических поверхностей	1	≥60	коэффициент отражения r≤0,007 и не более чем трёхслойное просветляющее покрытие 5)
7	Рассеяние	света на неоднородностях	1·		радиус корреляции rα≤10 мкм, дисперсия неоднородностей:α≤0,17 6)
8	Двухполосный ввод	А-ПВМС	1	≥70	эквивалентная линза на уровне АР с f₃≤10 см и вспомогательная линза на уровне ПВМС с f₃>f₀≥10/Пf₃ 7)
		Ф-ПВМС			
9	Нелинейность	А-ПВМС	≥0,999	≥70	εmax≤0,45 Ελ/₂ в режиме балансной модуляции света εmax≤1,85 Ελ/₂ Вεmax≤ .
		Ф-ПВМС	≥0,999	≥70	εmax≤0,45 Ελ/₂ без учета нулевого 0,45 Ελ/₂ εmax≤1,34 Ελ/₂ порядка дифракции 7)
10	Нулевой порядок дифракции	А-ПВМС	1	≥70	ΔЗут≥10⁻²(1%) в режиме балансной модуляции света 10)
		Ф-ПВМС	1	=70	ΔЗут=0,34(34%) для редуцированного КОП 11)

FOR OFFICIAL USE ONLY

Key Table 1:

A—System of tolerances of the coherent-optics processor of an arbitrary
    radio-optical antenna array
B—Distorting factor n
C—Pupil effects and mutual interference of space-time light modulator
D—Aberrations of the light wave front
E—Misalignment of elements of the optical system
F—longitudinal
G—transverse
H—Spatial incoherence of the readout beam
I—Time incoherence
J—chromatic aberration
K—dispersion of spatial frequencies
L—Re-reflections from optical surfaces
M—Light scattering on inhomogeneities
N—Two-band input
O—amplitude space-time light modulator
P—phase space-time light modulator
Q—Nonlinearity
R—Zero order of diffraction
S—Estimate of contribution
T—$Д\Phi_n$, relative units
U—$ДД_n$, dB
V—Requirements, limitations, tolerances
W—Dynamic range of coherent-optics processor $\geqslant 0.5[\Sigma ДД_n^{-1}]^{-1}$
X—In the presence of coherent-optics compensation
Y—Coefficient of utilization of the surface of the space-time light
    modulator $\geqslant 0.5$
Z—For long-focus astronomical objectives with $\Delta x/f \leqslant 4 \cdot 10^{-2}$ and $ПШП \leqslant 10^3$
1—If any of the elements of the optical system is set within $|\delta_z| \leqslant 100$ μm
2—$|\delta_y| \leqslant 1$ μm
3—$\gamma_{12мин} \geqslant 0.9995$ within the limits of the space-time light modulator
4—(coherence length)
5—coefficient of reflection $r \leqslant 0.007$, and no more than a three-layer
    reflection-reducing coating
6—Correlation coefficient $r_\alpha \leqslant 10$ μm; dispersion of inhomogeneities $\alpha \leqslant 0.17$
7—equivalent lens on the level of an antenna array with $f_e \leqslant 10$ cm and
    auxiliary lens on the level of a space-time light modulator with
    $f_e > f_0 > 10/11 f_e$
8—In the balanced light modulation mode
9—without consideration of zero order of diffraction
10—Diffraction efficiency of controllable transparency $\geqslant 10^{-2}$ (1%) in
    the mode of balanced light modulation
11—Diffraction efficiency of controllable transparency equal to 0.34 (34%)
    for a reduced coherent-optics processor

27

FOR OFFICIAL USE ONLY

FOR OFFICIAL USE ONLY

REFERENCES

1. A. Yu. Grinev, Ye. N. Voronin, "Antenna Arrays with Signal Process-
   ing by Coherent Optics Methods (Survey)," ZARUBEZHNAYA RADIOELEK-
   TRONIKA, No 9, 1977, p 69.

2. A. Yu. Grinev, Ye. N. Voronin, "Conversion of the Space-Time Spectrum
   by Antenna Arrays with Signal Processing by Coherent Optics Methods,"
   IZVESTIYA VUZov: RADIOELEKTRONIKA, Vol 21, No 2, 1978, p 74.

3. Ye. N. Voronin, A. Yu. Grinev, "Particulars of Conversion of the
   Space-Time Spectrum by Planar Antenna Arrays with Coherent-Optics
   Signal Processing," IZVESTIYA VUZov: RADIOELEKTRONIKA, Vol 22, No 11,
   p 3.

4. A. Yu. Grinev, Ye. N. Voronin, "The Formation of Reception Beams of
   Nonplanar Antennas by Radio-Optical Methods," IZVESTIYA VUZov:
   RADIOELEKTRONIKA, Vol 22, No 2, 1979, p 25.

5. A. Yu. Grinev, Ye. N. Voronin, "Cylindrical Antenna Arrays with
   Coherent-Optics Signal Processing," IZVESTIYA VUZov: RADIOELEKTRONIKA,
   Vol 22, No 5, 1979, p 29.

6. K. Preston, "Kogerentnyye opticheskiye vychislitel'nyye mashiny"
   [Coherent-Optics Computers], Moscow, Mir, 1974.

7. G. S. Kondratenkov, "Obrabotka informatsii kogerentnymi opticheskimi
   sistemami" [Information Processing by Coherent-Optics Systems],
   Moscow, Sovetskoye radio, 1972.

8. A. Yu. Grinev, Ye. N. Voronin, A. P. Kurochkin, "Planar Radio-
   Optical Antenna Arrays" in: "Radiogolografiya i opticheskaya
   obrabotka informatsii v mikrovolnovoy tekhnike" [Radioholography
   and Optical Data Processing in Microwave Equipment], Leningrad,
   Nauka, 1980.

9. A. Yu. Grinev, Ye. N. Voronin, "Nonplanar Antenna Arrays with Forma-
   tion of Reception Beams by Coherent Optics Methods" in: "Radio-
   golografiya i opticheskaya obrabotka informatsii v mikrovolnovoy
   tekhnike," Leningrad, Nauka, 1980.

10. Ya. S. Shifrin, "Voprosy statisticheskoy teorii antenn" [Problems of
    the Statistical Theory of Antennas], Moscow, Sovetskoye radio, 1970.

11. M. Born, E. Vol'f, "Osnovy optiki" [Principles of Optics], Moscow,
    Nauka, 1970.

12. A. Papulis, "Teoriya sistem i preobrazovaniy v optike" [Theory of
    Systems and Transformations in Optics], Moscow, Mir, 1971.

28

FOR OFFICIAL USE ONLY

13. L. M. Soroko, "Osnovy golografii i kogerentnoy optiki" [Principles
    of Holography and Coherent Optics], Moscow, Nauka, 1971.

[184-6610]

6610
CSO: 1860

PARALLEL PENCIL BEAM RECEPTION OF RADIO RADIATION USING CONFORMAL ANTENNA
ARRAYS WITH COHERENT OPTICAL PROCESSING

[Article by D.I. Voskresenskiy, A.Yu. Grinev and Ye.N. Voronin, Moscow
Aviation Institute]

[Text] A coherent optical method of producing the directional
pattern of aplanar receiving antenna arrays is proposed and
analyzed. The maximum capabilities of the method are estimated
and expressions are derived which make it possible to purpose-
fully design coherent optical processors.

Planar receiving antenna arrays (AR) having coherent optical (KO) shaping
of the directional patterns (DN) are known, a review of which is given in
[1]. A coherent optical method of producing the directional pattern of any
aplanar antenna arrays is treated in [2], the realization of which using
spherical optical components is possible only in a few special cases
(cylindrical, piecewise-planar antenna arrays and a few others).

A way of solving a similar problem is proposed below, which is different
from [2] and which is always feasible using spherical optical components,
but its capabilities are limited by the maximally permissible deviation of
the antenna array surface from a planar configuration.

As was shown in [2], parallel viewing of space with a continuous fan of
pencil-beam directional patterns is achieved through processing the signals
received by the antenna array elements, which are arranged on the aplanar
surface $R = R_\perp + n_z Z(R_\perp)$ (Figure 1a) using an algorithm of the form:

$$\hat{L}\{\cdots\} = \iint_\Sigma \cdots J_{opt}(R, K)\, d^2R, \tag{1}$$

where $\{\ldots\}$ are signals of the antenna array elements, Σ is the surface of
the antenna array, $J_{opt}(R, K) = |J_{opt}(R, K)|\exp(iKR)$ is the optimal ampli-
tude-phase distribution (AFR) (for example, in the sense of KU [gain] or
UBL [side lobe suppression]) which shapes the pencil beam reception from

the direction $\quad K = K_{\perp} + n_z \Omega_z (\Omega_z = \sqrt{K^2 - K_{\perp}^2} =$

$= K \cos\theta, \quad K_{\perp} = n_x K \sin\theta \cos\varphi + n_y K \sin\theta \sin\varphi,$

$K = 2\pi/\Lambda$ is the wave number, n_x, n_y and n_z are unit vectors, ϕ is the azimuth and θ is the elevation angle [3]), $d^2 R$ is a surface element.

In the case of a small Z (as compared to the size of the antenna array, see below):

$$| \dot{J}_{opt}(R, K) | \, d^2 R \approx J(R_{\perp}) d^2 R_{\perp}$$

($J(R_{\perp})$ is the AFR of a planar equivalent aperture, $d^2 R_{\perp}$ is an aperture element), i.e., it is permissible to neglect the amplitude distortions of the signals received by the antenna array elements [4]. In this case, we represent (1) in the form:

$$\hat{L} \{\cdots\} = \iint_{-\infty}^{\infty} \cdots J(R_{\perp}) \exp \{- i [K_{\perp} R_{\perp} + \Omega_z Z(R_{\perp})]\} \, d^2 R_{\perp}, \qquad (2)$$

where the infinite limits are taken considering the fact that $J(R_{\perp}) = 0$ outside the array.

For an arbitrary aplanar surface, the realization of operator (2) is impossible with a coherent optical procedure, since $\Omega_z = \sqrt{K^2 - K_{\perp}^2}$. We shall approximate the given function with the following step function:

$$\Omega_z \approx \sum_{n=1}^{N} H_n(K_{\perp}) \sqrt{K^2 - K_{\perp_n}^2}, \qquad (3)$$

where

$$H_n(K_{\perp}) = \begin{cases} 1, & K_{n-1} < | K_{\perp} | \leqslant K_n \\ 0, & \text{в противном случае} \quad \text{otherwise} \end{cases}$$

$$K_{n-1} < | K_{\perp_n} | \leqslant K_n, \ \text{причем} \ \sum_{n=1}^{N} H_n(K_{\perp}) = \begin{cases} 1, & | K_{\perp} | \leqslant K \\ 0, & | K_{\perp} | > K \end{cases}$$
where

Approximation (3) is more precise, the narrower the ring regions H_n are. At the limit ($N \to \infty$) it becomes an equality. Substituting (3) in (2), we find:

$$\hat{L}_N \{\ldots\} = \sum_{n=1}^{N} H_n(K_{\perp}) \hat{F} \{\ldots J(R_{\perp}) \exp [- i \sqrt{K^2 - K_{\perp_n}^2}] Z(R_{\perp}) \}, \qquad (4)$$

where $\quad \hat{F}\{\ldots\} = \iint_{-\infty}^{\infty} \ldots \exp(-i K_{\perp} R_{\perp}) d^2 R_{\perp} \quad$ is a Fourier transform operator.

The operator $\hat{L}_N \to \hat{L}$, when $N \to \infty$, by virtue of the continuity of the nucleus in (2). However, the smaller N is, the simpler it is for the realization of the approximated operator (4) using optical means. We shall establish the requisite number N and construct the coherent optical processor (KOP) corresponding to it, which provide for the specified directional gain of the antenna array throughout the entire viewing range

$$\left(0 \leqslant \theta < \frac{\pi}{2} \ \begin{matrix} \text{или} \\ \text{or} \end{matrix} \ |K_{\perp}| \leqslant \ \leqslant K \right) d_{\min} \leqslant \frac{D}{D_0} \leqslant 1$$

31

(D_0 is the directional gain of the array with processing using algorithm (2)). It can be shown that when K_n is

$$K_n = \sqrt{(2n-1)K\Delta K - \left(\frac{2n-1}{2}\right)^2 (\Delta K)^2}$$

(ΔK is the step of the stepwise approximation (3) defined below), we represent operator (4) in the form:

$$\hat{L}_N\{...\} = H_N(K_\perp)\hat{F}\{...J(R_\perp)\exp\{-i[K-(N-1)\Delta K]\}Z(R_\perp)\} + \qquad (5)$$

$$+\hat{L}_{N-1}\{...\} = H_N(K_\perp)(\hat{L}_0\hat{F}^{-1})^{(N-1)}\hat{L}_1\{...\} + \hat{L}_{N-1}\{...\},$$

где

where $\qquad \hat{L}_0\{...\} = \hat{F}\{...\exp[i\Delta K Z(R_\perp)]\},$

$$\hat{L}_1\{...\} = \hat{F}\{...J(R_\perp)\exp[-iKZ(R_\perp)]\}.$$

The finite step ΔK leads to an error in the AFR, and as a consequence, to a drop in the directional gain which in accordance with [3, 4] and (5) is equal to:

$$\frac{D_N}{D_0} \approx \{1 + [\Omega_z - K + (N-1)\Delta K]^2 \sigma_z^2\}^{-1},$$

$$\qquad (6)$$

where $\qquad \sigma_z^2 = \frac{1}{\Sigma} \iint\limits_{-\infty}^{\infty} |Z(R_\perp)|^2 d^2 R_\perp.$

We define the step $\Delta K = 2\sqrt{\dfrac{d_{min}^{-1}-1}{\sigma_z^2}}.$ from the condition $D_N/D_0 \geq d_{min}$.

A coherent optical processor which realizes algorithm (5) is depicted in Figure 1b. The signals of the antenna array elements (Figure 1a) control the corresponding channels of the multichannel light modulator in the plane Π_1. The coherent optical processor consists of a series of coaxial Fourier processors (according to the number of approximation steps), at the inputs to which (Π_1, Π_2, ...) there are transparencies with the corresponding AFR steps written on them, while at the outputs (Π_1, Π_2, ...) there are filters which realize the unperturbed transfer of the focused images in the hatch marked regions (H_1, H_2,...) to the common output of the coherent optical processor (Π_N). Phase transparencies with a transmittance of $\exp[-iR_0K_\perp]$, for example, can be used as these filters, which shift the Fourier images by $\hat{m}^{-1}R_0$ relative to the axis of the coherent optical processor ($\hat{m}$ is the modeling scale [3]).

We shall establish the requisite number of approximations N, with which the requirements placed on the directional gain are satisfied throughout the entire viewing region $|K_\perp| \leq K_N = K\sin\theta_{max}$ (θ_{max} is the maximum elevation

32
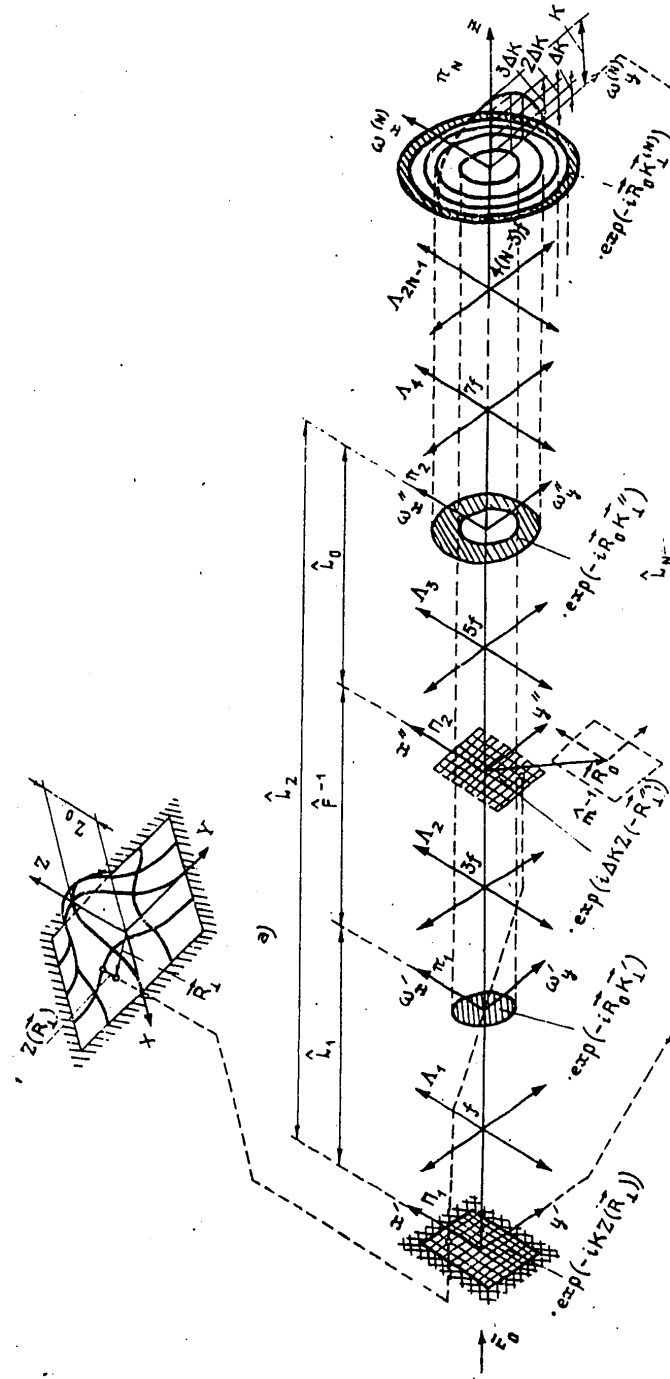
Рис. 1. Неплоская АР (a) и ее когерентно-оптический процессор (б).

Figure 1. The aplanar antenna array (a) and its coherent optical processor (b).

33

angle). We derive the following from the expression for K_n (see above):

$$N = \text{entier} \left[\frac{K \sigma_Z (1 - \cos \theta_{max})}{2 \sqrt{d_{min}^{-1} - 1}} + \frac{1}{2} \right], \tag{7}$$

where entier is the integer part of the number.

The number N, which determines the complexity of the coherent optical processor is limited.

Since the step ΔK should be greater than the width of the directional pattern $\Delta \Omega_X \simeq 2\pi/\Delta X$ (ΔX is the dimension of the antenna array), then:

$$\sigma_Z < \sigma_{Z max} = \frac{\Delta X}{\pi} \sqrt{d_{min}^{-1} - 1}.$$

From this, according to (7):

$$N < N_{max} = \text{entier} \left(\frac{\Delta X}{\Lambda} + \frac{1}{2} \right). \tag{8}$$

The quantity $\sigma_{Z\ max}$ characterizes the extremal root mean square value of the deviation of the aplanar surface of the antenna array from a planar one, permitted by the given method. Assuming $d_{min} = 0.9$, we obtain $\sigma_{Z\ max} = 0.1\ \Delta X$, something which exceeds the possibilities of the method of [3].

In conjunction with [2], the method considered here makes it possible to expand the class of aplanar antenna arrays which permit the production of a fan of pencil beam directional patterns using coherent optical means.

In conclusion, the authors would like to express their gratitude to B.Ye. Kinber for discussing the work.

<div style="text-align:center">BIBLIOGRAPHY</div>

1. A.Yu. Grinev, Ye.N. Voronin, ZARUBEZHNAYA RADIOELEKTRONIKA [FOREIGN RADIOELECTRONICS], No 9, 69, (1977).

2. A.Yu. Grinev, Ye.N. Voronin, IZV. VUZOV - RADIOELEKTRONIKA [PROCEEDINGS OF THE HIGHER EDUCATIONAL INSTITUTES - RADIOELECTRONICS], 22, No 2, 25 (1979).

3. A.Yu. Grinev, Ye.N. Voronin, IZV. VUZOV - RADIOELEKTRONIKA, 21, No 2, 74 (1978).

4. D.I. Voskresenskiy, L.I. Ponomarev, V.S. Filippov, "Vypuklyye skaniruyushchiye antenny" ["Convex Scanning Antennas"], Sovetskoye Radio Publishers, Moscow, 1978.

<div style="text-align:center">34</div>

5. L.D. Bakhrakh, V.A. Makeyev, RADIOTEKHNIKA I RADIOELEKTRONIKA [RADIO ENGINEERING AND RADIOELECTRONICS], 18, No 4, 741, 1973.

8225
CSO: 1860

35

COMMUNICATIONS; COMMUNICATIONS EQUIPMENT INCLUDING
RECEIVERS AND TRANSMITTERS; NETWORKS; RADIO PHYSICS;
DATA TRANSMISSION AND PROCESSING; INFORMATION THEORY

THE BLURRING OF THE MEAN DIFFRACTION PATTERN IN THE FOCAL PLANE OF A
RECEIVING LENS DUE TO RAIN IN A TURBULENT ATMOSPHERE

[Article by V.L. Mironov and S.I. Tuzova, Institute of Atmospheric
Optics of the Siberian Branch of USSR Academy of Sciences]

[Text] An expression is derived for the coherence
function of a plane wave which is scattered several
times in rain. It is shown that the distribution
of the mean intensity in the focal plane of a
receiving lens in the case of small optical thick-
nesses of the rain ($\mu < 1$) is of a two-scale nature.
In this case, the first scale is due to turbulent
fluctuations in the index of refraction., while the
size of the second is determined by the scale of the
diffraction for the dimensions of a drop. Where
$\mu \gg 1$, the characteristic scale of the mean dif-
fraction pattern is the scale of the diffraction
for the coherence radius of a plane wave scattered
at rain particles. The conditions under which it
is possible to determine the parameters of the rain
from measurements of the mean intensity in the focal
plane of the receiving lens are formulated.

A method of determining the structural characteristics of fluctuations
in the reffractive index, C_n^2 and the internal turbulence scale, l_0,
based on measurements of the mean intensity in the focal plane of the
receiving lens when the atmosphere is transilluminated by laser radiation
was proposed in paper [1]. The presence of precipitation in the atmos-
phere leads to a distortion of the mean diffraction pattern because of
additional wave field coherency losses in the case of scattering at
precipitation particles. The question of the nature and magnitude of
this distortion is an open one at the present time, while its solution
is of practical interest. An expression is derived in this paper for
the coherency function of a plane wave which is repeatedly scattered in
rain, and the nature of the blurring of the mean diffraction pattern

36

in the focal plane of the lens is analyzed for the purpose of studying the possibility of determining rain parameters. The combined action of atmospheric turbulence and rain is treated given specific assumptions.

According to [1], the distribution of the average current registered by the instrument,

$$\langle I(y) \rangle = \alpha \int_{-\infty}^{\infty} \langle J(y, z) \rangle dz \qquad \text{has the form:}$$

$$\langle I(y) \rangle = \alpha \Delta \frac{4 R^3 k}{\pi F} \int_0^1 d\eta \, \Gamma_2(L, 2 R \eta)(\arccos \eta -$$

$$- \eta \sqrt{1-\eta^2}) \cos\left(\frac{2 k R}{F} y \eta\right). \tag{1}$$

Here $\langle J(y, z) \rangle$ is the mean intensity in the focal plane of the lens; α is the sensitivity of the photomultiplier, Δ is the width of the receiver slot (the length of the slot along the z coordinate is chosen much greater than the width of the entire diffraction pattern), y is the current coordinate for the position of the slot, R and F are the radius and focal distance of the lens and $k = 2\pi/\lambda$ (λ is the wavelength of the radiation). The function which carries the information on the medium, $\Gamma_2(L, \rho = 2 R \eta) = \langle E(L, \rho_1) E^*(L, \rho_2) \rangle$ is a second order coherency function of a plane wave passing through a layer $0 \leq x \leq L$ with random inhomogeneities (a locally homogeneous and isotropic field), ρ is the spacing between the observation points ρ_1 and ρ_2 in the plane of the lens $x = L$, $E(L, \rho)$ is the optical wave field (depolarization is not taken into account because of its smallness) and the corner brackets indicate averaging over the ensemble.

We shall first derive the expression for the wave field coherency function, where the wave is scattered by rain in the absence of turbulent inhomogeneities, $\Gamma_2^a(L, \rho)$. We shall solve the problem in the phase approximation of [2], i.e., neglecting the amplitude fluctuations of the field. A plane wave $E(x, \rho) = e^{ikx}$, passing through a layer $0 \leq x \leq L$ of large scale, discrete inhomogeneities (ka >> 1, where a is the linear dimension of an inhomogeneity), acquires a random phase shift [3],

$$S(L, \rho) = \sum_{j=1}^{N} S_j(L - x_j, \rho - \rho_j),$$

, where x_j and ρ_j are the longitudinal and transverse directions of wave propagation of the coordinate for the position of the center of the j-th particle. Here, repeat scattering at an aggregate of N particles is taken into account approximately by summing the independent phase shifts $S_a(L - x_a, \rho - \rho_a)$ at the individual scatterers, something which is justified, as was shown in [3], for optical thicknesses of $\mu << 1/\langle\theta_0^2\rangle$, where $\langle\theta_0^2\rangle \simeq (ka)^{-2}$ is the mean square of the scattering angle of a particle. For a medium consisting of a large number of statically independent scatterers, the random positions of the particles $r_a = (x_a, \rho_a)$ are uniformly distributed in the scattering volume V_{pac} with a probability density of $P(x_a, \rho_a) = 1/V_{pac}$,

37

while the number of them, N, has a Poisson distribution $P(N) = e^{-<N>}$
$= e^{-<N>}<N>^N/N!$ with a mean value of $<N>$ [4]. Then the phase $S(L, \rho) =$
$= \sum_{j=1}^{N} S_j(L - x_j, \rho - \rho_j)$ is a Poisson random process [5]. Performing the
averaging in a manner similar to [5], we derive the expression for $\Gamma_2^a(L,\rho)$
in the   following form:

$$\Gamma_2^a(L, \rho_1, \rho_2) = \langle \exp \{ i [S(L, \rho_1) - S(L, \rho_2)] \} \rangle =$$

$$= \exp \left\{ n_0 \int_0^L dx_a \iint d\rho_a \int_0^\infty dan(a) [\exp \{ i [S_a(L - x_a, \rho_1 - \rho_a) - \quad (2) \right.$$

$$\left. - S_a(L - x_a, \rho_2 - \rho_a)] \} - 1] \right\}.$$

Where $n_0 = <N>/V_{pac}$ is the average particle concentration along the path
and $n(a)$ is the particle distribution with respect to size. Thus, the
problem is reduced to determination of the phase $S_a(L - x_a, \rho - \rho_a)$ of the
wave scattered by a single droplet. When a plane wave is scattered at an
isolated inhomogeneity, the field $E_a(L, \rho) = \exp[ikL + iS_a(L - x_a, \rho - \rho_a)]$
in the wave zone of a particle has the form: [6]:

$$E_a(L, \rho) = e^{ikL} + e^{ikx_a} f\left[\frac{k}{k}, k\frac{(r - r_a)}{|r - r_a|}\right] \frac{e^{ik|r-r_a|}}{|r - r_a|}. \quad (3)$$

for $ka \gg 1$ (a is the radius of a drop), the amplitude of the scattering
$f\left[\frac{k}{k}, k\frac{(r - r_a)}{|r - r_a|}\right]$ for small angles in the case of Fraunhofer diffraction
is equal to [6]:

$$f\left[\frac{k}{k}, k\frac{(r - r_a)}{|r - r_a|}\right] = ika^2 J_1\left(ka\frac{|\rho - \rho_a|}{L - x_a}\right) \Big/ \left(ka\frac{|\rho - \rho_a|}{L - x_a}\right),$$

where $J_1(t)$ is a Bessel function. Considering the small angle nature of
the scattering, and using in (3) the expansion of [12] $|r - r_a| \approx L - x_a +$
$+ \frac{1}{2}(\rho - \rho_a)^2/(L - x_a)$,   we obtain:

$$S_a(L - x_a, \rho - \rho_a) = \text{arctg}\frac{\Omega_a \cos u J_1(t)/t}{1 - \Omega_a \sin u J_1(t)/t},$$

where $\Omega_a = ka^2/2(L - x_a)$, $u = k(\rho - \rho_a)^2/2(L - x_a)$, $t = ka|\rho - \rho_a|/(L - x_a)$.

Since in the wave zone, $\Omega_a \ll 1$, the expression for the phase assumes the
form:

$$S_a(L - x_a, \rho - \rho_a) = \Omega_a \frac{J_1(t)}{t} \cos u. \quad (4)$$

In the following we shall utilize the approximation of the function
$2J_1(t)/t \approx \exp(-t^2/8)$ [7], which is a good description of the main
maximum of the scattering amplitude. Since $S_a(L - x_a, \rho - \rho_a) \ll 1$,
then the exponent under the integral sign in (2) can be expanded in a
series limited by second order smallness terms. Then:

38

$$\Gamma_2^a(L, \rho_1, \rho_2) = \exp\left[i \langle S(L, \rho_1) \rangle - i \langle S(L, \rho_2) \rangle - \right. \tag{5}$$

$$\left. -\frac{1}{2} \langle S^2(L, \rho_1) \rangle - \frac{1}{2} \langle S^2(L, \rho_2) \rangle + \langle S(L, \rho_1) S(L, \rho_2) \rangle \right],$$

$$\tag{5}$$

$$\langle S(L, \rho_1) \rangle = n_0 \int_0^L dx_a \iint d\rho_a \int_0^\infty da\, n(a) S_a(L - x_a, \rho_1 - \rho_a) =$$

$$= \langle S(L, \rho_2) \rangle,$$

$$\langle S^2(L, \rho_1) \rangle = n_0 \int_0^L dx_a \iint d\rho_a \int_0^\infty da\, n(a) S_a^2(L - x_a, \rho_1 - \rho_a) = \langle S^2(L, \rho_2) \rangle,$$

$$\langle S(L, \rho_1) S(L, \rho_2) \rangle = n_0 \int_0^L dx_a \iint d\rho_a \int_0^\infty da\, n(a) S_a(L - x_a, \rho_1 - \rho_a) \times$$

$$\times S_a(L - x_a, \rho_2 - \rho_a).$$

Thus, the expression derived for the field coherency function
$$\Gamma_2^a(L, \rho_1, \rho_2) = \exp\left\{ -\frac{1}{2} \left\langle \left[S(L, \rho_1) - S(L, \rho_2) \right]^2 \right\rangle \right\}$$ corresponds to
the case of a normal distribution of the phase S [5]. We will note
that the possibility of going over to a normal phase statistic in the
case of small mean square phase shifts at one inhomogeneity $(\langle S_a^2 \rangle)^{1/2} \ll 1$
was demonstrated in paper [8] using a geometric-optic representation of
the phase. In our case $(\langle S_a^2 \rangle)^{1/2} \simeq \Omega_0^2/4$ $(1 - L_0/L) \ll \Omega_0 \ll 1$, since
the linear dimension of the scattering layer satisfies the condition for
scattering in the wave zone $ka^2/L - L_0) \ll 1$ and $\Omega_0 = ka^2/L \ll 1$. As
w s shown in [9], for paths with a length of $L \gg ka^2$, the contribution
to $\Gamma_2^a(L, \rho)$ of the path section $L - ka^2 \ll x \leq L$, where the approximation
of geometric optics is applicable, as well as the contribution of the
intermediate Fresnel diffraction region can be neglected. Using formulas
(4) and (5), following some simple computations with a precision of down
to the small terms on the order of Ω_0, we obtain the following expressions
for the dispersion and the correlation function of the phase fluctuations
of a plane wave:

$$\langle S^2 \rangle = \int_0^\infty da\, n(a) \frac{1}{2} n_0 \pi a^2 L, \quad \langle S(L, \rho_1) S(L, \rho_2) \rangle = \int_0^\infty da\, n(a) \frac{1}{2} n_0 \pi a^2 L \exp\left(-\frac{\rho^2}{a^2} \right).$$

Then $\Gamma_2^a(L, \rho)$ is written in the form:

39

$$\Gamma_2^a (L, \rho) = \exp \left[-\frac{1}{2} D_s^a (\rho) \right], \tag{6}$$

where $D_s^a(\rho) = \dfrac{\langle [S(L, \rho_1) - S(L, \rho_2)]^2 \rangle = \int\limits_0^\infty dan_1^t(a) \mu [1 - \exp(-\rho^2/a^2)]}{}$ is the

structural function of the fluctuations of the phase of a plane wave scattered in rain. The quantity $\mu = n_0 \pi a^2 L$ has the sense of the optical thickness which determines the attenuation of the average field $\langle u \rangle \sim \exp(-\mu)$ [4].

The question of the influence of precipitation on the turbulence mode of the atmosphere has been inadequately studied at the present time. At the same time, existing experimental literature [10, 11] point towards the necessity of taking into account the joint action of turbulence and rain in certain meteorological situations. For this reason, the attempt undertaken in this paper to approximately account for the contribution of turbulent fluctuations in the refractive index to the function being studied <I(y)> is justified at least for preliminary estimates. In following [12], we assume that the fluctuations of the wave field which are caused by rain and turbulence are not correlated. In this approximation, the coherency function Γ_2 (L, ρ), of the wave field which has experienced the combined action of turbulence and rain is equal to:

$$\Gamma_2 (L, \rho) = \Gamma_2^a (L, \rho) \Gamma_2^\tau (L, \rho), \tag{7}$$

where Γ_2^τ (L, ρ) is the coherency function of the wave scattered by turbulent inhomogeneities. The expression for Γ_2^τ(L, ρ) derived in [13] has the form:

$$\Gamma_2^\tau (L, \rho) = \exp \left[-\frac{1}{2} D_1 (\rho) \right], \tag{8}$$

where $D_1 (\rho) = 2.91 \, C_n^2 \, k^2 L \, \rho^{5/3}$ is the structural function of the fluctuations in the plane wave phase. We presuppose here that the spectrum of fluctuations in the index of refraction in a turbulent atmosphere with rain remains a Kolmogorov spectrum. Based on formulas (1) and (6)–(8), we shall analyze the nature of the washing out of the mean diffraction pattern separately for small and large optical thicknesses μ.

1. Small Optical Thicknesses ($\mu < 1$)

For simplicity, we shall consider the case of monodisperse rain with a drop radius equal to a. The results of a numerical calculation of the normalized function V(ρ) = <I(ρ)>/<I(0)> (ρ = 2kRy/F) are shown in Figures 1a and 1b for three values of C_n^2 as a function of the quantity μ, which is related to the intensity of the rain $\overline{J}$ by the expression $\mu = 0.21 \, (\overline{J})^{0.74} L$ [14]. It can be seen from the curves that the

40

distribution of the mean intensity in the focal plane of the lens is of a two-scale nature. Without considering the turbulent inhomogeneities $(C_n^2 = 0$, Figure 1a), the first-scale y_1 is the scale for the diffraction at a lens size $y_1 = 2F/kR$. The size of the second scale y_2 is determined from the asymptotic formula ($\mu \ll 1$):

$$V(y) \approx \mu \frac{\sqrt{\pi}}{4} \frac{\bar{a}}{R} \exp\left[-\frac{y^2}{(2F/k\bar{a})^2}\right] \qquad (y \gg y_1, \bar{a} \ll R) \qquad (9)$$

as the scale of the diffraction for a drop size $y_2 = 2F/k\bar{a}$. (The asymptote $\log V(\rho)$ for $\mu = 0.62$, which is plotted in FIgure 1a with the dashed line, is in good agreement with the calculated curve). As follows from the graphs, with an increase in μ, y_2 also increases, something which is due to the reduction in the coherency radius of the field ρ_k. The quantity $V(y)$ likewise increases the region $y > y_1$ in this case, something which signifies a redistribution of the mean intensity in the focal plane of the lens between the regions $y < y_1$ and $y > y_1$. Taking turbulent inhomogeneities into account, where the coherency radius of a plane wave due to turbulence, [13], is $\rho_0 = (1.46C_n^2k^2L)^{-3/5} \ll R$, the asymptotic expression for the function $V(y)$, derived from (1) and (6)-(8) where $\mu \ll 1$, has the following form:

$$V(y) \approx \left[1 + \frac{\mu}{2}\left(1 + \frac{\rho_0^2}{\bar{a}^2}\right)^{-1/2}\right]^{-1} \left\{\exp\left[-y^2\left(\frac{k\rho_0}{2F}\right)^2\right] + \right.$$
$$\left. + \frac{\mu}{2}\left(1 + \frac{\rho_0^2}{\bar{a}^2}\right)^{-1/2}\right] \exp\left[-\frac{y^2}{(2F/k\rho_0)^2 + (2F/k\bar{a})^2}\right]\right\} \qquad (10)$$
$$(\bar{a} \ll R, \rho_0 \ll R).$$

A square-law approximation of the function $D_1(\rho)$, equivalent to the substitution of $\exp(-\alpha\rho^{5/3}) \to \exp(-\alpha^{6/5}\rho^2)$, was used in the derivation of (10) [7]. In the region $y > y_1$, where the approximation error becomes significant, the contribution of the function $\Gamma_2^T(L, \rho)$ to $V(y)$ proves to be neglectably small as compared to the contribution of the function $\Gamma_2^a(L, \rho)$. For $\bar{a} \ll \rho_0$, there is a clear division of the diffraction pattern into two characteristics sections, where the first scale, which is defined by the drop in $V(y)$ by $1/e$, is $y_1' = 2F/k\rho_0$. (This fact points to the possibility of determining C_n^2 in rain, within the framework of the indicated assumptions, in a manner similar to that for the absence of rain [1]). In the region $y > y_1'$ the asymptote of (10) assumes the form:

$$V(y) \approx \frac{\mu}{2} \frac{\bar{a}}{\rho_0} \exp\left[-\frac{y^2}{(2F/k\bar{a})^2}\right] \qquad (\bar{a} \ll \rho_0 < R), \qquad (11)$$

i.e., the second scale, just as in the case of $C_n^2 = 0$, is defined as $y_2 = 2F/k\bar{a}$. A comparison of the calculated curve (Figure 1b) with the asymptote of (11) shows good agreement when $\mu = 0.62$. We will note that the
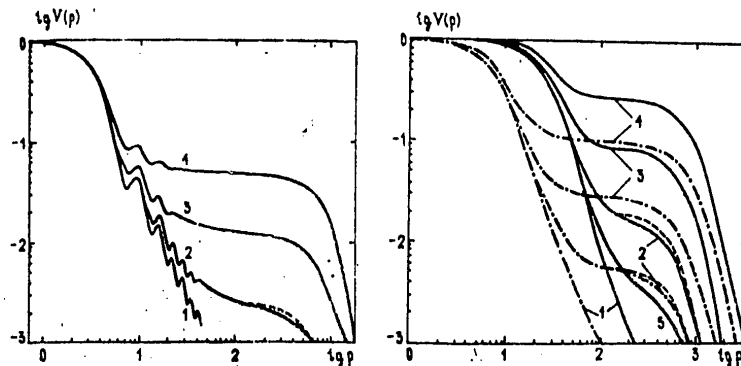
Figure 1. The function $V = <I(p)>/<I(0)>$ as a function of the generalized parameter $p = 2kRy/F$.

Key: 1. $-\mu = 0$ $(\overline{J} = 0)$; 2. $-\mu = 0.62$ $(\overline{J} = 3$ mm/hr$)$; 3. $-\mu = 2.38$ $(\overline{J} = 10$ mm/hr$)$; 4. $-\mu = 5$ $(\overline{J} = 50$ mm/hr$)$; 5. $- = 0.27$ $(\overline{J} = 1$ mm/hr$)$;

a) $C_n^2 = 0$ (the dashed curve is the asymptote of (9) when $\mu = 0.62$);

b) $C_n^2 = 5 \cdot 10^{-17}$ cm$^{-2/3}$ (the dashed and dotted curves) and

$C_n^2 = 5 \cdot 10^{16}$ cm$^{-2/3}$ (the solid curves), the dashed curves

are the asymptote of (11) when $\mu = 0.62$ $(L = 1,300$ m,

$\lambda = 0.63 \cdot 10^{-6}$ m, $R = 8 \cdot 10^{-2}$ m, $F = 1.6$ m, $\overline{a} = 5 \cdot 10^{-4}$ m).

conclusion concerning the division between the turbulent and hydrosol components was drawn for the first time [10] because of the considerable difference in their characteristic scales, and thereafter in 11] using the example of the frequency spectra of the intensity fluctuations.

Thus, for $\mu < 1$, based on the drop in the function being measured, $V(y)$ to the 1/e level in the region $y \gg y_1$, y_1', it is possible to determine the mean radius $\overline{a}$ of the droplets, and based on the quantity $V(y)$, the values of μ and consequently the mean intensity of the rain $\overline{J}$ in the region $y_1 \ll y \ll y_2$. The calculated curves shown in Figure 2 for various values of μ and typical values of $\overline{a}$ indicate the considerable dependence of $V(y)$ on the parameters of the rain being sought. The practicability of measurements of the light flux, which amounts to 10^{-3} times its value in the center of the diffraction pattern, was demonstrated in paper [15].
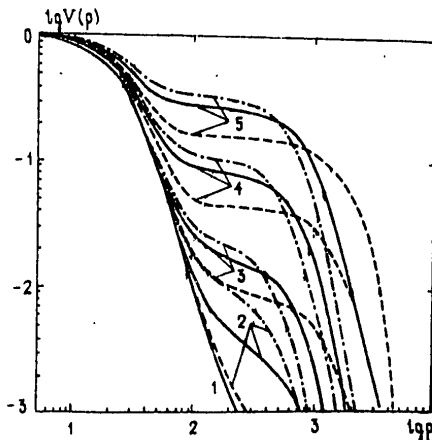
Figure 2.

Key: $c_n^2 = 5 \cdot 10^{-16} \, cm^{-2/3}$; 1. $-\mu = 0$; 2. $-\mu = 0.27$; 3. $-\mu = 0.62$
4. $-\mu = 2.38$; 5. $-\mu = 5$;

The solid curve is for $-\overline{a} = 5 \cdot 10^{-4}$ m; the dashed curve is for
$-\overline{a} = 2.5 \cdot 10^{-4}$ m; the dashed-and-dotted curve is for $-\overline{a} = 7 \cdot 10^{-4}$ m.
($L = 1,300$ m; $\lambda = 0.63 \cdot 10^{-6}$ m; $R = 8 \cdot 10^{-2}$ m; $F = 1.6$ m).

2. Large Optical Thicknesses ($\mu \gg 1$)

Based on the decline of the function $\Gamma_2^a(L, \rho)$ to the $1/e$ level, we shall
determine the coherency radius ρ_k of a plane wave scattered in rain, where
$\mu \gg 1$. For monodisperse particles, we find by working from (6) that $\rho_k = (2/\pi n_0 L)^{1/2} < \overline{a}$. As follows from formulas (1) and (6) - (8), when $\overline{a} \ll \rho_0$ (something which is practically always observed in the atmosphere),
the influence of turbulence on the function $\langle I(y)\rangle$ can be disregarded.
When $\mu \gg 1$, the determining factor in (1) is the region $\eta \lesssim \overline{a}/2R \ll 1$,
so that the asymptotic formula for $\langle I(y)\rangle$ is written in the form:

$$\langle I(y)\rangle \approx \alpha\Delta \frac{2R^3k}{F} \int\limits_0^\infty d\eta \exp\left[-\frac{1}{2}\int\limits_0^\infty da\, n(a)\,\mu\left(\frac{2R\eta}{a}\right)^2\right] \times$$

$$\times \cos\left(\frac{2kR}{F}\eta y\right).$$

From this we derive a simple expression for the normalized spectrum of the
coherency function:

$$V(y) = \exp\left[-\frac{y^2}{(2F/k\rho_k)^2}\right] \qquad (\mu \gg 1).$$

(12)

43
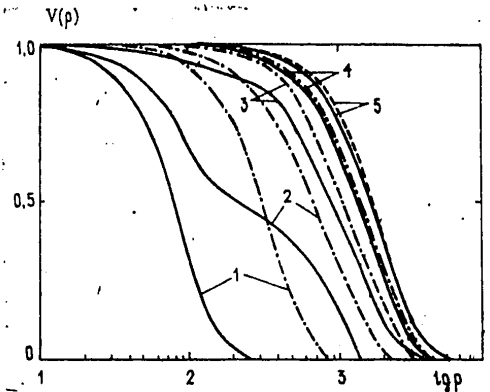
Figure 3.

Key: The solid curves for $C_n^2 = 5 \cdot 10^{-16}$ $cm^{-2/3}$; the dashed-and-dotted curves are for $C_n^2 = 5 \cdot 10^{-15}$ $cm^{-2/3}$;

1. $-\mu = 0$; 2. $-\mu = 5$; 3. $-\mu = 10$; 4. $-\mu = 15$; 5. $-\mu = 20$;

The dotted curve is the asymptote of (12) when $\mu = 20$ ($L = 10$ km;

$\lambda = 0.63 \cdot 10^{-6}$ m; $R = 8 \cdot 10^{-2}$ m; $F = 1.6$ m; $\overline{a} = 5 \cdot 10^{-4}$ m).

Graphs of the function $V(p)$ are shown in Figure 3 for two values of C_n^2 and various values of μ. A comparison of the asymptote (12) with the calculated curves shows that the asymptotic expression (12) yields good results even for $\mu = 20$. Consequently, for $\mu \gtrsim 20$, the mean concentration of particles along the path in rain, n_0, can be uniquely determined from measurements of the half-width y_0 of the spectrum of $V(y)$ [9]. (We will note that the size of the particles plays no role here).

Thus, the analysis performed here shows that in the case of small optical thickness of the rain ($\mu < 1$), because of the separation of the turbulence and hydrosol contributions to the mean diffraction pattern, it is possible to determine the size $\overline{a}$ of the droplets and the intensity of the rain $\overline{J}$. When $\mu \gg 1$, where the influence of turbulence can be neglected, and the spectral width of the coherency function is determined by the scale of the diffraction at the coherency radius of the plane wave scattered in rain, it is possible to determine the average concentration of rain particles along the path n_0.

BIBLIOGRAPHY

1. A.V. Artem'yev, A.S. Gurvich, IZV. VUZOV – RADIOFIZIKA [PROCEEDINGS OF THE HIGHER EDUCATIONAL INSTITUTES – RADIOPHYSICS], 14, No 5, 734 (1971).

2. V.A. Banakh, V.L. Mironov, OPT. LETT., 1, No 5, 172 (1977).

3. N.P. Kalashnikov, M.I. Ryazanov, ZhETF [JOURNAL OF EXPERIMENTAL AND THEORETICAL PHYSICS], 50, No 2, 459 (1966).

4. A.G. Borovoy, M.V. Kabanov, V.A. Saveliev, APPL. OPT., 14, No 11, 2731 (1975).

5. V.I. Klyatskin, "Statisticheskoye opisaniye dinamicheskikh sistem s fluktuiruyushchimi parametrami" ["The Statistical Description of Dynamic Systems with Fluctuating Parameters"], Nauka Publishers, Moscow, 1975.

6. N'yuton, R., "Teoriya rasseyaniya voln i chastits" ["Wave and Particle Scattering Theory"], Mir Publishers, Moscow, 1969.

7. A.S. Gurvich, A.I. Kon, V.L. Mironov, S.S. Khmelevtsov, "Lazernoye izlucheniye v turbulentnoy atmosfere" ["Laser Radiation in a Turbulent Atmosphere"], edited by V.I. Tatarskiy, Nauka Publishers, Moscow, 1976.

8. L.M. Yerukhimov, P.I. Shpiro, IZV. VUZOV – RADIOFIZIKA, 17, No 6, 879 (1974).

9. V.L. Mironov, S.I. Tuzova, "V Vsesoyuznyy simpozium po lazernomu i akusticheskomu zondirovaniyu atmosfery. Tezisy dokladov" ["The Fifth All-Union Symposium on Laser and Acoustic Sounding of the Atmosphere. Abstracts of Reports"], Tomsk, 1978.

10. A.S. Gurvich, V.V. Pokasov, FIZIKA ATMOSFERY I OKEANA [PHYSICS OF THE ATMOSPHERE AND OCEAN], 8, No 8, 878 (1972).

11. N.V. Galakhov, A.V. Yefremov, A.F. Zhukov, V.V. Reyno, R.Sh. Tsvyk, FIZIKA ATMOSFERY I OKEANA, 12, No 12, 1251 (1976).

12. Ting-i Wang, S.F. Clifford, J. OPT. SOC. AM., 65, No 8, 927 (1975).

13. V.I. Tatarskiy, "Rasprostraneniye korotkikh voln v srede so sluchaynymi neodnorodnostyami v priblizhenii markovskogo sluchaynogo protsessa" [The Propagation of Short Waves in a Medium with Random Inhomogeneities in an Approximation of a Markov Random Process"], Preprint, Department of Oceanology, Atmospheric Physics and Geography of the USSR Academy of Sciences, Moscow, 1970.

14. O.D. Barteneva, Ye.N. Dovgyallo, Ye.A. Polyakova, TRUDY GLAVNOY GEOFIZICHESKOY OBSERVATORII IMENI A.I. VOYEYKOVA [PROCEEDINGS OF THE MAIN GEOPHYSICAL OBSERVATORY imeni A.I. VOYEYKOV], No 220, Leningrad, Gidrometeoizdat, 1967.

15. V.A. Banakh, V.V. Boronoyev, N.Ts. Gomboyev, E.V. Zubritskiy, V.L. Mironov, Ch.Ts. Tsydypov, in the collection "Rasprostraneniye opticheskikh voln v sluchayno-neodnorodnoy atmosfere" ["The Propagation of Optical Waves in a Randomly Inhomogeneous Atmosphere"], Nauka Publishers, Novosibirsk, 1979.

8225
CSO: 1860

DIGITAL DEVICES USING INTEGRATED CIRCUITS IN COMMUNICATIONS ENGINEERING

[Text] The fundamentals of the theory of the synthesis of combination devices and finite automats are presented. Methods of realizing digital filters and systems for the automatic tuning of tuned circuits are given special treatment. A number of digital devices used for control and communications are described.

The book is intended for engineering and technical workers interested in questions of the design and practical use of modern digital devices using integrated logic circuits.

Table of Contents

FOR OFFICIAL USE ONLY

8225
CSO: 1860

FOR OFFICIAL USE ONLY

UDC 621.373.826:621.39

THE USE OF LASERS FOR OPERATIONAL COMMUNICATIONS WITH INDUSTRIAL UNITS

Moscow LAZERNAYA OPERATIVNAYA SVYAZ' S PROMYSHLENNYMI OB'YEKTAMI in Russian
1979 signed to press 5 Jul 79 pp 1-3, 104

[Annotation, Foreword, and Table of Contents from the book by Vitold'
Trofimorovich Zagorodnyuk and Dmitriy Yakovlevich Parshin, Izd. "Svyaz',"
1979, 4000 copies, 104 pages]

/Text7 The book examines the construction principles of laser systems for op-
erational communications with industrial units, and describes the basic ele-
ments of the transmitting and receiving equipment involved; a method is given
for the engineering design of these systems.

The book is intended for communications engineers, radio engineers, and speci-
alists in problems of communications with industrial units.

FOREWORD

The current state of development of the national economy poses a problem in re-
gard to the creation of systems for the operational control of industrial-tech-
nological processes. The performance effectiveness of technological processes
in various industrial sectors is determined in large part by the capabilities
of the communications system--operator to industrial unit. This substantiates
the advisability of creating wireless, small-scale, reliable, and convenient
systems for transmitting information.

Crowding of the radio-frequency spectrum, mutual interference, and other tech-
nical causes are leading to exploration and investigation of new channels for
the transmission of operational information. The use of laser radiation for
these purposes is highly promising. At the present time, work is being con-
ducted both in the USSR and abroad on the creation of optical systems of oper-
ational communications in which laser radiation will be employed for the trans-
mission of information. The systems so far developed possess a number of ad-
vantages over those presently employed. There are currently works in publica-
tion which deal with laser communications theory, but the absence of systema-
tized material reflecting the specific nature of laser systems for operational
communication with industrial units impedes the development of such systems.

50

FOR OFFICIAL USE ONLY

FOR OFFICIAL USE ONLY

The book sets forth fundamental problems related to the development of equipment and systems in which laser radiation is employed as a communications channel for the transmission of operational information. It systematizes material on laser channel communication and offers basic recommendations for the selection and construction of systems and their primary elements. The book details for the first time a method for engineering design of laser systems for operational communication with industrial units.

The book is intended for communications engineers and electronics engineers specializing in the design of laser communication systems and the management of industrial units.

The authors express their thanks to V.P. Petrukhin, Candidate in Technical Sciences, who aided in the writing of sections 1.1, 2.2, 3.2-3.4, and to A.G. Muradyan, Candidate of Technical Sciences, for his painstaking review of the manuscript and critical commentary which facilitated improvement of the book.

Comments concerning the book should be sent to this address: Moscow, 101000, Chistoprudnyy Bul'var, 2.

TABLE OF CONTENTS

FOR OFFICIAL USE ONLY

UDC 621.396.61:621.3.029.6(075)

THE DESIGN OF MICROWAVE RADIO TRANSMITTING DEVICES

Moscow PROYEKTIROVANAIYE RADIOPEREDAYUSHCHIKH USTROYSTV SVCH in Russian
1979 signed to press 2 Oct 79

[Annotation and table of contents from the book edited by G.M. Utkin,
Sovetskoye Radio Publishers, Moscow, 320 pages, 19,000 copies]

[Text] The major questions in the design of decimeter and centimeter
wavelength transmitting devices using semiconductor devices and metal-
ceramic vacuum tubes are treated. Engineering methods of designing
transmitter stages are given, including power amplifiers, frequency
multipliers, and exciters with improved frequency stability. The design
methods are illustrated by specific examples.

The textbook is intended for students in the radio engineering specialties
of the higher educational institutes. It can also be useful to special-
ists engaged in the design of radio engineering equipment.

Table of Contents

53

56

A TRANSMITTING ACCESSORY FOR THE R-250M2

Moscow RADIO in Russian No 2, 1980 pp 19-22

[Conclusion of article by Ye. Sukhoverkhov, Moscow, amateur call letters UA3AJT; first part of article published in RADIO, No 1, 1980, p 19]

[Text] An external view of the accessory is shown in Figure 3. With the exception of block 10, the RF units are structurally mounted on one printed circuit board made of foil covered glass textolite [laminated resin on a glass fabric base] 3 mm thick. The layout of the components on it is shown in Figure 4 (the circuit board is arbitrarily broken down into two sections). The bandswitch wafers and the crystals are mounted on the circuit board by means of posts or corner braces. The layout of the printed circuit board (distinguished by the color), the output stage and the power supply unit inside the accessory housing are shown in Figure 5.
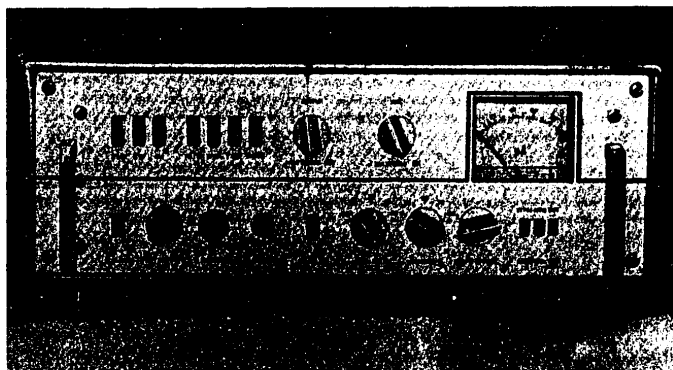
Figure 3.

The partition shields between the units are made of strips of double-sided foil covered glass textolite 1.5 mm thick and 40 to 45 mm high. Those forming the grid are installed after the installation of all components on

57

FOR OFFICIAL USE ONLY

Table 2

Катушка (1)	Число витков (2)	Провод (3)	Диаметр каркаса, мм (4)	Длина намот-ки, мм (5)	Зазор между обмотками на общем карка-се, мм (6)
1L1—1L3	18	ПЭШО 0,31	9	—	—
3L1	3000	ПЭЛ 0,06	5	—	—
5L1—5L3	16	ПЭШО 0,31	9	—	—
7L1, 7L2	7	ПЭШО 0,44	9	4	5
7L3, 7L4	8	ПЭШО 0,44	9	5	5
7L5, 7L6	11	ПЭШО 0,31	9	5	5
7L7, 7L8	18	ПЭШО 0,31	9	7	5
7L9, 7L10	30	ПЭШО 0,31	9	12	1
8L1	11	ПЭШО 0,44	9	—	—
8L2	17	ПЭШО 0,31	9	—	—
8L3	30	ПЭШО 0,31	9	—	—
8L4	25	ПЭШО 0,31	9	—	—
9L3	10	ПЭШО 0,44	9	6	—
9L4	12	ПЭШО 0,44	9	7	—
9L5	14	ПЭШО 0,31	9	6	—
9L6	17	ПЭШО 0,31	9	7	—
9L7	30	ПЭШО 0,31	9	12	—
10L1, 10L2	8	ПЭВ-2 1,0	(МЛТ-2)	—	—
10L3	9	ПЭВ-2 1,5	12	15	—
10L4	4+7*	ПЭВ-2 1,0	18	20	—
10L5	9+13*	ПЭВ-2 0,8	30	24	—

Key: 1. Coil;
2. Number of turns;
3. Wire;
4. Coil form diameter, mm;
5. Length of the winding;
6. Gap between the windings on the common coil form, mm;

* Figured from the "hot" end of the coil.

the circuit board and are soldered to the circuit board using copper pins. The only thing to keep in mind is the fact that the grid should not make contact with the "grounded" areas of the units. It is connected to the chassis at only one point. The partitions should be provided with holes for the shaft of the bandswitch and the electromechanical filter. The shields for the filters can be fabricated in a similar manner. The block of variable capacitors is placed alongside the filter of the second mixer and is well shielded.

The connection of the "grounded" areas of the units to each other is not shown in Figure 4. In principle, they can be connected together by jumpers in an arbitrary fashion, but during operation as an exciter, it can prove useful to pick a ground point in each of the units of the accessory.

The hookup schematic of the low frequency units is not shown. The circuit board, with dimensions of 200 x 40 mm having these units, is shielded and positioned on the left front panel of the accessory.

The winding data for the inductance coils is given in Table 2. It is desireable to wind the coils in the bandpass filters on toroidal cores made of 30 VCh or 50 VCh ferrite. In this case, the transmission factor of the filters will increase.

58

FOR OFFICIAL USE ONLY
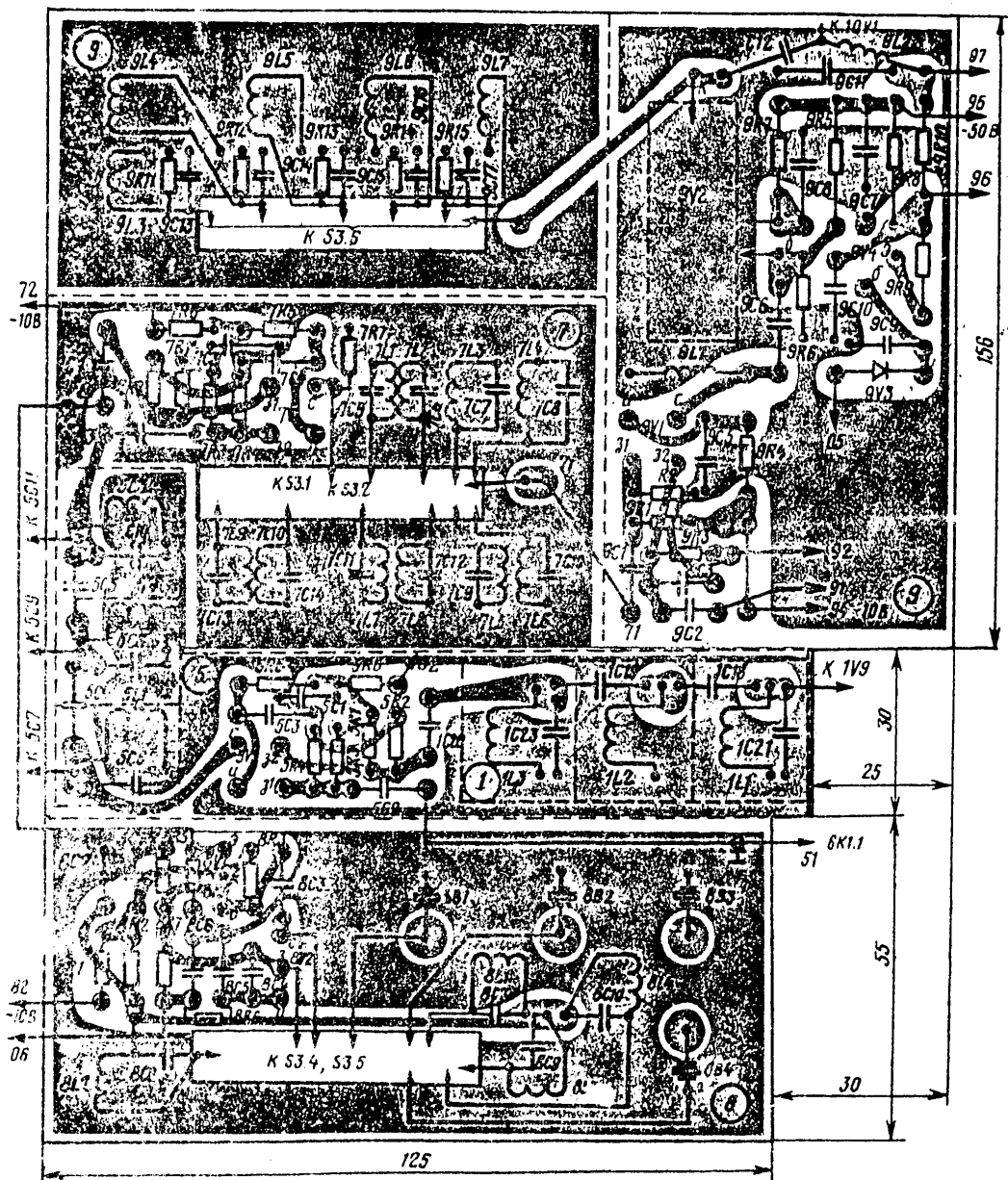
Figure 4 [First half]

59

FOR OFFICIAL USE ONLY
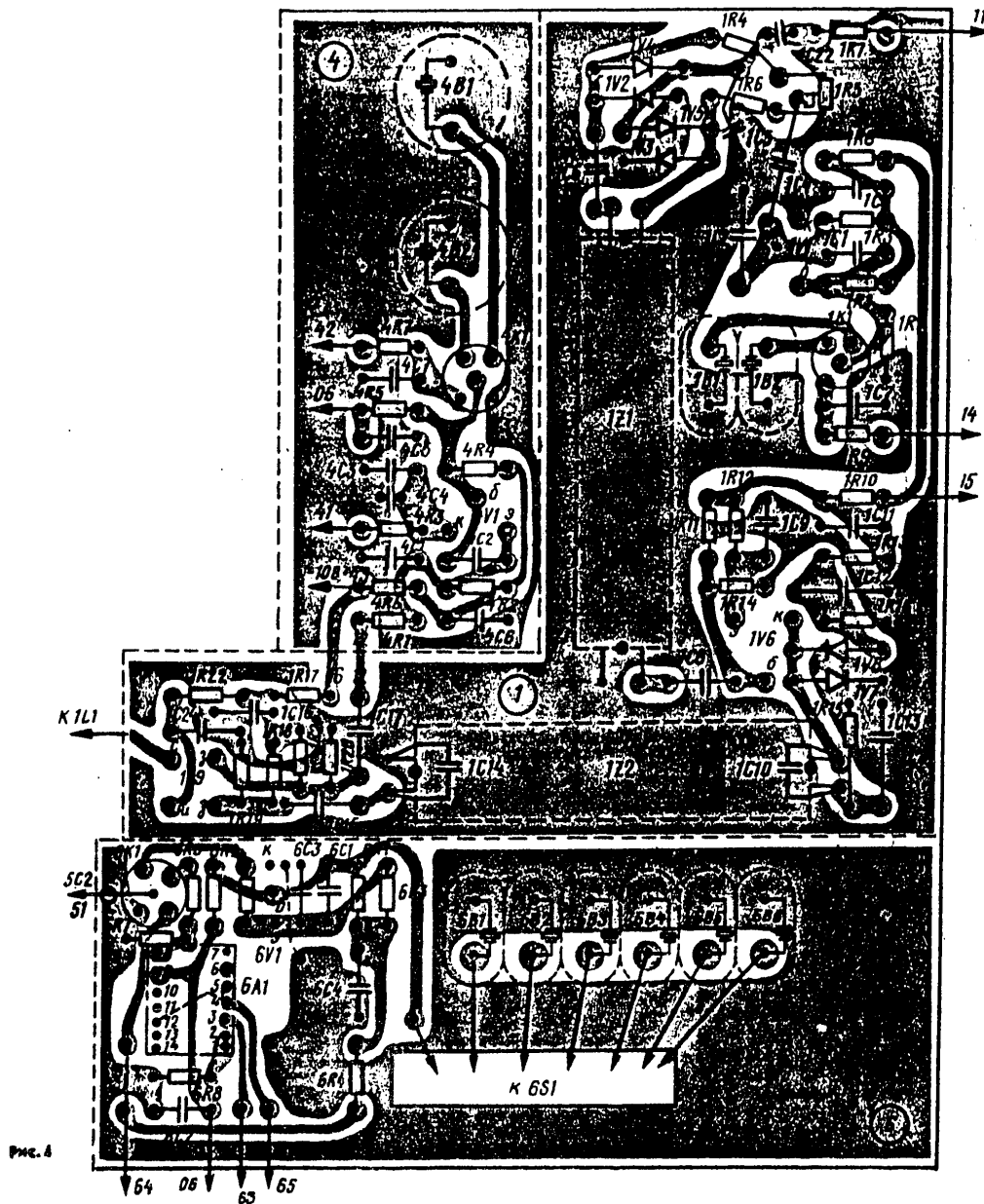
Figure 4 [Continued from preceding page].

60

Рис. 5
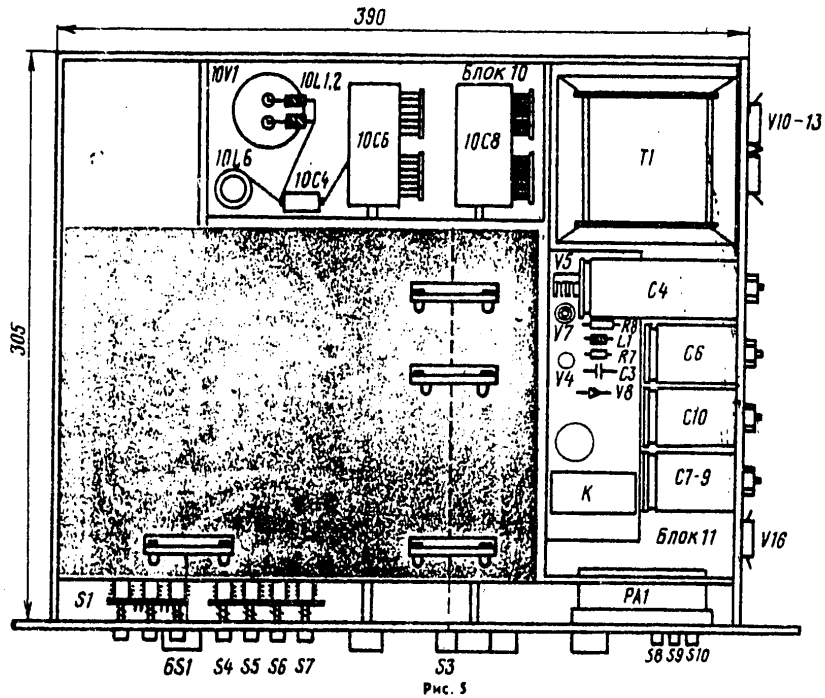
Figure 5.

The power transformer is made of ShL20x40 magnetic core material. Winding I has 884 turns of PEV-2 0.47 wire. The taps are made at the 478th turn ("127 v"), the 806th turn ("+10 v"), the 845th turn ("common") and 884th turn ("-10 v"). Winding II has 1,050 + 1,050 turns of PEV-2 0.27 wire, winding III has 165 + 165 turns of PEV-2 0.33 wire, winding IV has 27 + 27 turns of PEV-2 0.96 wire and winding V has 45 turns of PEV-2 0.47 wire.

Switches S1 - S13 are P2K switches and the remaining ones are wafer types. Relay K1 has an actuation voltage of 12 volts. The relay contacts are designed for switching circuits at a voltage of 1,000 v. The remaining relays are RES-15 types, data sheet number RS4.591.003. The PA1 meter is a microammeter with a full scale current of 100 microamps.

The preliminary alignment of the accessory is accomplished using conventional procedures - the correctness of the wiring, the operation of the power supply, the crystal oscillators and the microphone amplifier are checked. The operation of the SSB driver and all mixers are checked using the well-known procedure.

61

FOR OFFICIAL USE ONLY

When aligning the filters in the first and second mixers, the gates of the field effect transistors are disconnected from the preceding stages, and a signal from a generator is fed to one of the gates.

The alignment of the mixer stages should be accomplished by achieving the maximum undistorted signal at their outputs (monitored with an oscilloscope). Because of the considerable scatter in the parameters of the field effect transistors, the values of the levels in the mixers are not given. Some approximate levels and recommendations for the alignment of such assemblies are indicated in the article by Ya. Lapovka "A Transceiver Accessory" (see RADIO, 1978, No 8, pp 12-16).

Operation with the Accessory. The RF input to the accessory, X6, must be be connected to the output of the second heterodyne stage of the R-250M2 receiver. The tuning of the accessory to a frequency is accomplished with the high voltage cut off. By pressing the "Tune" button and setting the appropriate band, the filter of the second mixer is tuned for a maximum of the grid current of the output tube.

The output stage is powered from a combination rectifier. When the high voltage is cut off, a reduced voltage is applied to the plate and screen grid of the output tube, where this voltage is determined by the zener diode circuit in the screen circuit. This makes it possible not only to tune the Pi-network with the high voltage cut off, but also carry on local communications. For long range traffic, it is necessary to cut on the high voltage.

In conclusion, it must be said that radio amateurs of category II or III can add the 160 meter amateur band to the accessory (instead of the 15 m band). For this, an 8 MHz crystal is to be used instead of the 10 MHz crystal. The corresponding tuned circuits in the third mixer, the RF amplifier, and the output stage must be rewound and tuned to a frequency of 1,850 - 1,950 KHz.

When working in this band, the output power of the exciter should be reduced to 5 watts.

COPYRIGHT: Radio, 1980 No 2
[196-8225]

8225
CSO: 1860

62

UDC 681.322:621.391.28

USE OF COMPUTERS DURING DESIGN OF URBAN TELEPHONE EXCHANGES

/Annotation and Table of Contents from the book by Yuriy Vital'yevich Danilov, Aleksandr Borisovich Murdasov, and German Vasil'yevich Furtikov, Izd. "Svyaz'," 1979, 2200 copies, 113 pages]

/Text/ Described herein are the basic principles of the application of EVM /electronic computers/ to the design of GTS/urban telephone exchanges/ as a means to the identification of optimal designing solutions and the automation of design engineering. To this end, a model for GTS is offered in the form of a G graph, and a procedure is indicated by which one may, on the basis of this model, identify the optimal variants of GTS multi-exchange nets and toll switch planning. Investigation is made of algorithms for the automation of calculations of load densities, planning estimates, custom specifications, and cross-connection field charts. A broad range of technical equipment and programming provisions for the creation of automated planning systems is examined.

The book is intended for technical engineering personnel of planning organizations which are carrying out practical work in EVM, or developing new GTS planning programs with the use of computer technology.

TABLE OF CONTENTS

63

ELECTROMAGNETIC WAVE PROPAGATION; ELECTRODYNAMICS

INVESTIGATION OF IONOSPHERIC INHOMOGENEITIES

[Article by V.V. Kitayev]

[Text] For the purpose of creating a theoretical model of the dynamics of the inhomogeneous F-layer of the ionosphere, it is necessary to have sufficient information on the inhomogeneities of this layer. One of the possible sources of this information is ionospheric sounding (vertical (VZ), oblique (NZ) and oblique-incidence (VNZ)), in particular, with Doppler processing of the signal (the Doppler method [1]).

Determination of the parameters of ionospheric processes from the Doppler frequency shift, Δf, is a complex problem. The interpretation is complicated primarily by the integral nature of the results arrived at in space (the accumulation of effects along the path of radio waves) and in time (the possibility of the simultaneous influence of various factors on the same region of the ionosphere). For example [1], for vertical propagation with slight variations in electron concentration, N, in a nondeflecting region and with the rate of its change, $\partial N/\partial t$, depending on the altitude, h, the relationship between Δf and the sounding frequency, f_0, is inversely proportional:

$$\Delta f = \frac{e^2}{\pi m c} \frac{1}{f_0} \int_0^{h_0} \frac{\partial N}{\partial t} \, dh,$$

(1)

where h_0 is the echo altitude, e and m are the charge and mass of an electron and c is the speed of light in a vacuum.

And if variations in the frequency are caused by slight variations in the echo altitude, h_0, with maintenance of the shape of the layer, then Δf is directly proportional to the frequency, f_0:

65

FOR OFFICIAL USE ONLY

$$\Delta f = 2 \frac{f_0}{c} \frac{dh_0}{dt}.$$

(2)

With a combination of dependences of both types the relationship between Δf and f_0 can be more complicated.

Another example. It is known [2] that in the ionosphere there are large-scale ionized inhomogeneities (with linear dimensions of dozens and hundreds of kilometers) as well as small-scale ionized clouds (a few kilometers in size and smaller). These inhomogeneities are in a dual type of motion. One is the chaotic motion of the scattering center with a component v along the line of sight--the direction of the radius vector--and the second is the regular drift of the chaotic deflector of scattering centers in the horizontal direction with a velocity of V . It is difficult to distinguish the influence of drift from chaotic motion, since the chaotic velocities, v , are close in order of magnitude to the values of the velocity component, V , along the line of sight, and both velocities are on the order of dozens of meters per second, corresponding to Doppler frequencies of 0.5 to 10 Hz [2,3].

These examples demonstrate that for the purpose of identifying Doppler frequency shifts it is necessary to enlist other methods, and that it is possible to interpret the data of the Doppler method only by having additional information on the reason for the frequency shift.

In this communication an analysis is made of the possibility of separating the component of the Doppler frequency caused by regular motion (V) from the component caused by random motion (v), without involving other possible causes for the Doppler shift.

Let the sounding signal represent a train of square pulses with coherent occupation. Then after the reflection of each pulse from the ionosphere the initial phases of high-frequency occupation will have random values caused both by the chaotic and regular movement of inhomogeneities, i.e., the mid-range frequency of the signal spectrum, f_0 , will be shifted by a certain Doppler frequency equal to

$$\Delta f = \pm \frac{2 v f_0}{c} + \frac{2 V f_0}{c} \sin \theta \cos \psi,$$

(3)

where θ and ϕ are the spherical coordinates of the radius vector.

The channel's transmission coefficient, $u(j\omega,t)$, can be represented in the form

$$\mu(j\omega,\ t)=x(\omega,\ t)+jy(\omega,\ t)=\mu(\omega,\ t)e^{j\psi(\omega,\ t)},$$

(4)

where $x = \mu \cos \phi$ and $y = u \sin \phi$ are the orthogonal components of the channel's transfer function, whereby $\mu = \sqrt{x^2 + y^2}$, $\phi = \arctan (y/x)$ $(x = x(\omega,t)$, $y = y(\omega,t)$ and $\phi = \phi(\omega,t)$).

If it is assumed that orthogonal components x and y are distributed normally, then the phase, ϕ , is generally distributed according to the so-called four-parameter law [4]; in particular, with $m_x = m_y = 0$ and $\sigma_x^2 = \sigma_y^2 = \sigma^2$,

$$w(\varphi) = \frac{1}{2\pi};$$

(5)

and with $m_x \neq 0$, $m_y = 0$ and $\sigma_x^2 = \sigma_y^2 = \sigma^2$,

$$w(\varphi) = \frac{1}{2\pi} e^{-m_x^2/2\sigma^2} + \frac{m_x \cos \varphi}{\sigma\sqrt{2\pi}} F\left[\frac{m_x}{\sigma}\cos \varphi\right] e^{-(m_x^2/2\sigma^2)\sin^2\varphi},$$

(6)

where m_x , m_y , σ_x and σ_y are the mathematical expectations and standard deviations of the orthogonal components x and y , respectively, and $F[a]$ is the Laplace function.

In [3] are indicated a number of shortcomings of this model of the channel's transfer function, and there also is given a phase distribution of the type (with $m_x = m_y = 0$)

$$w(\varphi) = \frac{1}{2\pi} \frac{E_R}{2} \frac{\Gamma^2\left(\frac{2}{E_R}+\frac{1}{2}\right)}{\Gamma^2\left(\frac{2}{E_R}\right)} {}_2F_1\left(\frac{1}{2},1,1+\frac{2}{E_R},\cos^2 2\varphi\right),$$

(7)

where E_R is the excess of the probability density function for this process as compared with the Rayleigh probability density function, $\Gamma(a)$ is a gamma function and ${}_2F_1$ is a hypergeometric function.

67

Distributions (5) and (6) in 70 to 95 percent of cases agree well with the experimental data in [2,4,5]. In 95 percent of cases a phase distribution law of type (7) agrees with the experimental data [3]. Furthermore, it has been established [4,5] that for several minutes (for an interval of local stationarity of T_{st}) the parameters of the distribution of ortho-gonal components x and y (and consequently of processes μ and ϕ) are constant, i.e., the processes themselves are stationary, at least in the broad sense.

The conclusion regarding the local stationarity of processes, e.g., in [5], was made on the basis of the data of coherent processing of signals in vertical sounding. But in vertical sounding ($\theta \sim 0$) the influence on the phase of the reflected signal of regular horizontal drift of the reflecting region is excluded. Generally, when this influence is not excluded, the instantaneous phase of the received signal brought about, as was indicated above, by chaotic and regular motion, can be represented in the form of the sum of the regular, ϕ_r, and random, ϕ, components:

$$\varphi_\Sigma = \varphi_p + \varphi,$$

(8)

whereby ϕ_r is a determined magnitude unambiguously determined by velocity V; for ϕ^r are valid, obviously, distributions (5), (6) and (7) and the conclusion regarding the local stationarity of processes. For the total phase, ϕ_Σ, will be valid the four-parameter distribution, whereby m_x, m_y, σ_x and σ_y are quantities constantly varying over time, i.e., the overall process is nonstationary (equal to the sum of the determined func-tion and the stationary random process).

This distribution of the overall process makes it possible to conclude that it is possible to separate components V and v with their simultaneous effect on Δ_f (the oblique sounding case).

In coherent processing of the reflected signal (as the reference is em-ployed an oscillation coherent with high-frequency occupation of sounding pulses) at the output of the phase detector (FD) is gotten a train of video pulses whose amplitudes are proportional to $\cos \phi_\Sigma$ (fig 1a), i.e., the amplitudes of the pulses are random and are caused by the total effect of chaotic and regular motion of inhomogeneities of the ionosphere. Obviously, the mean values (mathematical expectations) of the components of $\cos \phi$ and, accordingly, of the amplitudes of pulses at the output of the FD caused by the chaotic motion of inhomogeneities will be constant, and the mean values of $\cos \phi_r$ and of the amplitudes of pulses caused by the regular motion of inhomogeneities will equal these same quantities (varying in accordance with V).

In fact, having computed the mathematical expectations of $\cos \phi$ as the mathematical expectations of functions of random values according to the equation

68

$$m_1 = \int_{-\pi}^{+\pi} \cos \varphi \, w(\varphi) \, d\varphi,$$

(9)

for phase distributions (5), (6) and (7) we get [6] for (5)

$$m_1 = 0;$$

(10)

for (6) with $m_x/\sigma \ll 1$

$$m_1 = \frac{1}{2} \sqrt{\frac{\pi}{2}} \cdot \frac{m_x}{\sigma};$$

(11)

with $m_x/\sigma \sim 1$ or $m_x/\sigma \gg 1$

$$m_1 = \frac{1}{2} \sqrt{\frac{\pi}{2}} \frac{m_x}{\sigma} \left[I_0 \left(\frac{m_x^2}{4\sigma^2} \right) + I_1 \left(\frac{m_x^2}{4\sigma^2} \right) \right] e^{-m_x^2/4\sigma^2},$$

(12)

where $I_\nu(a)$ is a modified Bessel function of the first kind and of the ν-th order; for (7)

$$m_1 = 0.$$

(13)

It follows from equations (10), (11), (12) and (13) that in all cases the mean values (including for (7), too) are either identically equal to zero or depend only on parameters m_x and σ, which, as indicated above, are constant over the range of local stationarity.

Thus, it is possible to present the following algorithm for processing the reflected signal for the purpose of separating the random component of the Doppler frequency from the regular (fig 2). The signal reflected from the ionosphere is subjected to coherent processing; the oscillation produced is fed to a unit (m_1) for calculating the mathematical expectation from a great number of realizations; from the mathematical expectation for the overall process (fig 1b) is filtered the constant component (the product of chaotic motion of the reflecting region). The remaining oscillation represents a train of video pulses whose envelope equals the Doppler frequency, caused by regular motion of the reflecting region (fig 1c).
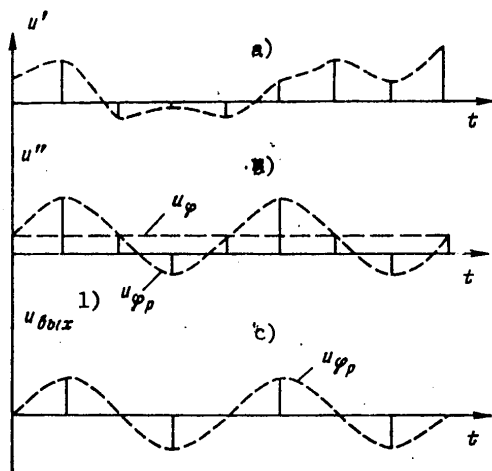
Figure 1. a--Signal at the Output of the Phase Detector; b--Signal
at the Output of the Mathematical Expectation Calculator;
c--"Pure" Doppler Frequency Signal

Key:

1. u_{vykh} [output]
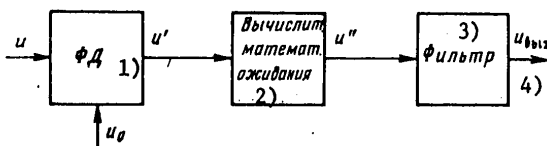
Figure 2. Functional Diagram of Signal Processing

Key:

1. Phase detector
2. Mathematical expectation
    calculator
3. Filter
4. u_{vykh}

70

In implementing the proposed algorithm an additional problem is the simultaneous obtainment of a great number of realizations of the random process (of the reflected signal); this problem is totally solvable.

This procedure for excluding the random component of the Doppler frequency of the ionosphere can be useful also in processing beyond-the-horizon shortwave radar signals (the VNZ case), when the regular component of the Doppler frequency is caused by motion of the target.

Bibliography

1. Namazov, S.A., Novikov, V.D. and Khmel'nitskiy, I.A. IZV. VUZOV MVSSO SSSR, RADIOFIZIKA, 1975, 18, 473.

2. Al'pert, Ya.L. "Rasprostraneniye elektromagnitnykh voln i ionosfera" [Propagation of Electromagnetic Waves and the Ionosphere], Izdatel'stvo Nauka, 1972, 563.

3. Vsekhsvyatskaya, I.S. "Statisticheskiye svoystva signalov, otrazhennykh ot ionosfery" [Statistical Properties of Signals Reflected from the Ionosphere], Izdatel'stvo Nauka, 1973, 135.

4. Klovskiy, D.D. "Peredacha diskretnykh soobshcheniy po radiokanalam" [Transmission of Discrete Messages Through Radio Channels], Izdatel'stvo Svyaz', 1969.

5. Mirkotan, S.F., Vologdin, A.G. and Smorodinov, V.A. RADIOTEKHNIKA I ELEKTRONIKA, 1978, 18, 3, 509.

6. Gradshteyn, I.S. and Ryzhik, I.M. "Tablitsy integralov, summ, ryadov i proizvedeniy" [Tables of Integrals, Sums, Series and Products], Fizmatgiz, 1962, 1100.

8831
CSO: 1860

ELECTRON TUBES; ELECTROVACUUM TECHNOLOGY

FORMATION OF BROAD HOMOGENEOUS ELECTRON STREAMS

[Article by L.P. Shanturin and V.I. Fedorov]

[Text] A description is given of an electrooptical system with a periodic
structure of filamentary thermionic cathodes for the purpose of forming
broad homogeneous streams of electrons with an energy of 100 to 500 keV
to be extracted into gaseous media with elevated pressure.

Good agreement is obtained between calculated and experimental results,
which can be used in creating electrooptical systems with assigned beam
parameters.

The problem of forming broad homogeneous electron streams arose in connec-
tion with the development of guns which release these streams into gaseous
media with pressure on the order of atmospheric through foil windows up to
10^3 cm^2 in area which let electrons through.

In [1] is described an electrooptical system for forming a broad electron
stream with a periodic structure of filamentary thermionic cathodes placed
in the field of a diode interelectrode gap. Each cell of the periodic
structure creates on a plane anode a line focus coupled with the line foci
of the neighboring cells.

Work relating to the investigation of electrooptical systems with a line
focus was done earlier [2,3], e.g., in connection with the creation of
x-ray tubes. In this paper a study is made of the features of the periodic
electrooptical system described in [1] for forming a broad homogeneous
stream, and the results of calculation on a digital computer are given, as
well as the results of experimental research reduced to tables, making it
possible for each specific case to select the geometrical relationships of
the electrooptical system.

The main specifications for electrooptical systems for forming homogeneous
broad streams are associated with the aspiration of increasing the mean

current density of electrons passing through the foil windows. It has been established that the degree of homogeneity of the electron stream necessary for an effective discharge is reached with deviations in the density of the electron current on the surface of the foil window (plane anode) not greater than 10 percent; the angles of incidence of the electron trajectories to the plane of the anode must not differ from the normal line by an amount greater than approximately 15°, and the current efficiency factor (k_{vykh} --the ratio of the current striking the foil window to the current passing through it) must not be less than 30 percent. The energy of electrons is on the order of hundreds of kiloelectronvolts.

A diagram of a periodic electrooptical system is given in fig 1.
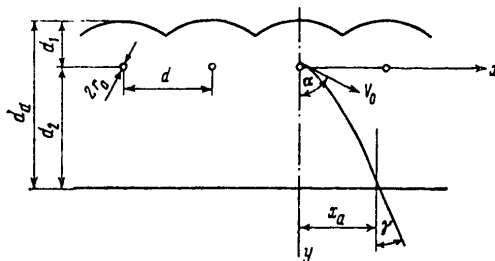
Figure 1. Electrooptical System with a Periodic Structure of Filamentary Cathodes: r_0 --radius of filamentary cathode; d_1 --distance between cathodes and focusing electrode under the same potential, $\phi_{fe} = 0$; d_2 --distance between cathode and anode with potential of $\phi_a = 1$; d -- distance between electrodes creating a plane electric field; a --spacing of periodic structure; α --initial angle of emission of electrons from surface of cathode, read from the plane of symmetry; γ --angle of incidence of electron onto plane of anode; x_a --half value of width of line focus

Generally the focusing electrode has a curvilinear surface with deformations whose period agrees with the spacing of the cathode filaments. Let us consider an electrooptical system infinitely extended along the direction of coordinate axes X and Z , which makes it possible to limit ourselves to solving a two-dimensional problem. In designs used in practice, at the edges are installed special electrodes which compensate edge effects.

The formation and acceleration of electrons takes place in the electric field of the gap, in which the potential of the focusing electrode equals the potential of the cathode filaments, $\phi_{fe} = \phi_k = 0$; at the anode the potential is $\phi_a = 1$.

73

In a system with postdeflection acceleration the anode is designed in the form of a grid and is the first anode of the acceleration gap.

The problem reduces to finding the geometrical relationships and form of the focusing electrode making possible an assigned breadth and homogeneity of the stream.

We will arrive at a solution by the method of analysis employing a digital computer, with the subsequent optimization of the results obtained. The problem has a peculiarity associated with the presence of parts of different scales (the diameter of the cathode is considerably smaller than the interelectrode gaps) and the relatively extended sections in which it is necessary to assign boundary conditions.

Therefore, we will first separate, by means of an approximate analytical calculation, the region of variation of interesting parameters and we will establish the key relationships of geometrical dimensions.

For the purpose of finding the distribution of potential in the system of electrodes illustrated in fig 1, let us employ the familiar analytical expression obtained by the method of conformal transformation as applied to the theory of a plane triode [4],

$$\varphi(x, y) = \frac{\frac{1}{2} d_1 \ln\left(\sin^2\frac{\pi x}{a} + \mathrm{sh}\frac{\pi y}{a}\right) + y\left(\ln\sin\frac{\pi d_1}{a} - \ln\sin\frac{\pi r_0}{a}\right) - d_1 \ln\sin\frac{\pi r_0}{a}}{d_1 \ln\mathrm{sh}\frac{\pi d_2}{a} + d_2 \ln\sin\frac{\pi d_1}{a} - (d_1 + d_2)\ln\sin\frac{\pi r_0}{a}},$$

(1)

which is valid with $r_0 \ll d_1$ and $r_0 \ll d_2$.

Analysis of equation (1) makes it possible to conclude that when the spacing of the cathode structure (a) is increased, beginning with a certain value the neighboring elements have a slight influence on the distribution of potential. For example, with $a/d_a > 0.2\pi$ the maximum change in potential associated with the influence of neighboring elements is not greater than hundredths of a percent. Therefore, we will make an approximate analysis of only one element of the periodic structure.

In addition, from the diagram of the field plotted according to (1), fig 2, it can be seen that a cathode grid with a spacing of $a/d_a = 0.07\pi$ introduces insignificant perturbations into the field of the interelectrode gap (perturbations of the field take place in small regions near the cathode

FOR OFFICIAL USE ONLY

in the form of equipotential cylindrical surfaces with a potential of ϕ_0 and surrounding the cathode filament), whereby potential ϕ_0 is equal to the natural potential of the plane field determined by the position of the cathode structure relative to the external electrodes. Therefore, in an approximate trajectory analysis we assume equipotential surfaces with ϕ_0 to be the surfaces of an emitter of electrons having initial velocities of $v_0 = \sqrt{2\eta\phi_0}$.
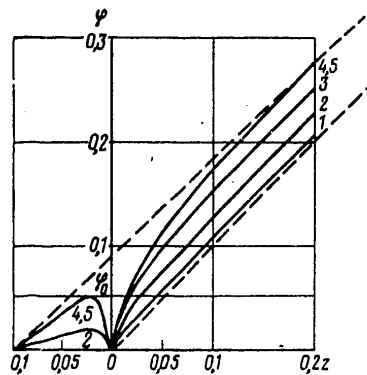
Figure 2. Distribution of Potential for a Periodic Cathode Structure in the Field of a Plane-Parallel Capacitor: a—spacing of cathode structure: 1—a = 0.032π, 2—a = 0.32π, 3—a = π, 4—a = 3.2π, 5—a = 32π

Then for the case illustrated in fig 1, with a plane focusing electrode the equations of motion are written in the following simple form:

$$\frac{d^2y}{dt^2} = \eta E_y,$$

$$\frac{d^2x}{dt^2} = 0,$$

(2)

where E_y is the field of the plane interelectrode gap. The trajectory equations have the form

$$y = \frac{1}{4} d_1 \frac{\varphi_0 - \varphi_{\phi_0}}{\varphi_0} x^2 (ctg^2\alpha + 1) + x \, ctg\,\alpha,$$

(3)

75

FOR OFFICIAL USE ONLY

where α is the angle of emission of electrons from the cathode. Electrons emitted along the normal line to the cylindrical surface of the cathode with an initial velocity of $v_0 = \sqrt{2\eta\phi_0}$ describe parabolic trajectories, and the field deflects the electrons in the direction toward the plane of symmetry, $x = 0$.

The distribution of the density of the electron current in the anode is determined by the equation

$$j_a = \frac{1}{l_a}\frac{di}{dx_a},$$

(4)

where di is the elementary current and $l\,dx_a$ is an element of the anode's area. In disregarding the space charge and with an infinitely great number of trajectories leaving a uniformly heated cathode over identical angular intervals, each of them carries an identical elementary current of di . In this case the distribution of current density in the anode can be brought into agreement with the distribution of trajectories. We get the distribution of trajectories from (3), assuming that $\phi_{fe} = 0$, $\phi_a = 1$ and $d_a = 1$.

The results of calculation of the distribution of current density in the anode plane as a function of the change in the angle of emission (a) of an electron from the cylindrical surface of a cathode in the range of $0 \le \alpha \le \pi$ and as a function of the position of the cathode (d_2) are presented in fig 3.

The characteristic nonlinearity in the distribution of the electron current at the boundary of the beam formed is caused by the focusing effect of the transitional region of the field from accelerating to retarding in relation to electrons emitted from the cathode over the range of initial angles (α):

$$\sim \frac{7}{12}\pi < \alpha < \frac{3}{4}\pi.$$

Electrons radially diverging from the cylindrical surface of the cathode can have angles of incidence (γ) onto the surface of the cathode which differ from zero. Their value depends on the angle of emission (α) of the electron from the surface of the cathode and on the position of the cathode (d_2) in the field of the interelectrode gap.

In the plane of the anode the angle of incidence (γ) is determined by the ratio of the transverse and longitudinal components of the electron's velocity. The expression for γ we get in the form

76

$$\gamma = \operatorname{arctg} \sqrt{\frac{(1-d_2)\sin\alpha}{(1-d_2)\cos\alpha+d_2}}$$

(5)
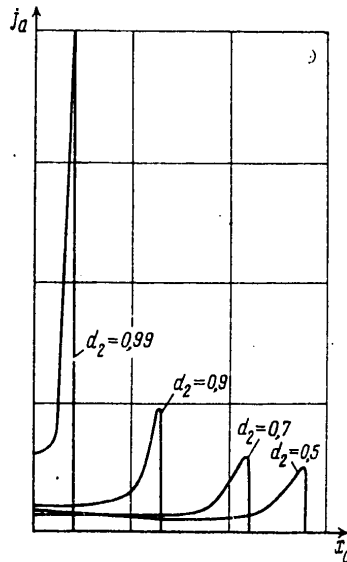
Figure 3. Dependence of the Size of the Line Focus and Distribution
of Current Density in the Anode on Position of the Cathode
in the Interelectrode Gap; γ_a --Current Density in the
Anode Plotted in Relative Units

We are interested in electrons with trajectories close to normal to the
anode's plane ($\gamma = 0$). From (5) it follows that $\gamma = 0°$ with $\alpha = 0°$
and $\alpha = \pi$. The trajectory of an electron with an initial angle of emis-
sion of $\alpha = \pi/2$ has the widest angle of incidence. On the other hand,
γ tends toward $0°$ with d_2 tending toward one (the case when the axis of
the cathode is in line with the plane of the focusing electrode). Here
the divergence of the electron stream tends toward zero.

The range of possible values of d_2 is determined from the condition
$0 < \gamma \leq 15°$ for an electron trajectory with the initial angle of emission
($\alpha = \pi/2$). Substituting these conditions in (5) gives

77

$$1 > d_2 \geqslant 0{,}933. \tag{6}$$

The value of the divergence (x_a/r_0) of the electron stream accordingly varies from 1 to approximately 1000, whereby the maximum width of the line focus in the plane of the anode equals part of the distance between the cathode and anode:

$$2x_{a\,\text{макс}} \leqslant 0{,}632 d_2. \tag{7}$$

It follows from the approximate trajectory analysis that the range of possible variations of dimension d_2 is determined by the permissible angle of inclination of electron trajectories, γ. In addition, the distribution of the current density of the beam in the anode is nonuniform and has two sections—a uniform (the amplitude deviation of the current density is not greater than 10 percent) and nonuniform. The nonuniform section is formed by electrons which leave the cathode with initial angles of emission close to $2\pi/3$. A homogeneous stream can be achieved by collimating the inhomogeneous sections. Experience gained by the authors in using guns with a periodic EOS [electrooptical structure] has demonstrated that condition $k_{\text{уукh}} \geq 30$ percent is fulfilled if the collimated current equals not more than 30 percent of the total beam current. For the purpose of solving the problem of forming a homogeneous stream with minimal losses in collimation it is necessary to optimize the EOS. The problem of optimizing the EOS in terms of uniformity of the distribution of current density in the anode was solved by us numerically by the method of finite differences on the basis of the compiling system for the BESM-6 computer (the KSI BESM) [5].

The electrooptical system consists of a periodic structure of filamentary cathodes, a plane anode and a focusing electrode symmetrically deformed in relation to planes passing through the axes of the cathodes perpendicular to the plane of the anode. This system of electrodes represents a system of cylindrical lenses with planes of symmetry passing through the axis of the cathode.

The calculation of many variants made it possible to reveal the key rules for the formation of a stream from a cylindrical cathode when changing the form of the focusing electrode. On the cathode there are two considerably different regions: the region of the cathode facing the anode, electrons from which are formed only in the accelerating field, and the region of the cathode facing the focusing electrode, electrons from which are first accelerated and, passing through the potential maximum corresponding to potential ϕ_0 (fig 2), fall into the retarding field. Starting at the instant when the longitudinal component of the velocity of the electrons (v_y) becomes equal to zero, electrons are accelerated toward the anode.

A change in parameters of the retarding field exerts a considerable influence on the formation of electrons from the region of the cathode facing the focusing electrode, practically not disturbing the flow of electrons from the region of the cathode facing the anode. This fact makes it possible independently to control the electrons emitted from various regions of the cathode.

Calculation of a great number of variants of an electrooptical system with different configurations of focusing electrodes demonstrated that from a cylindrical cathode in the field between a plane anode and a focusing electrode cannot be formed a stream with a uniform distribution of current density in the anode. At the boundaries of the stream formed there always exist sections with increased current density. The major portion of the current of these sections is made up of electrons emitted from the portion of the cathode facing the focusing electrode. However, it was possible to find a solution (fig 4 on the condition that $x_{a1} = x_{a2}$) whereby part of the electrons forming the current density maximum at the boundaries of the stream are distributed over the entire breadth of the line focus. In fig 4 is presented the path of the trajectories of electrons emitted from characteristic sections of the cathode, as well as current density diagrams (for the purpose of clarity the scale has not been observed). This solution is obviously optimal for the EOS selected (the size of the uniform section is maximal) and is implemented by means of a focusing electrode of simple form. In plotting current density diagrams it has been assumed that the electrons leave the cathode over identical angular intervals and that the emission is uniform over the entire surface of the cathode. For a predetermined breadth of the line focus an optimal solution can be arrived at with different relationships between the geometrical dimensions of the EOS, whereby the degree of homogeneity of the stream is also different. The necessity of optimizing the geometrical relationships of the EOS is obvious. The geometry of the EOS has been optimized over the stream divergence range of 10^2 to 10^3 for varying parameters d_2, d_{shch} and c. With fixed values of d_2 and d_{shch} the breadth of the line focus (x_{a1}, fig 4) is a function of c. We arrive at an optimal solution for each c by selecting dimension b so that condition $x_{a2} = x_{a1}$ is fulfilled. The minimum value of d_2 is determined by the assigned value of the breadth of the line focus ($2x_a$), equal in our case to the spacing (a) of the periodic electrooptical system. Taking (7) into account, we have

$$d_{2\ \text{мин}} = 3,17 x_a. \tag{8}$$

The period of the cathode structure limits dimension d_{shch}, since it cannot exceed the value of the spacing (a) of the periodic electrooptical system:

$$d_{m\ \text{макс}} \leqslant 0,7 x_{a\ \text{макс}}. \tag{9}$$
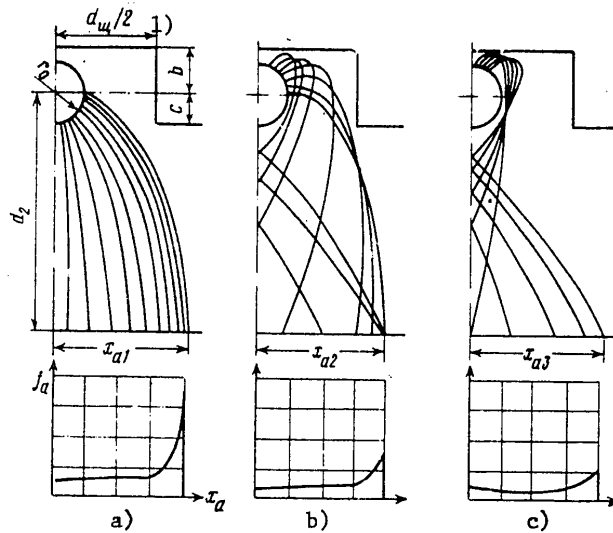
Figure 4. Form of Electron Trajectories and Current Density Distri-
bution Curves for an Optimal Electrooptical System as a
Function of the Initial Angle of Emission of an Electron
from the Surface of the Cathode: a--$0 \leq \alpha \leq \pi/2$; b--
$\pi/2 \leq \alpha \leq 3\pi/4$; c--$3\pi/4 \leq \alpha \leq \pi$

Key:

   1. $d_{shch}/2$

Taking (8) and (9) into account, the ratio d_{shch}/d_2 (determining the de-
gree of homogeneity of the stream and the amount of the error in the re-
lative setting of electrodes) is limited by the condition $d_{shch}/d_r \leq$
≤ 0.22 .

The results of the calculation of EOS variants for selected ranges of geo-
metrical relationships with $d_2/r_0 = 2.5 \cdot 10^3$ are summarized in table 1,
where $k_x = A/2x_a$ is the degree of homogeneity of the stream at the anode
(in keeping with the symbols in fig 5 A is the length of the section with
uniform current density distribution); k_i is the degree of current colli-
mation (the ratio of the portion of current contained in inhomogeneous
sections to the total current of the beam); and δ is the maximum per-
missible deviation of the cathode (calculated from the condition that the
change in stream parameters thereby is not greater than 10 percent). Cal-
culations were performed by taking into account the relativistic effect

FOR OFFICIAL USE ONLY

of the change in the mass of an electron in the energy range up to 500 keV and without taking it into account.

Table 1.

1) $d_{\text{ш}}/d_{\text{s}}$	$c/d_{\text{ш}}$	$b/d_{\text{ш}}$	$2x_a/d_s$			k_x	k_t	$\delta/d_{\text{ш}}$
			*	2) 150 кВ	500 кВ			
0,2	0,128	0,347	0,43	0,42	0,41	0,89	0,21	0,020
	0,185	0,278	0,35	0,34	0,33	0,83	0,26	0,016
	0,238	0,232	0,27	0,26	0,25	0,77	0,34	0,012
	0,293	0,140	0,19	0,19	0,18	0,72	0,40	0,009
	0,349	0,074	0,11	0,11	0,11	0,66	0,47	0,006
0,15	0,086	0,399	0,38	0,38	0,37	0,83	0,25	0,014
	0,123	0,345	0,35	0,34	0,33	0,79	0,28	0,012
	0,194	0,255	0,27	0,26	0,25	0,74	0,35	0,009
	0,261	0,197	0,19	0,19	0,18	0,68	0,45	0,006
	0,336	0,151	0,11	0,11	0,11	0,62	0,57	0,003
0,10	0,092	0,355	0,31	0,30	0,29	0,77	0,32	0,008
	0,165	0,272	0,23	0,23	0,22	0,71	0,38	0,006
	0,256	0,195	0,15	0,15	0,14	0,58	0,49	0,004
	0,296	0,161	0,11	0,11	0,11	0,49	0,58	0,003
0,07	0,072	0,378	0,26	0,26	0,25	0,73	0,35	0,006
	0,149	0,271	0,19	0,19	0,18	0,64	0,43	0,004
	0,199	0,222	0,15	0,15	0,14	0,58	0,48	0,003
	0,263	0,166	0,11	0,11	0,11	0,52	0,59	0,002

3) * Без учета релятивизма.

Key:
1. d_{shch}/d_2
2. 150 kv
3. Without taking relativism into account

An analysis of the results presented in table 1 demonstrated the possibility of the formation of an electron stream from a filamentary cathode with a uniform distribution of current density in a section equaling 52 to 89 percent of the breadth of the line focus, whereby the size of the homogeneous section increases with an increase in the divergence of the stream and dimension d_{shch}.

The range of d'~ensions of the line focus for the optimal case has an upper limit determined by the transverse velocity ($\gamma = 15°$) and has a value of

$$2x_{\text{s макс}} \leqslant 0,43 d_2.$$

The range of permissible deviations (δ) for the relative setting of electrodes is expanded by increasing the divergence of the stream and dimension d_{shch}. The relativistic effect is but slightly pronounced. The change in

81

FOR OFFICIAL USE ONLY

FOR OFFICIAL USE ONLY

beam parameters is not greater than five percent in the indicated range of accelerating voltages.

For the purpose of testing the admissibility of the assumptions made in calculation, experimental studies were made of the calculated electrooptical system, employing an electron beam analyzer making possible relative positioning of the electrodes of the electrooptical system and changing of the form of the focusing electrode. The analyzer is furnished with a power supply with a regulated voltage from 10 to 150 kV. The measuring unit is in the form of a specially developed collector of the Faraday cylinder type with a resolution of approximately one percent. A unit with mechanical scanning and remote control makes it possible to move the collector in the specified direction. The signal arriving from the collector is recorded by a high-speed recorder.

Experimental diagrams of the current density distribution (fig 5) for boundary values of the range (a--c/d_{shch} = 0.128 and b--c/d_{shch} = 0.349) with d_{shch}/d_2 = 0.2 were arrived at for the following absolute values: a VA-1 tungsten wire cathode with a dimension of r_0 = 0.1 mm ; size of the acceleration gap equaling d_2 = 260 mm ; an acceleration voltage of 150 kV; and a characteristic dimension of the collector's aperture of 1.5 mm.

a)

b)
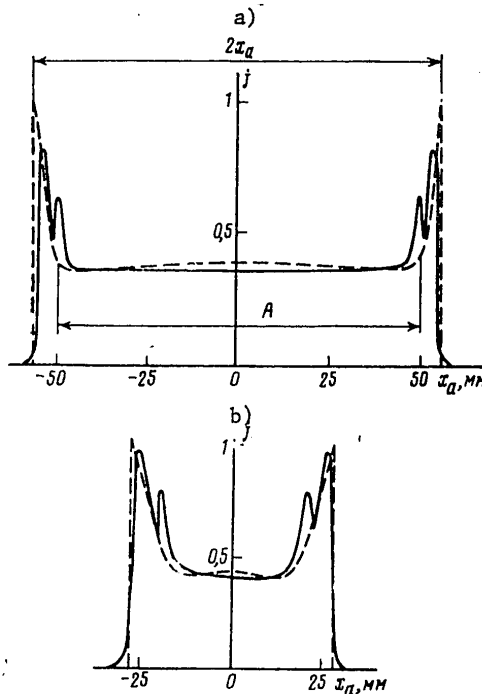
[Caption on following page]

82
FOR OFFICIAL USE ONLY

FOR OFFICIAL USE ONLY

Figure 5. Current Density Distribution Diagram for $d_{shch}/d_2 = 0.2$ with Differing Beam Divergence: Solid-Line curves—Experimental; Dotted-Line—Results of Numerical Calculation

The calculated EOS's were studied experimentally for $d_{shch}/d_2 = 0.2$ and the results of these studies are given in table 2.

Table 2.

d_{III}/d_1	c/d_{III}	b/d_{III}	$2x_a/d_1$	k_x	k_1	δ/d_{III}
0,2	0,128	0,347	0,42	0,84	0,29	0,020
	0,185	0,278	0,34	0,79	0,34	0,017
	0,238	0,232	0,27	0,74	0,41	0,012
	0,293	0,140	0,19	0,66	0,50	0,009
	0,349	0,074	0,11	0,60	0,55	0,006

The difference from the calculation results consists in a slight (less than five percent) reduction in the line focus and in the appearance of an additional current density maximum resulting from violation of the optimality condition ($x_{a_1} > x_{a_2}$). This somewhat reduces the degree of homogeneity of the stream. The necessary distribution ($k_1 \leq 0.3$) is achieved with maximum divergence of the stream. A smaller degree of current collimation can be arrived at for streams with greater divergence, in an EOS with an increased ratio of d_{shch}/d_2, as well as by adjusting the geometry of the focusing electrode by selecting dimension b consistent with condition $x_{a_1} = x_{a_2}$.

The authors thank A.I. Pokras for his assistance in making numerical calculations.

Bibliography

1. Fedorov, V.I. and Shanturin, L.P. PRIBORY I TEKHNIKA EKSPERIMENTA, 1976, 1, 153.

2. Kharadzha, F.N. "Obshchiy kurs rentgenotekhniki" [General Course in Radiography], GEI, 1956.

3. Samoylov, I.M. PRIBORY I TEKHNIKA EKSPERIMENTA, 1959, 1, 24.

4. Strashkevich, A.M. "Elektronnaya optika elektrostaticheskikh sistem" [Electrooptics of Electrostatic Systems], Izdatel'stvo Energiya, 1966.

FOR OFFICIAL USE ONLY

FOR OFFICIAL USE ONLY

5. Il'in, V.P. "Chislennyye metody resheniya zadach elektrooptiki"
   [Numerical Methods of Solving Electrooptics Problems], Izdatel'stvo
   Nauka, Novosibirsk, 1974.

8831
CSO: 1860

FOR OFFICIAL USE ONLY

OSCILLATORS, MODULATORS, GENERATORS

RADIO BAND SELF-EXCITED OSCILLATOR WITH STOCHASTIC BEHAVIOR

[Article by S.V. Kiyashko, A.S. Pikovskiy and M.I. Rabinovich]

[Text] A radio engineering self-excited oscillator is discussed which is
distinguished from an ordinary sine-wave oscillator with a filter circuit
in the grid circuit by a tunnel diode added in series with the filter cir-
cuit's inductance. A qualitative and numerical analysis is made of the
dynamics equations describing the circuit. The structure of the attracting
region in the phase space (the attractor) is investigated by reduction to a
unidimensional point transformation the attracting nature of which makes
possible stochastic behavior of the oscillations produced. Experimentally
observed realizations and spectra of the noise signal are presented.

Introduction

In quite recent times in radio engineering have appeared subjects of invest-
igation which are attractive both from the theoretical and practical points
of view--self-excited noise generators per se [1,2] in which the statistics
of the output signal are determined not by the intensification of fluctua-
tions, but by the intrinsic complex dynamics of a system not containing
noise sources. A self-excited oscillator of this sort, even one put to-
gether from a very simple circuit [2,4], separates out in the load, unlike
periodic-wave generators (sine-wave generators or relaxation oscillators
[3]), a signal possessing all the traits of a random one (continuous spec-
trum, a decline in autocorrelation, etc.). The appearance of simple noise
generators--stochastic self-excited oscillators--is associated with recent
successes in the theory of nonlinear oscillations of systems with a number
of degrees of freedom greater than two.

The fact is that some time ago only one mathematical representation of
self-oscillations was known--the asymptotic cycle responsible just for the
generation of periodic signals. Any more complicated structures in the
phase space of self-oscillating systems appeared to be unstable and, con-
sequently, physically unrealizable. However, at the end of the 60's

FOR OFFICIAL USE ONLY

mathematicians discovered that in addition to simple stable structures (attractors) complicated ones can also exist which are responsible for the stochastic behavior of the dynamic system--the generation of a random signal [5,6]. Thus appeared a mathematical representation of stochastic auto-oscillations--the "strange attractor" [7].* The words "stochastic behavior of the dynamic system" must be understood in the sense that although the precise assignment of the starting point in the phase space completely determines the subsequent trajectory, this trajectory can be very complicated and practically indistinguishable from a random process [8,9,10]. For the purpose of visualization it is possible to refer to the analogy with random number generators used in computers: Although the operations performed by the computer are determinate, the sequence of numbers produced does not differ from random.

After the discovery of strange or stochastic attractors, practically immediately attempts were made to describe by means of them the origin of hydrodynamic turbulence [7,11]. Now there have been notable successes along this line, associated chiefly with the investigation of the so-called Lorenz system [12]--a maximum-simple model of freely convective turbulence. Detailed numerical calculations and qualitative considerations supported by the theory of bifurcations made it possible to conclude with sufficient confidence that in the Lorenz system over a broad range of variation of parameters there are no other attractors except the stochastic [13,14]. Now are known a few more fairly simple systems in the numerical investigation of which stochastic behavior has been observed. These systems describe the kinetics of chemical reactions [15], the work of a dynamo [16] and the nonlinear interaction of waves [10,17].

Historically it happened that in the development of ideas regarding strange attractors and stochastic auto-oscillations the classical area of application of the theory of dynamic systems--radio engineering--turned out to have been bypassed. The idea of designing radio engineering noise generators based on a stochastic attractor was expressed for the first time only four years ago [14], although the greater number of known systems with stochastic attractors (e.g., the Lorenz system) have proven to be simple enough to be able to model them on an analog computer and thus produce an actual noise generator. Let us mention also the experiments in which noise was observed in distributed radio band systems--LC lines [19]. It is possible that the noise observed owes its origin to a stochastic attractor.

In this paper the results are given of a theoretical, numerical and experimental investigation of one of the simplest self-excited noise generators-- a relaxation oscillator similar to that in [4].

---

*We will still use the term "stochastic attractor" suggested by Sinay [8].

FOR OFFICIAL USE ONLY

1. Operation of Circuit and Experiment

Let us consider an oscillator assembled according to the circuit in fig 1a.
It is distinguished from a classical self-excited sine-wave oscillator with
a filter circuit in the grid circuit only by a tunnel diode connected in
series with the inductance. The operation of this circuit is described by
the following equations:

$$C\dot{U} = -I,$$
$$L\dot{C}I = (MS - rC)I + C(U - V),$$
$$C_1\dot{V} = I - I_{\text{тд}}(V).$$

$$(1)$$

Here C_1 is the capacitance of the tunnel diode, S is the transconduct-
ance of the tube and M is the mutual inductance factor. In discussing
the circuit's operation we will consider the tube's characteristic to be
linear. This is justified by the fact that in the mode of interest to us
the oscillations are limited by the nonlinear characteristic of the tunnel
diode, $I_{td}(V)$ (fig 1b), at a level at which the nonlinearity of the tube
is not evidenced.
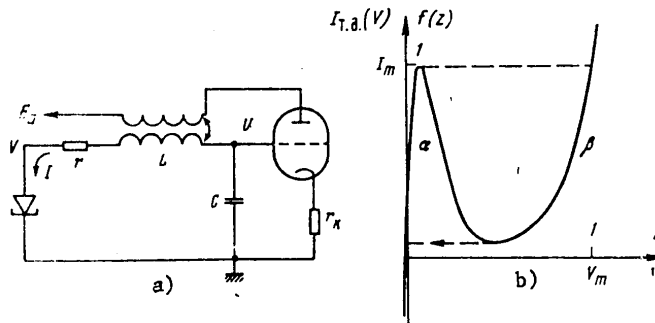
Figure 1.   a--Circuit Diagram of Self-Excited Noise Generator; b--
Volt-Ampere Characteristic of Tunnel Diode

Qualitatively the operation of the oscillator can be described in the
following manner. While the current, I , and voltage, U , are low, the
tunnel diode does not exert a substantial influence on oscillations in the
circuit and these increase on account of the energy introduced by the tube.
Here current I flows through the tunnel diode and the voltage in it is
determined by branch α of characteristic $I_{td}(V)$. But when current I
reaches a value of I_m , almost instantaneous switching of the tunnel diode
takes place (the speed of this switching is associated with the triviality
of capacitance C_1)--voltage V_m is established abruptly. Then the
current through the tunnel diode is reduced and it is switched back--from

87

FOR OFFICIAL USE ONLY

section β to α . As a result of the two switching events, the tunnel diode almost completely "kills" the energy entering the circuit and the oscillations begin to grow again.

Thus, the signal generated, $U(t)$, is in the form of a sequence of trains of increasing oscillations, and the end of each train is accompanied by a voltage pulse, $V(t)$. From this description it is not clear, of course, whether the steady-state mode is periodic or stochastic. It is possible to investigate this by a close mathematical examination of equations (1), which, however, we will set aside until the next section, and now we will give the results of the experiment.

The circuit in fig 1 was implemented with half of a 6N1P triode (E_a = = 250 V , r_k = 30 Ω). The filter circuit consisted of a capacitance of C = 1.5 μF and an inductance of L = 5.7 MH . To this filter circuit were connected four 3I306G tunnel diodes connected in parallel (I_m $\sim$ 7.15 mA , V_m $\sim$ 1.08 V and C_1 $\sim$ 30 pF). The dimensionless parameters of the circuit (cf. equations (2) below) in this case equal g $\sim$ 2.4 and ε $\sim$ 4.8$\cdot$10^{-5} . The increment of the increase in oscillations in the circuit, i.e., magnitude h , it was convenient to vary by varying resistance r . The minimum achievable losses in the filter, determined by the elements of the circuit themselves, equaled r_0 $\sim$ 8.2 Ω .

With R = r - r_0 $\sim$ 14.5 Ω , in the circuit were excited purely periodic oscillations which were limited by the tube's nonlinearity to such a low level that the diodes were not switched (I < I_m). With R $\sim$ 13.5 Ω the amplitude of the oscillations reached the threshold value and signal U(t) was in the form of long packets of oscillations occasionally interrupted by switching of the diodes. And only with R < 11 Ω was the nonlinearity of the triode not felt--a signal was generated in the form of trains within each of which the oscillations grew exponentially, and the transition from one train to another was accompanied by a voltage pulse in the tunnel diode, V(t) . With no single value of R < 11 Ω was it possible to detect a periodic mode--a random signal was generated with a continuous spectrum. From the spectra and oscillograms presented in fig 2 it is obvious that with a reduction in R the increment in oscillations, h , increases and the mean duration of the train is reduced--here in the spectrum the peaks at the train repetition frequencies are leveled off. The greater part of the energy is contained in the main maximum corresponding to the frequency of the circuit's oscillations.

2. Analysis of Mathematical Model

In investigating equations (1) let us go to the dimensionless variables $x = I/I_m$, $\tau = V/V_m$, $y = UC^{1/2}/(I_m L^{1/2})$ and $\tau = t(LC)^{-1/2}$. As a result we get

88

$$\dot{x} = 2hx + y - gz,$$
$$\dot{y} = -x,$$
$$\varepsilon \dot{z} = x - f(z).$$

(2)

Here $h = 0.5(MS - rC)(LC)^{-1/2}$ is the increment in the increase in oscillations in the circuit in the absence of a diode; $g = V_C C^{1/2}/(I_r L^{1/2})$ is a parameter determining the degree of the influence of the tunnel diode on processes in the circuit; $\varepsilon = gC_1/C$ is a minor parameter proportional to the capacitance of the tunnel diode; and $f(z) = I_{td}(V_m z)/I_m$ is the normalized characteristic of the diode (cf. fig 1b).

Figure 2.   Oscillograms of the Output Signal, U(t) , (Right) and Its Spectra on a Logarithmic Scale (Left) with Different Figures of Merit for the Circuit (In the Top Figure R is Minimal)

Key:
   1.   f , kHz

System (2) has minor parameter ε as the result of a derivative; there-fore, all motion in the phase space (fig 3) can be divided into rapid--switching of the diode (straight lines x = const and y = const)--and slow--oscillations at which the voltage in the diode follows the current (the respective trajectories lie on surfaces A and B (x = f(z) and f'(z) = 0), corresponding to sections α and β of the diode's charac-teristic [20].
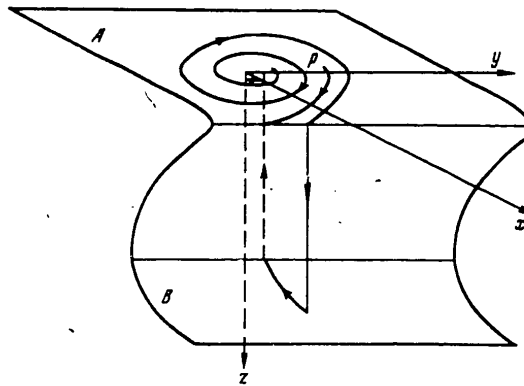
Figure 3. Phase Space of System (2)

The approximate form of the phase space of system (2) is presented in fig 3. The system has one unstable (with $2h > g/f'(0)$) state of equilibrium, x = y = z = 0 . Trajectories lying on surface A uncoil around the un-stable focus and ultimately reach the edge of surface A . Here takes place a breakaway of the mapping point along the line of rapid motion toward surface B . Passing along B , the mapping point breaks away back to surface A and falls into the neighborhood of the state of equi-librium--a new train of increasing oscillations begins.

Further analysis is simplified substantially if we go from a description, continuous over time, of the trajectory to a discrete description. This means that we will note only those points on the trajectory in which y (i.e., the output voltage, U) reaches a maximum--we will construct a map of T -- $y_i \rightarrow y_{i+1}$ = $\phi(y_i)$ --step by step becoming itself by means of half-line Σ (x = z = 0 , y > 0). All trajectories beginning and ending at Σ can be divided into two classes: 1) lying entirely on surface A --they rotate around the state of equilibrium; and 2) those reaching surface B . These two groups are separated by trajectory P , which approaches the breakaway line at a tangent.

An analytical expression for the map of $\phi(y)$ is possible only if f(z) is approximated by a piecewise linear function. Let us assume, for

90

FOR OFFICIAL USE ONLY

example, that $f(z) = z/\kappa$ when $z < \kappa$, $f(z) = (1 - \kappa - z)/(1 - 2\kappa)$ when $\kappa < z < 1 - \kappa$ and $f(z) = (z - 1 + \kappa)$ when $1 - \kappa < z$. Then the equations for slow motion become linear:

$$\dot{x} = 2\nu x + y + k \ , \quad \dot{y} = -x \ , \tag{3}$$

where $k = 0$ on A (now A and B are planes) and $k = b = g/(1 - \kappa)$ on plane B , and $\nu = h - 0.5\kappa g$. Joining solutions (3) in the standard manner on planes A and B [3], it is not difficult to arrive at an expression for $\phi(y)$ similarly to how this was done in [4,18]. Without writing out cumbersome equations, we present only the division of region of parameters b, ν into different types of behavior of $\phi(y)$ (fig 4).
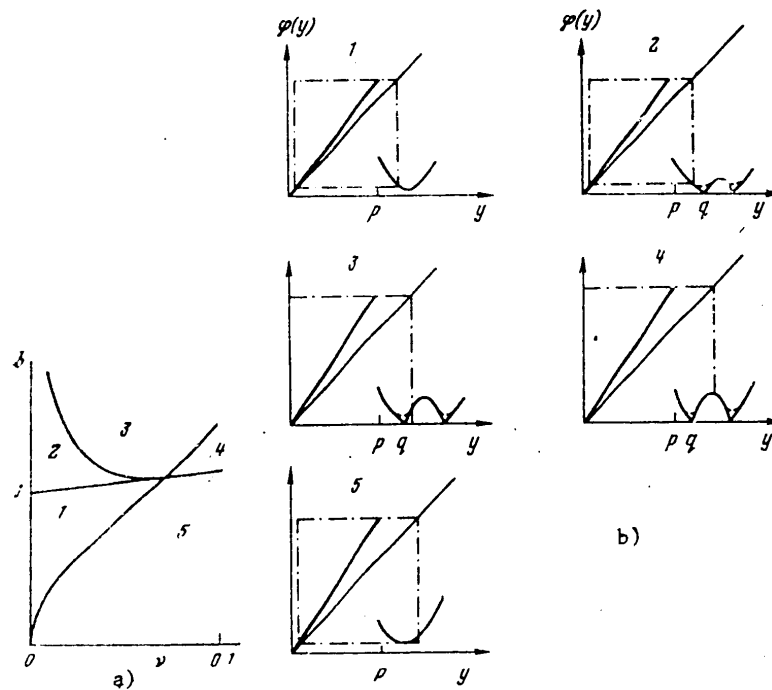
Figure 4. a--Division of Plane of Parameters b, ν into Regions of the Different Behavior of T ; b--Maps of T Arrived at with a Piecewise Linear Approximation of $f(z)$

The maps in fig 4b have in addition to discontinuity p (corresponding to trajectory P) point of discontinuity q . The appearance of a discontinuity at point q is associated with the fact that with this selection of

91

FOR OFFICIAL USE ONLY

$f(z)$ ($f(z) = 0$ with $x = 1 - \kappa$) the state of equilibrium lies precisely below the breakaway line. If it is taken into account that $f(z) \neq 0$ with $z \neq 0$, then the discontinuity will disappear, as indicated in fig 4b by the broken line. On all the maps in fig 4b there is a region of attraction which all trajectories enter. Within this region there first occur several iterations with $y_i < p$ (corresponding to this is an increase in oscillations in the train), and then an iteration with $y_i > p$ returns the mapping point to the linear section (one train is replaced by another).

With low ν within the region of attraction is fulfilled the condition $|\phi'| > 1$, i.e., the map is one of attraction--in successive iterations the two near points diverge. The divergence of close trajectories is one of the traits of stochastic behavior [8,10] and at once ensures the absence of stable limiting cycles. In this case the transformation has an invariant ergodic measure in relation to which it is a mixing transformation (this follows from the results of [14]).

However, the conclusions arrived at when employing a piecewise linear approximation of $f(z)$ can prove to be incorrect, since with this description the behavior of trajectories close to P is incorrectly reflected. Therefore, we plotted transformation T numerically. The values of parameters were selected as follows: $h = 0.074$, $q = 2.8$ and $\varepsilon = 0.004$; characteristic $f(z)$ was approximated by the function $f(z) = z \exp \exp (3.61 = 13.5z) + \exp (6.5(z - 1)) - \exp (-6.5)$. Integration was performed on a BESM-6 computer by the Runge-Kutta method with an interval of $2 \cdot 10^{-4}$. Function $\phi(y)$ arrived at is presented in fig 5. Near P now appeared a critical point at which $\phi' = 0$, but it was not completely possible to resolve the region of discontinuity. Obviously transformation T is really continuous, but $\phi' \sim \exp (\varepsilon^{-1})(!)$, i.e., the assumption that the piecewise linear approximation describes the real situation sufficiently well has been confirmed. And nevertheless the existence within the region of attraction of critical points worsens the stochastic behavior of the system.

As follows from [21,22], transformations with critical points with almost all values of parameters have a stable asymptotic cycle. However, firstly, the stable cycle is surrounded by a stochastic non-attracting region [23]; secondly, the period of the cycle can be very great and over long intervals of time the realization appears to be random; and, thirdly, the region of the space of parameters in which this cycle is stable is as a rule very small. Therefore, in the numerical experiments in [24] transformations with critical points demonstrate stochastic behavior; however, here possibly more appropriate would be the term "complex dynamics" [18]. And although the stochastic behavior observed here is the consequence of low noise (e.g., of rounding errors), the statistical properties of the signal are determined, judging from the whole, not by the statistics of noise, but by the characteristic dynamics of the system.
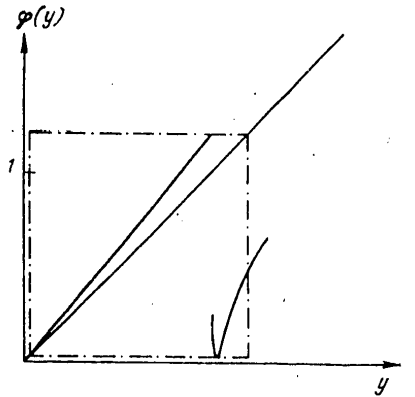
Figure 5. Transformation $y \rightarrow \phi(y)$ Plotted for System (2) Numerically with $h = 0.074$, $g = 2.8$ and $\varepsilon = 0.004$. The Attractor is Indicated by the Dot-Dash Line

Thus, system (2) demonstrates a behavior practically indistinguishable from stochastic, and the signal produced in the self-excited oscillator is random.

In the self-excited noise generator described here is realized only one of the possible mechanisms for the origin of a stochastic process in self-oscillating systems. In radio engineering equipment other mechanisms can also be realized--the decay mechanism associated with the time lag of non-linearity, and others [10]. In connection with the investigation of self-excited noise generators per se, of obvious interest are questions relating to the effect on them of an external signal, to the interaction of several generators of this sort and many more. Studies along this line have still just begun.

The authors wish to express their gratitude to A.V. Gaponov for his continued interest in this paper and to A.A. Andronov, Yu.B. Kobzarev and S.M. Rytov for their helpful discussions.

Bibliography

1. Gollub, J.P., Brunner, T.O. and Danley, B.G. SCIENCE, 1978, 200, 48.

93

2. Kiyashko, S.V., Pikovskiy, A.S. and Rabinovich, M.I. "Radio Band Random Signal Generator," Patent No 698118, OTKRYTIYA, IZOBRETENIYA, PROMYSHLENNYYE OBRAZTSY, TOVARNYYE ZNAKI, 1979, 42, 227.

3. Andronov, A.A., Vitt, A.A. and Khaykin, S.E. "Teoriya kolebaniy" [Theory of Oscillations], Fizmatgiz, 1959.

4. Pikovskiy, A.S. and Rabinovich, M.I. DOKL. AN SSSR, 1978, 239, 301.

5. Smeyl, S. USPEKHI MATEM. N., 1970, 25, 113.

6. Williams, R. TOPOLOGY, 1967, 6, 473.

7. Ruelle, D. and Takens, F. COMM. MATH. PHYS., 1971, 20, 167.

8. Sinay, Ya.G. "Nelineynyye volny" [Nonlinear Waves], edited by A.V. Gaponov, Izdatel'stvo Nauka, 1979.

9. Alekseyev, V.M. "Symbolic Dynamics" in "XI letnyaya matematicheskaya shkola" [The 11th Summer Mathematics School], Izdatel'stvo Instituta Matematiki AN USSR, Kiev, 1976.

10. Rabinovich, M.I., USPEKHI FIZ. N., 1978, 125, 123.

11. McLaughlin, J.B. and Martin, P.C. PHYS. REV. A, 1975, 12, 186.

12. Lorenz, E.N. J. ATMOS. SCI., 1963, 20, 130.

13. Afraymovich, V.S., Bykov, V.V. and Shil'nikov, L.P. DOKL. AN SSSR, 1977, 234, 336.

14. Bunimovich, L.A. and Sinay, Ya.G. Collection "Nelineynyye volny," edited by A.V. Gaponov, Izdatel'stvo Nauka, 1979.

15. Rossler, O.E. Z. NATURFORSCH., 1976, 31a, 259.

16. Rikitake, T. PROC. CAMBR. PHIL. SOC., 1958, 54, 89.

17. Sherman, J.S. and McLaughlin, J. COMM. MATH. PHYS., 1978, 27, 1.

18. Mira, C. In "Convegno internazionale su equazioni differenziali ordinarie ed equazioni funzionali" [International Conference on Ordinary Differential Equations and Functional Equations], edited by R. Conti, G. Sestini and G. Villari, 1978, Firenze [Florence], p 25.

19. Kiyashko, S.V. and Rabinovich, M.I. ZHETF, 1974, 66, 1626.

20. Mishchenko, Ye.F. and Rozov, N.Kh. "Differential'nyye uravneniya s malym parametrom i relaksatsionnyye kolebaniya" [Differential

Equations with a Minor Parameter and Relaxation Oscillations],
Izdatel'stvo Nauka, 1975.

21. Yakobson, M.V. DOKL. AN SSSR, 1978, 243, 866.

22. Mira, C. "VII Int. Conf. on Nonl. Oscill.," Academic-Verlag, Berlin,
    1977, p 81.

23. Li, T.Y. and Yorke, J.A. AMER. MATH. MONTHLY, 1975, 82, 985.

24. Lorenz, E.N. TELLUS, 1964, 16, 1.

8831
CSO: 1860

QUANTUM ELECTRONICS

THE INFLUENCE OF THE THERMOPHYSICAL PROPERTIES OF A TARGET ON VAPORIZATION WITH THE ACTION OF LASER RADIATION

[Article by V.I. Luchin, Institute of Applied Physics of the USSR Academy of Sciences]

[Text] The influence of the thermophysical properties of opaque substances on the vaporization process with the action of laser radiation at flux densities of $q = 10^8 - 5 \cdot 10^9$ W/cm^2 is treated. It is determined that materials are broken down according to the quantity and composition of erosion products and the structure of the plasma flare. A breakdown parameter is the ratio of the ionization potential to the critical temperature of the substance (I/kT_c). Differences in the vaporization mechanisms of the materials of the given groups are discussed.

An analysis of the vaporization process of metals with the action of laser radiation in a shielding mode, as a rule, is made without considering the influence of the thermophysical parameters of the target material (for example, in the self-consistent model of [1]). As experiments have shown, this approximation is not observed, at least in the range of radiation flux density of $q = 10^8$ to $5 \cdot 10^9$ W/cm^2 (the Q switched mode with a pulse width of $\tau_i \simeq 30$ nsec). A significant difference is observed in the nature of the vaporization of materials with different thermophysical properties; in this case, it proves to be possible to split all of the absorbing condensed materials into two groups. The difference is manifest, in particular, in the number of vaporization products, which is determined from the depth of the crater in the target surface and the thickness of the film on the substrate, which is located along the scatter path of the erosion products in a vacuum. The crater depth for a number of materials (difficultly fusible metals for example), $h = 0.04$ μm, is approximately an order of magnitude smaller than for the other group (for example, $h = 0.2 - 0.8$ μm for Cd, Sb, Pb and Bi). The thicknesses of the films condensed on the substrates also differ by several times.

96

Attention is drawn to the fact that in a large series of investigated materials with different, but close thermophysical parameters, a sharp division of the materials into the indicated groups is observed. This makes it possible to presuppose a difference in the vaporization mechanisms, which is of a threshold nature.

The large mass removal for a number of materials cannot be due to surface vaporization with the action of the energy flux (reradiation, thermal flux) from the plasma shielding the target from the laser radiation. The arrangement of the materials studied in a series with respect to the surface vaporization threshold, $q_* \simeq \kappa T_i / \sqrt{a \tau_p}$ (where T_i is the vaporization temperature, κ and a are the heat conductivity and temperature conductivity coefficients and the arrival time for the energy flux from the plasma $\tau_p \simeq \simeq \tau_i$) is not in agreement with experimental data.

The best agreement with experiment is given by the breakdown of the materials into groups according to the specific heat of vaporization Ω. The only possible mechanism for the vaporization of metals, the threshold of which would depend on this thermophysical parameter is vaporization with the action of the ultraviolet radiation of an erosion plasma. Only in the ultraviolet range in the given mode is the condition $\alpha^{-1} \gg \sqrt{a \tau_p}$ met (where α is the absorption coefficient), for which the vaporization threshold is $q_* \simeq \Omega / \alpha \tau_p$.

Figure 1. The crater depth at the surface of a bismuth (1) and titanium (2) target as a function of the radiation flux density (where the diameter of the irradiated area is d = 300 µm).

A number of facts contradict the mechanism of vaporization with the action of energy flux from the plasma.

1) The experimental division of materials into the indicated groups does not depend on the laser radiation flux density q.

2) The depth of a crater at the surface of a target depends slightly on q for all materials (the curves shown in Figure 1 for bismuth and titanium are characteristic representatives of the groups). It is clear that the

97

energy flux from the plasma should depend greatly on q, since the bulk of the radiation energy in the shielding mode goes to heating the plasma.

3) The shielding influence decreases in the case of small dimensions of the irradiated area (Figure 2), because of the non-one-dimensional scattering of the plasma. We shall turn our attention to the similarity of the curves for both groups of materials; the difference in the depth of the craters does not depend on the diameter. This means that the characteristic dimension for the process which assures the large mass removal during evaporation of materials of the second group is much less than the characteristic shielding dimensions ($\simeq 100$ μm).

A dependence of the laser flare structure on the properties of the target material is likewise established in this paper. A complex structure with an opaque nucleus at the surface of the target [2] is not observed for all materials in the range considerdd here. The opaque region is absent in shadow photographs of the flares of a series of materials. In this case, the division of materials into two groups precisely corresponds to position in the series arranged according to the depth of the craters.
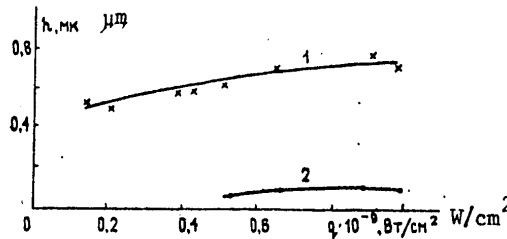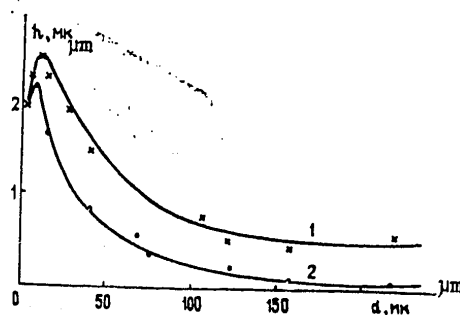

Figure 2. The crater depth at the surface of a bismuth (1) and titanium (2) target as a function of the light spot diameter (where the radiation flux density is q $\simeq 10^9$ W/cm²).

The flare structure and the crater depth were recorded in the same experiment. The projection configuration with a phase corrector of [3] made it possible to produce a uniform a uniform light spot on the target (nonuniformity of no more than 20%), as well as change the diameter of the spot given a specified radiation flux density. The structure of an erosion flare was studied by the shadow method with various delays relative to the irradiating pulse. The second harmonic of the radiation comprising the plasma was utilized for the photography; the exposure time (≤ 30 nsec) was determined by the pulse width. The delay line was composed of a resonator with coaxial spherical reflectors and provided for delay of the transilluminating pulse of up to 120 nsec.

98

A shock wave is observed in the shadow photographs (the experiment was performed at atmospheric pressure), the front of which propagates with a velocity which is the same for all materials: $v \simeq 10^6$ cm/sec. Under the conditions of the experiment, a point explosion approximation [4] can be used to estimate the shock wave parameters, where the position of the front is determined by the energy liberated (E) during the explosion: $R_f = \xi_0 (E/\rho_0)^{1/5}$ • $\cdot t^{2/3}$, where $\xi_0 \simeq 1$ and ρ_0 is the density of the undisturbed medium. The independence of the shock wave velocity from the target material means that energy liberation in vapors as a result of shielding is the same for the various materials. This is a natural result, since in the shielding mode, the bulk of the radiation energy goes to heating the plasma.

It is important to note that not only the overall liberated energy is the same for the various materials, but also the heating of that portion of the plasma from which the fast electrostatically accelerated ions are emitted. This conclusion is drawn on the basis that in this mode, the quantity, energy and amount of charge of the fast ions registered in a laser mass spectrometer depends only slightly on the target material [5]. It follows from the energy balance that the portion of the plasma emitting fast ions carries a greater share of the energy, though the bulk of the vaporization products are of low energy.

Thus, the process of the vaporization of metals with a complex flare structure should occur in two stages. In the stage common to all materials, there is the onset of shielding, fast ions are formed and a shock wave is excited (for the case of vaporization in a gas atmosphere); during the second stage, a considerable mass of vapor and liquid phase droplets are removed for a number of materials, where these form an opaque nucleus, the front of which propagates at a velocity of $(1 - 3) \cdot 10^5$ cm/sec.

We will note that the presence of liquid phase droplets in the composition of the vaporization products registered on the substrate during vaporization in a vacuum precisely correlates with the presence of an opaque zone in the flare and deep craters in the surface of the target. The absorption and scattering of the radiation at droplets is inherently due to the opaqueness of the nucleus. The plasma opaqueness is possible only at densities much greater than those attainable in an experiment (less than 10^{20} cm^{-3}); the electron concentration, which corresponds to the plasma frequency, is equal to the frequency of the transilluminating radiation, $n = 4 \cdot 10^{21}$ cm$^{-3} \gg 10^{20}$ cm^{-3}. There remains the absorption and scattering at the droplets; in this case, to explain the sharp boundary of the region of opaqueness, it is necessary to meet the condition $\alpha^{-1} \ll R$ (α is the absorption coefficient, R is the dimension of the opaque nucleus). This condition, as estimates show [6], is not met when the size of the droplets is $r \ll \lambda = 0.53$ μm, or vice versa, when $r \gg \lambda$. The requisite size of the droplets, $r \simeq \lambda$, corresponds to that observed experimentally ($r \simeq 0.1 - 1$ μm).

As was shown above, the second vaporization stage cannot be due to energy flux from the plasma. The energy needed for the vaporization of the bulk

99

of the material is apparently stored in the target prior to the shielding of the surface. Photographing a flare at small delays has shown that the opaque nucleus appears at the onset of the pulse. The major mass removal cannot be due to this load relief of the material following the completion of the pressure pulse, something which is presupposed in the case of several large fluxes [2]. The energy which is stored in the shock wave over a small portion of the pulse is insufficient for intense vaporization. The second stage likewise cannot be related to surface vaporization of the layer heated up prior to the onset of shielding in view of the rapid cooling of the surface during vaporization.

The experimentally observable removal of mass can be due only to the bulk explosion of the heated layer. The most acceptable model is that of explosive decay of a metastable state of a superheated liquid phase [7]. We have to expand the model by explaining why the explosion of the superheated liquid does not occur for a number of materials.

The assumption of liquid metal dielectrification effects and the explosion of the superheated melt is made in paper [7] to explain the special features of the behavior of the recoil pressure pulse during the vaporization of lead [8]. Lead belongs to materials having a complex flare structure.

We shall turn our attention to a qualitatively different kind of pressure pulse in the case of the vaporization of aluminum [8] - a material which belongs to the other group. We explain the absence of explosive decay of a metastable state during the vaporization of materials of this group by the fact that the shielding begins earlier than the heating of the superheated alloy up to the temperature of absolute instability. Since the radiation heating of the liquid is terminated due to shielding, while the temperature and pressure of the vapors rise, the degree of superheating of the melt decreases and explosive decay of the metastable state does not occur.

We divide the materials into groups based on a parameter which defines the development of shielding at a vapor temperature corresponding to the temperature of absolute instability of the melt ($T \simeq 0.9\ T_c$). We shall assume that prior to shielding, the vapor temperature is proportional to the surface temperature of the target [6]. Then the condition for explosive boiling of the melt will be absence of shielding at a certain vapor temperature $T_* = \beta T_c$ ($\beta \leq 1$). The proportionality factor β does not depend on the target material, and for this reason, various materials at the point in time of the explosion are in corresponding states with the cited temperature $T' = T_*/T_c = \beta$. The exponential factor $e^{-\varepsilon/kT*}$ (ε is the vaporization energy per atom) which enters into the shielding criteria [9] is the same for different materials. The single strong parameter which defines the shielding process will be the ratio I/kT_*, which enters into the absorption factor of a weakly ionized gas $\kappa \simeq e^{-I/2kT}$ [4] (I is the ionization potential).

100

Thus, the ratio $\gamma = I/kT_c$ will determine whether the explosion of a super-heated liquid has time to occur ($\gamma > \gamma_*$) or the shielding will set in earlier and prevent explosive boiling ($\gamma < \gamma_*$). The materials investigated here are arranged in order in the Table according to the parameter γ. Tin can be considered a threshold material ($\gamma = \gamma_* = 10.3$) under the conditions of the experiment: an opaque nucleus was not always observed in the flare.

Table

(1) Материал мишени	Ti	Al	Sn	Pb	Bi	Cd	Sb
(2) I/kT_c	6,7	8,6	10,3	17,3	22,5	37,1	38,9
Непрозрачное ядро в факеле*	—	—	±	+	+	+	+
(3) Глубина** кратера, мк/имп.	0,04	0,04	0,3	0,4	0,8	0,2	0,4

Key: 1. Target material;
2. Opaque nucleus in the flare*
3. Depth of the crater**, micrometers/pulse;

* The "+" sign corresponds to the presence of a nucleus in the flare and the "-" sign corresponds to the absence of a nucleus.
** The crater depth at the surface of the target was measured following irradiation with a series of 100 - 200 pulses.

The thickness of the superheated liquid layer is $h \simeq 1/\alpha$ (α is the radiation absorption factor in the condensed medium), since thermal conductivity is not significant at the point in time of the explosion. The absorption factor of metals, $\alpha \simeq 10^5 - 10^6$ cm^{-1} cannot assure the deep heating corresponding to the crater depth of $h \simeq 10^{-4}$ cm. Drawing on the effect of liquid metal transmission augmentation for the model [10] provides agreement within an order of magnitude of the thickness of the superheated layer [7] with the experimental values of the depth of the crater at the target surface.

The model treated here is in agreement with a number of experimental facts. The depth of the crater depends slightly on the radiation flux density (Figure 1) just as the thickness of the superheated melt layer [7].

With a reduction in the size of the irradiated area, an increase is observed in the depth of the crater for all of the materials studied (Figure 2). For materials with an opaque nucleus in the flare, the curve is elevated by the amount of the depression corresponding to the explosive stage of vaporization (for all sizes). Nonuniformity should be manifest for the other presupposed mechanisms, something which would lead to the absence of a similarity in the curves of the two groups of materials. In the

proposed model, the characteristic dimension - the size of the nucleation of the gas phase in the melt - is much less than the diameter of the irradiated area and does not manifest itself.

The influence of uniformity in the distribution of the flux density over the cross-section of the light beam on the subdivision of the materials into two groups argues in favor of the mechanism considered here. In the case of poor uniformity, the lifetime of the metastable state of the melt decreases, since bulk boiling in the pure liquid begins at the thermal inhomogeneity. As a result, the boundary between the groups should shift in the d ..·tion of the materials with a lower γ, something which is also observed experimentally. With the vaporization of aluminum by focused radiation, droplets of the liquid phase are observed in the erosion products, while the depth of the crater is increased by an order of magnitude as compared to the case where a spatial corrector is utilized.

The author would like to express his gratitude to Yu.I. Nikitin for assisting in the performance of the experiments and S.V. Gaponov and N.N. Salashchenko for their useful discussions of the work.

BIBLIOGRAPHY

1. Yu.V. Afanas'yev, O.N. Krokhin, TRUDY FIAN [PROCEEDINGS OF THE INSTITUTE OF PHYSICS OF THE USSR ACADEMY OF SCIENCES IMENI R.N. LEBEDEV], 52, 118, (1970).

2. N.G. Basov, O.N. Krokhin, G.V. Sklizkov, TRUDY FIAN, 52, 171, (1970).

3. S.V. Gaponov, N.N. Salashchenko, Ya.I. Khanin, KVANTOVAYA ELEKTRONIKA [QUANTUM ELECTRONICS], No 7, 48, (1972).

4. Ya.B. Zel'dovich, Yu.P. Rayzer, "Fizika udarnykh voln i vysokotemperaturnykh gidrodinamicheskikh yavleniy" ["The Physics of Shock Waves and High Temperature Hydrodynamic Phenomena"], Nauka Publishers, Moscow, 1966.

5. G.G. Devyatykh, N.V. Larin, G.A. Maksimov, ZH. ANALIT. KHIM. [JOURNAL OF ANALYTICAL CHEMISTRY], 29, 1516, (1974).

6. S.I. Anisimov, Ya.A. Imas, G.S. Romanov, Yu.V. Khodyko, "Deystviye lazernogo izlucheniya bol'shoy moshchnosti na metally" ["The Action of High Power Laser Radiation on Metals"], Nauka Publishers, Moscow, 1970.

7. B.M. Kozlov, A.A. Samokhin, A.B. Uspenskiy, KVANTOVAYA ELEKTRONIKA, 4, 524, (1977).

8. Ya.T. Gnoyevoy, A.I. Petrukhin, Yu.Ye. Pleshanov, V.A. Sulyayev, PIS'MA V ZhETF [LETTERS TO THE JOURNAL OF EXPERIMENTAL AND THEORETICAL PHYSICS], 11, 440, (1970).

9. G.G. Vilenskaya, I.V. Nemchinov, ZhPM i TF [JOURNAL OF APPLIED MATHEMATICS AND ENGINEERING PHYSICS], No 6, 3, (1969)

10. V.A. Batanov, F.V. Bunkin, A.M. Prokhorov, V.B. Fedorov, ZHETF, 63, 586, (1972).

8225
CSO: 1860

FOR OFFICIAL USE ONLY

RADARS, RADIO NAVIGATION AIDES, DIRECTION FINDING, GYROS

ON SPATIAL FLUCTUATIONS OF STRENGTH OF RADAR SIGNAL REFLECTED BY
SEA SURFACE

[Article by L. S. Dolin and V. V. Rodin]

[Text] Expressions for the spatial spectra of fluctuations
of the strength of a radar signal reflected by a sea surface
are derived within the framework of "resonance" theory of
the scattering of a microwave field on the sea surface. It
is shown, in particular, that large-scale formations in a
radar image of a water surface may occur as a result of non-
linearity of the relation between radar signal strength and
the slopes of surface waves (the "detection" effect). The
possible influence of irregularities of the wind field above
the sea surface on the formation of its image is discussed.

Radar systems have been attracting increasing attention in recent years for
studying the wavy sea surface and, in particular, for recording different
kinds of surface formations, for example ocean swells, pollution (oil
slicks), currents, etc. They provide quality images of a surface and of
large-scale disturbances on it (see, for example, [1-3]), but the latter
have to be identified against a background of spatial noises of different
origins. A statistical analysis of some of these noises is the subject of
this article.

1. Strength Structure of Echo from Wavy Sea Surface

We assume that the radar observation system uniformly irradiates the sea
surface within the scanning sector (Figure 1) and performs reception-
transmission of quasimonochromatic pulses of identical polarization p
(which in the numerical calculations is assumed to be vertical). A radar
(RL) image of the surface is defined as the intensity of the backscatter
field (E_p) as a function of the coordinates of the center of the resolution
area (pulse area). We will find the characteristics of the reflected
signal from the formulas of the "resonance" theory of the scattering of

FOR OFFICIAL USE ONLY

ultrashort radio waves [4], developed for a two-scale model of the surface. According to this model the profile of the sea surface is approximated by the sum $z(\mathbf{r}, t) = \zeta(\mathbf{r}, t) + \xi(\mathbf{r}_\zeta, t)$, in which the first term describes large flat surfaces with a radius of curvature much larger than working wavelength λ of the radar, and the second describes level irregularities of relief with a small, in the scale of λ, characteristic height ("ripples"). Through $\mathbf{r}_\zeta$ we denote the radius-vector on the profile of a large wave: $\mathbf{r}_\zeta = \mathbf{r} + \zeta(\mathbf{r}, t)z^0$, where $\mathbf{r}$ is the radius-vector of a point on median plane $z = 0$. The spectrum of the spatial correlation function of the large-scale component of wind wave action

$$W_\zeta(\varkappa) = \frac{1}{(2\pi)^2} \iint\limits_{-\infty}^{\infty} \langle \zeta(\mathbf{r} + \mathbf{\rho}, t)\zeta(\mathbf{r}, t) \rangle\, e^{-i\varkappa\rho}\, d\mathbf{\rho} \qquad (1)$$

is assumed to be [5]

$$W_\zeta(\varkappa) = \frac{\beta}{\varkappa^4} \exp\left[-0{,}74\, \frac{g^2}{u^4 \varkappa^2} \right] \frac{2}{\pi} \cos^2(\varphi - \varphi_0), \qquad (2)$$

where $\varkappa = |\varkappa|,\ \varphi = (\widehat{\varkappa, x^0}),\ u = |u|,\ u$ is the wind velocity 19.5 m above sea level, and $\varphi_0 = (\widehat{u, x^0}),\ g = 9{,}8\ \text{м/c}^2,\ \beta \approx 8\cdot 10^{-3}$ (the Pearson-Moskowitz spectrum).
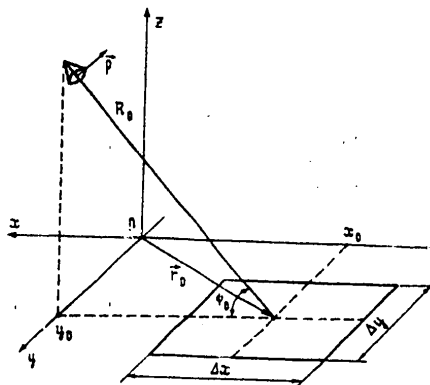

Figure 1. Geometry of problem: x^0 -- direction of propagation of probing pulse, Δx, Δy -- dimensions of resolution area (rectangular), $r_0(x_0, y_0)$ -- radius-vector of its center, R_0 -- distance between radar and point (x_0, y_0), ψ_0 -- grazing angle of incident wave, p -- polarization vector of receiving-transmitting antenna.

105

FOR OFFICIAL USE ONLY

The ripple spectrum

$$W_\xi(\varkappa) = \frac{1}{(2\pi)^2} \iint_{-\infty}^{\infty} \overline{\xi(r_\xi + \rho, t)\,\xi(r_\xi, t)}\, e^{-i\varkappa\rho}\, d\rho,$$ (3)

in accordance with Phillips [5], is written as

$$W_\xi(\varkappa) = C\varkappa^{-4},$$ (4)

and we will assume that the parameter C that characterizes the mean square height of a ripple may depend on r and t: $C = C_0[1 + \mu(r, t)]$. This assumption does not contradict spectral representation (3), if the characteristic scales of an irregularity $\mu(\cdot)$ -- spatial (Δr_μ) and time (Δt_μ) -- are large in comparison with the radius and correlation time of the ripples. The symbols — and <···> denote statistical averaging of sets of samples of ripples and large wave.

Intensity I of the echo from the described type of surface, based on results published in the literature [4], is expressed as

$$I(r_0, t) \equiv \frac{1}{2} E_p(r_0, t) E_p^*(r_0, t) = K(r_0, t)N(r_0, t);$$ (5)

$$K(r_0, t) = \frac{k^4}{2\pi^2 R_0^4} |B_p^p[\nu(r_0, t)]|^2 \frac{1 + \mu(r_0, t)}{1 - \nu^2(r_0, t)};$$ (6)

$$N = J J^*,$$

$$J = \iint_{-\infty}^{\infty} \Phi(r_1)\,\xi^{cr}(r_0 + r_1, t)\exp[-iq(r_0, t)r_1]\,dr_1,$$ (7)

$$q(r_0, t) = -2k\cos\psi_0\, x^0 - 2k\sin\psi_0\,\nabla\zeta(r_0, t);$$

$$\Phi(r) = \begin{cases} 1 \text{ for } |x| \leqslant \Delta x/2 \text{ and } |y| \leqslant \Delta y/2 \\ 0 \text{ for } |x| > \Delta x/2 \text{ or } |y| > \Delta y/2 \end{cases},$$ (8)

where $\nu(\cdot)$ is the projection of vector $\zeta(\cdot)$ of the unit external normal to the surface onto plane z = 0, the expression for $B_p^p[\nu(\cdot)]$ is presented in the literature [6] [see formula (4)], $\xi^{st}(\cdot)$ is a statistically homogeneous field with space spectrum $C_0\varkappa^{-4}$, $k = 2\pi/\lambda$.

Formulas (5)-(7) are based on the following assumptions: 1) the resolution area $(\Delta x, \Delta y)$ is small in comparison with Δr_μ and characteristic wavelength of a large wave Λ; 2) $\xi(r, t)$, $\zeta(r, t)$, $\mu(r, t)$ changes slowly in scale $2R_0/c$ (c is the speed of light); 3) the self-shading effect of the surface

is insignificant ($\psi_0 > |v|_{max}$); 4) the pulse area is located in the Fraunhofer zone of the radar antenna.

A radar image of a sea surface is made by real systems by means of repeated irradiation of each element of the surface (with dimensions (Δx, Δy)) and accumulation (in time Δt_Σ) of the energy of a sufficiently large number n of samples of the reflected signal. An image made in this way can be described as

[н=init] $$I_{im}(\mathbf{r}_0) = K(\mathbf{r}_0, t_{\text{н}}) \sum_{m=1}^{n} N(\mathbf{r}_0, t_{\text{н}} + m/F_n), \qquad (9)$$

where t_{init} is the initial time of observation of a given element of the surface ($t_{init} = y_0/V_{init}$ if the discussion refers to a side-looking radar, installed on an airplane flying at velocity V_{init} along y^0); we assume that $\zeta(t_{init} + \Delta t_\Sigma) \approx \zeta(t_{init})$; F_n is the probing pulse repetition frequency ($F_n \Delta t_\Sigma \ll 1$); $n < F_n \Delta t_\Sigma$.

I_{im} may be expressed as

$$I_{im} = \overline{I_{im}} + \Delta I_{im} = \overline{I_{im}}(1 + \delta I_{im}) \qquad (10)$$

($\overline{I}_{im}$ is the result of averaging of I_{im} from samples of ripples on the frozen relief of large waves);

$$\delta I_{im} = \frac{\Delta I_{im}}{\overline{I_{im}}} = \sum_{m=1}^{n} \Delta N(\mathbf{r}_0, t_{\text{н}} + m/F_n)/\overline{N}n,$$

$$\Delta N(\cdot) = N(\cdot) - \overline{N}; \qquad (11)$$

$$\overline{I}_{im} = nK(\cdot)\overline{N}. \qquad (12)$$

Image (10), generally speaking, is random in nature in view of the irregularity of wind wave action. It represents an additive mixture of two noise components, one of which $\overline{I}_{im}$ depicts the structure of a specific sample of the large-scale component of wave action and spatial irregularities of the ripple distribution [see (12), (6)], and the other $\Delta\overline{I}_{im}$ is noise with zero mean [see (11)], modulated by the function $\overline{I}_{im}$. The analogous representation can also be found for I_{im} in Zagorodnikov's work [7].

Spatial noise ΔI_{im} occurs because the field scattered on the resolution area has a random, very "choppy" angular distribution, since it is the

result of the interference of many uncorrelated waves, coming from different "elementary scatterers." We will call this noise interference noise to distinguish it from noise $\overline{I}_{im}$, which, in turn, is called modulation noise. We will examine two varieties of the latter below. In part 3 we will talk about modulation noise (linear and nonlinear), which occurs during the observation of spatially homogeneous wind wave action ($\mu \equiv 0$), while the noise examined in part 4 ($\mu \neq 0$), modulation wind noise, owes its origin entirely to turbulent pulsations of the wind velocity in the near-surface layer of the atmosphere.

2. Interference Noise

An echo from a fixed resolution area, as is known, fluctuates in time and has a finite correlation time Δt_c. In the time it takes to accumulate signal Δt_Σ from the element $n_{init} = \Delta t_\Sigma/\Delta t_c$ uncorrelated parcels of pulses will be received, each of which will contain n/n_{init} correlated pulses. Converting in (11) from the adding up of pulses to the adding up of uncorrelated parcels, we write the expression for a sample of interference noise in the form

[k=c]
$$\delta I_{im} = \frac{n}{n_n} \sum_{m=1}^{n_n} \mathcal{J}! \mathcal{N}(r_0, \, t_n + m\,\Delta t_k)/\overline{N}n. \tag{13}$$

In accordance with (7) the real and imaginary parts of the scattered field may be viewed as being the sum of a large number of independent random variables with zero mean. Therefore Re J and Im J can be expected to have normal distribution, the modulus of the complex amplitude of the radar signal can be expected to have a Rayleigh* distribution, and $N = (\text{Re } J)^2 + (\text{Im } J)^2$ has an exponential probability distribution:

$$P(N) = \frac{1}{\overline{N}} \exp\left(-\frac{N}{\overline{N}}\right), \qquad \overline{(\Delta N)^2} = (\overline{N})^2. \tag{14}$$

Then it follows from (13) and (14) that $\overline{(\delta I_{im})^2} = 1/n_{init}$.

Assuming random field $\xi^{st}(\cdot)$ to be normal with a radius of correlation much smaller than Δx, Δy, we obtain from (5) and (13) for the spatial correlation function of interference noise the expressions

---

*This assumption does not conflict with existing experimental data on deviations of the statistics of a radar signal, scattered by a sea surface, from Rayleigh (see, for example, [8]). On the contrary, as was shown in [9], such deviations (for Δx, $\Delta y \ll \Lambda$) may be viewed as being the result of chaotic modulation of the amplitude of the echo signal by large waves and the signal has Rayleigh statistics during the time the large-scale relief is "frozen."

108

$$B_{\delta I_{lm}}(\rho) = \overline{\delta I_{lm}(\rho + r_0) \, \delta I_{lm}(r_0)} = [b_\Phi(\rho)]^2 / [b_\Phi(0)]^2 \, n_{\text{H}};$$

$$b_\Phi(\rho) = \frac{1}{(\Delta x \Delta y)} \iint\limits_{-\infty}^{\infty} \Phi(r + \rho) \, \Phi(r) \, dr, \tag{15}$$

$$\iint\limits_{-\infty}^{\infty} b_\Phi(\rho) \, d\rho = 1. \tag{16}$$

The correlation function of relative fluctuations, as we see, does not depend on the parameters of ripples and is determined entirely by the kind of "system" function $\Phi(r)$, i.e., by the size and shape of the pulse area. In the case when $\Phi(r)$ is given by formula (8), we obtain from (15) and (16)

$$B_{\delta I_{lm}}(\rho) = \frac{1}{n_{\text{H}}} \left(1 - \frac{|\rho_x|}{\Delta x}\right)^2 \left(1 - \frac{|\rho_y|}{\Delta y}\right)^2 \begin{cases} 1 & \text{for } |\rho_x| \leqslant \Delta x \text{ and } |\rho_y| \leqslant \Delta y \\ 0 & \text{for } |\rho_x| > \Delta x \text{ or } |\rho_y| > \Delta y \end{cases} \tag{17}$$

Here the energy spectrum of spatial noise is

$$W_{\delta I_{lm}}(\varkappa) = \frac{1}{(2\pi)^2} \iint\limits_{-\infty}^{\infty} B_{\delta I_{lm}}(\rho) \, e^{-i\varkappa \rho} d\rho =$$

$$= \frac{4\Delta x \Delta y}{n_{\text{H}} \pi^2 \alpha_x^2 \alpha_y^2} \left(1 - \frac{\sin \alpha_x}{\alpha_x}\right) \left(1 - \frac{\sin \alpha_y}{\alpha_y}\right), \tag{18}$$

where $\alpha_x = \Delta x \varkappa_x$, $\alpha_y = \Delta y \varkappa_y$. In the range of low space frequencies ($\varkappa_x \ll$ $\ll 1/\Delta x$, $\varkappa_y \ll 1/\Delta y$) expression (18) yields a spectral density that does not depend on $\varkappa$:

$$W_{\delta I_{lm}} \approx \frac{\Delta x \Delta y}{2\pi^2 n_{\text{H}}}. \tag{19}$$

3. Modulation Noise in Homogeneous Wind Wave Action

We now will calculate the spatial fluctuations of $\overline{I}_{lm}$. According to the formulas in section 1

$$\overline{I}_{lm}(r_0) = \frac{2\pi k^4}{R_0^4} \iint\limits_{-\infty}^{\infty} f[\nu(r)][1 + \mu(r)]\Phi^2(r - r_0) dr,$$

$$f(\nu) = \frac{1}{1 - \nu^2} \, |B_p^p(\nu)|^2 \, W_\xi \left[-2k \cos \psi_0 \, x^0 + \frac{2k \sin \psi_0}{\sqrt{1 - \nu^2}} \, \nu \right]. \tag{20}$$

(We note that when writing (20) we are not required to satisfy the condition $\Delta x, \Delta y \ll \Lambda, \Delta r_\mu$.)

Table 1

ψ_0, deg	2	5	8	10	20	30	50	70
$f(0)$	10^{-2}	0,13	0,34	0,5	1,2	1,5	1,4	1,1
a_x	90	27	14	9,9	3,9	2,9	4,2	10,4
a_{xx}	$2,5 \cdot 10^3$	160	21	5,5	0,8	3,0	12	70
a_{yy}	−2,5	−2,2	−2,0	−1,8	−1,7	−2,0	−4,0	−16

Comment: $a_y \equiv 0$. The data in the table pertain to the case when λ = 3 cm, ε = 60.5 - i30 (ε is the dielectric constant of water), p = -sin $\psi_0 x^0$ + cos $\psi_0 z^0$ (radiated and received signals vertically polarized).

We expand f(ν) into a series by powers of $\nu(\nu_x, \nu_y)$ (see Table 1):

$$f(\mathbf{v}) = f(0)[1 + a_x \mathbf{v}_x + a_{xx}\mathbf{v}_x^2 + a_{yy}\mathbf{v}_y^2 + \ldots], \qquad (21)$$

and, after substituting (21) into (20), we obtain the function

$$\overline{T}(r_0) = \overline{T}_{lm}(r_0)/[\overline{T}_{lm}]_{\mu=0}^{\nu=0} = \frac{1}{(\Delta x \Delta y)} \int\!\!\int_{-\infty}^{\infty} [1 + a_x \mathbf{v}_x(r) +$$
$$+ a_{xx}\mathbf{v}_x^2(r) + a_{yy}\mathbf{v}_y^2(r) + \ldots][1 + \mu(r)]\Phi^2(r - r_0)dr, \qquad (22)$$

which yields the amount of contrast at an arbitrary point on the radar image in relation to the horizontally oriented (ν = 0) elements of the profile of a large wave with an undisturbed spectrum of small-scale irregularities (μ = 0).

Equation (22) shows that in the absence of a large wave ($\nu \equiv 0$) the radar will give a linear image of spatial variations of the mean square height of a "resonance" ripple (the latter has the wave vector $\kappa \approx 2k \cos \psi_0 x^0$, see (7)). When $\nu \neq 0$, but $\mu \equiv 0$, and the terms of series (21) with powers ν_x, ν_y higher than the first are ignored, the radar image may be viewed as being the result of linear filtration of the spatial distribution of the slopes of the profile of the surface in the plane of sight [10]. Now, however, when the quadratic terms (which we shall stipulate below) in (21) are taken into consideration a unique kind of space noise, produced by "detection" of a "linear" image on a quadratic nonlinearity (ν_x^2, $\nu_x\nu_y$, etc.), will appear in the image of the surface. The strength of this noise is determined by the mean square fluctuations of the normalized intensity of the echo signal $\langle(\Delta\overline{T}(r_0))^2\rangle$ $(\Delta\overline{T}(r_0) \equiv \overline{T}(r_0) - \langle\overline{T}\rangle)$, assuming that wind

wave action produces a homogeneous random field of irregularities $\zeta(r)$ (with spatial spectrum (1), (2)), and assuming $\mu(r) \equiv 0$ (the case $\mu(r) \neq$ $\neq 0$ will be examined in the next part). We find the desired estimate by finding the space spectrum $W_{\overline{\Delta T}}(\kappa)$ of fluctuations $\Delta\overline{T}(r_0)$. The corresponding calculation (it is not presented here because it is unwieldy), carried out on the assumption that $\nu(r)$ has a normal distribution [11]*, using formula (22)**, yields

$$W_{\Delta\overline{T}}(\varkappa) = 4\pi^2 w^*(\varkappa)\left[a_x^2\,W_{\nu_x}(\varkappa)' + \right.$$

$$\left. + 2a_{xx}^2 \iint\limits_{-\infty}^{\infty} W_{\nu_x}(\varkappa - \varkappa_1)\,W_{\nu_x}(\varkappa_1)\,d\varkappa_1\right], \qquad (23)$$

where

$$W_{\Delta\overline{T}}(\varkappa) = \frac{1}{(2\pi)^2} \iint\limits_{-\infty}^{\infty} \langle\Delta\overline{T}(r_0 + \rho)\,\Delta\overline{T}(r_0)\rangle\,e^{-i\varkappa\rho}\,d\rho,$$

$$W_{\nu_x}(\varkappa) = \frac{1}{(2\pi)^2} \iint\limits_{-\infty}^{\infty} \langle\nu_x(r_0 + \rho)\,\nu_x(r_0)\rangle\,e^{-i\varkappa\rho}\,d\rho, \qquad (24)$$

$$w(\varkappa) = \frac{1}{(2\pi)^2}\left[\frac{\sin(\varkappa_x\Delta x/2)}{\varkappa_x\Delta x/2}\,\frac{\sin(\varkappa_y\Delta y/2)}{\varkappa_y\Delta y/2}\right],$$

$w(\kappa)$ is the spectrum of the function $B_{\Phi}(\rho) = \dfrac{1}{(\Delta x\,\Delta y)^2} \iint\limits_{-\infty}^{\infty} \Phi^2(r+\rho)\,\Phi^2(r)\,dr$,

with the condition that $\Phi(r)$ is of the form (8).

To simplify the ensuing calculations we will replace spectrum (24) with the "equivalent step spectrum," which satisfies the conditions

$$w_{\mathfrak{d}}(0) = w(0), \qquad \iint\limits_{-\infty}^{\infty} w_{\mathfrak{d}}(|\varkappa|)\,d\varkappa = \iint\limits_{-\infty}^{\infty} w(\varkappa)\,d\varkappa$$

and is written in the form

$$w_{\mathfrak{d}}(\varkappa) = \begin{cases} 1/4\pi^2 & \text{for} \quad |\varkappa| \leqslant \varkappa_0 \\ 0 & \text{for} \quad |\varkappa| > \varkappa_0 \end{cases}, \qquad \varkappa_0 = \left(\frac{4\pi}{\Delta x\Delta y}\right)^{1/2}.$$

---

*This assumption enables us to express the fourth-order moments of field ν through the second-order moments.

**We keep the first two terms in the integrand in (22), since (see Table 1) $a_{yy} \ll a_{xx}$ everywhere, where $a_{xx} \gtrsim a_x$ (i.e., the term that is quadratic in terms of ν_x may make an appreciable contribution to $\Delta\overline{T}$).

In (23) we replace $w(\kappa)$ with $w_e(\kappa)$, integrate the resulting expression for $W_{\Delta\overline{T}}(\kappa)$ (considering the fact that when $|\nu| \ll 1$ $W_{\nu_x}(\kappa) = (\kappa x^0)^2 W_\zeta(\kappa)$) and find the desired value $\langle(\Delta\overline{T})^2\rangle$. It is the sum of the linear $(\langle(\Delta\overline{T})^2\rangle_{lin})$ and nonlinear $(\langle(\Delta\overline{T})^2\rangle_{nl})$ (in terms of ν_x) terms

[л=lin;
нл=nl]

$$\langle(\Delta\overline{T})^2\rangle = \iint\limits_{-\infty}^{\infty} W_{\Delta\overline{T}}(\varkappa)\,d\varkappa = \langle(\Delta\overline{T})^2\rangle_{\pi} + \langle(\Delta\overline{T})^2\rangle_{нл},$$

$$\langle(\Delta\overline{T})^2\rangle_{\pi} = -a_x^2\frac{\beta}{8}\,\text{Ei}\left(-\frac{1}{m}\right)(1+2\cos^2\varphi_0),$$

(25)

where

$$\langle(\Delta\overline{T})^2\rangle_{нл} \approx \begin{cases} a_{xx}^2\left(\dfrac{\beta}{8}\right)^2 m\left[59\cos^4\varphi_0 + \sin^2\varphi_0\left(\dfrac{1}{2}+\cos^2\varphi_0\right) + \right.\\ \qquad\qquad \left. + 3\sin^4\varphi_0\right] \quad \text{for} \quad m \ll 1 \\ 2a_{xx}^2(\langle v_x^2\rangle)^2 \quad \text{for} \quad m \gg 1 \end{cases}$$

(26)

$$m = \frac{4\pi\,u^4}{0,74\,g^2(\Delta x\,\Delta y)}, \quad \langle v_x^2\rangle = \frac{\beta}{8}\left[\ln\frac{4\pi^2\,u^4}{0,74\,g^2\lambda^2} - 0,58\right](1+2\cos^2\varphi_0).$$

The form of $\langle v_x^2\rangle$ is found, as in [11], by integrating $W_{\nu_x}(\kappa)$ in the interval $0 < |\varkappa| \leqslant 2\pi/\lambda$.

Table 2

ψ_0, deg	m_i 0,5		1,0		∞ $\left(\begin{matrix}u=3\text{ м/с}\\ \Delta x,\,\Delta y \to 0\end{matrix}\right)$	
	$\langle(\Delta\overline{T})^2\rangle_{нл}$	$\langle(\Delta\overline{T})^2\rangle_{\pi}$	$\langle(\Delta\overline{T})^2\rangle_{нл}$	$\langle(\Delta\overline{T})^2\rangle_{\pi}$	$\langle(\Delta\overline{T})^2\rangle_{нл}$	$\langle(\Delta\overline{T})^2\rangle_{\pi}$
2	9,3	$8,3\cdot10^{-11}$	37	$7,3\cdot10^{-2}$	$7,8\cdot10^3$	200
5	$4\cdot10^{-2}$	$7,5\cdot10^{-12}$	0,16	$6,6\cdot10^{-3}$	32	18
8	$7\cdot10^{-4}$	$2\cdot10^{-12}$	$2,7\cdot10^{-3}$	$1,8\cdot10^{-3}$	0,55	4,9
10	$4,5\cdot10^{-5}$	10^{-12}	$1,8\cdot10^{-4}$	$8,8\cdot10^{-4}$	$3,8\cdot10^{-2}$	2,4
20	$9,6\cdot10^{-7}$	$1,6\cdot10^{-13}$	$3,9\cdot10^{-6}$	$1,4\cdot10^{-4}$	$8\cdot10^{-4}$	0,38
30	$1,3\cdot10^{-5}$	$8,5\cdot10^{-14}$	$5,4\cdot10^{-5}$	$7,5\cdot10^{-5}$	$1,1\cdot10^{-2}$	0,21
50	$2,1\cdot10^{-4}$	$1,8\cdot10^{-13}$	$8,4\cdot10^{-4}$	$1,6\cdot10^{-4}$	0,18	0,44
70	$7\cdot10^{-3}$	10^{-12}	$2,9\cdot10^{-2}$	10^{-3}	6,1	2,7

FOR OFFICIAL USE ONLY

The values of $<(\Delta\overline{T})^2>_{lin}$ and $<(\Delta\overline{T})^2>_{nl}$ for different grazing angles ψ_0 and for different values of the parameter $m_1 = u^2(\varkappa/c)/\sqrt{\Delta x(\varkappa)\Delta y(\varkappa)}$ are presented in Table 2 ($\phi_0 = 30°$, $\lambda = 3$ cm, vertical polarization). The data in the table, with the exception of the last column, pertain to the case when the resolution area (Δx, Δy) is substantially larger than the characteristic wavelength of wind wave action $\Lambda \sim 2\pi u^2/g$.

A comparison of $<(\Delta\overline{T})^2>_{lin}$ with $<(\Delta\overline{T})^2>_{nl}$ in accordance with formulas (25) and (26) and Table 2* shows that when $m_1 \lesssim 1$ the linear component of modulation noise is small in comparison with the nonlinear one. As Δx, Δy decreases the relative contribution of the linear component increases.

The dependence of the fluctuations of a radar signal on the size of the pulse area was analyzed previously by Pereslegin [12] in linear (in terms of v_x) approximation. The latter, as was shown above, has a limited range of application (Δx, $\Delta y < \Lambda$).

4. Modulation Wind Noise

Up until now, for calculating the average characteristics of an echo signal, we have been using as the ripple spectrum Phillips' equilibrium spectrum (4). However, there are some theoretical considerations and experimental data [13, 14], according to which the spectrum of short gravity and capillary waves (they scatter the microwave field) depends on the wind velocity above the sea. Because of this dependence rather large-scale inhomogeneities of wind field u(**r**), "printed" on the surface (through ripples), are converted to the corresponding variations of the reflected signal. We shall analyze this effect on the basis of ripple spectrum (3) in the Leykin-Rozenberg notation [15]:

$$W_\xi(\varkappa) = \alpha\, u\, \varkappa^{-3,5},$$

where $\alpha \approx 10^{-5}$ s/cm, $\kappa = 0.6\text{-}6$ rad/s, u is the wind velocity at a height of 19.5 m, u < 10 m/s.

Modulation noise related to the radar mapping of large surface waves, examined above, will not be considered in this part. Then, denoting through the symbol ($\sim$) the operation of statistical averaging of samples u(**r**) and assuming in (22) $\mu(\mathbf{r}) = \Delta u(\mathbf{r})/\tilde{u}$ ($\Delta u(\cdot) \equiv u(\cdot) - \tilde{u}$), $v(\cdot) \equiv 0$, we obtain

---

*We note that the results of the calculations for $\psi_0 = 2°$, $5°$ have poor accuracy, since the requirement that there be no shadows ceases to be satisfied at the indicated grazing angles. It is easy to see that the shadows that appear can amplify low-frequency space noise in an image of the surface (i.e., increase $<(\Delta\overline{T})^2>_{nl}$).

113
FOR OFFICIAL USE ONLY

$$W_{\Delta\overline{T}_u}(\varkappa) = \frac{1}{(2\pi)^2} \iint\limits_{-\infty}^{\infty} \widetilde{\Delta\overline{T}_u(r_0 + \rho)\,\Delta\overline{T}_u(r_0)}\, e^{-i\varkappa\rho}\, d\rho =$$

$$= 4\pi^2\, w(\varkappa)\, W_{\Delta u}(\varkappa)/(\widetilde{u})^2, \tag{27}$$

where $\Delta\overline{T}_u(\cdot) = \overline{T}(\cdot) - \widetilde{\overline{T}}$, $W_{\Delta u}(\varkappa) = \dfrac{1}{(2\pi)^2} \iint\limits_{-\infty}^{\infty} \widetilde{\Delta u(r_0 + \rho)\,\Delta u(r_0)} e^{-i\varkappa\rho}\, d\rho$, $w(\varkappa)$ is determined by formula (24).

If the resolution area is small enough, so that its filtering effect [see (27) and (24)] is negligible during the imaging of the basic energy-carrying (large) scales of wind turbulence, then

$$\widetilde{(\Delta\overline{T}_u)^2} = \iint\limits_{-\infty}^{\infty} W_{\Delta\overline{T}_u}(\varkappa)\, d\varkappa \approx \widetilde{(\Delta u)^2}/\widetilde{(u)^2}.$$

The dispersion of horizontal pulsations of wind velocity $\widetilde{(\Delta u)^2}$ at a fixed height (19.5 m in our case) depends on u and on the stratification of the air mass above the sea. Thus, for neutral stratification (Richardson's number is zero), using the results of measurements [16], we find $\widetilde{(\Delta\overline{T}_u)^2} \approx$
$\approx 9.8 \cdot 10^{-3}$; $1.06 \cdot 10^{-2}$; $1.4 \cdot 10^{-2}$ for $\tilde{u} = 3, 5, 10$ m/s, respectively.

A comparison of these data with the data in Table 2 shows that space noise produced by turbulent pulsations of wind velocity makes an appreciable contribution to the overall spatial fluctuations of an image. The relative role of these turbulent pulsations of wind velocity apparently will increase as the intensity of the wave action decreases and Δx, Δy increase, when the noise produced by wind waves is effectively smoothed by virtue of the finite size of the resolution area.

Modulation wind noise, on the one hand, may hamper the recording of any expansive formations on the surface (an oil slick, let us say) and, on the other hand, is a basis for certain conclusions regarding the status of the wind situation in an investigated region of the sea (the authors of the experimental work [1], in particular, point to this possibility).

It is important to note that the material presented in this part is more or less preliminary, because the question of the ripple spectrum and of its interaction with large waves and wind remains largely unanswered.

5. Total Dispersion of Fluctuations of Filtered RL Image of Sea Surface

Returning to formula (10), we see that spatial variations of a radar image of a wavy sea surface are made up of modulation noise (they are produced by large waves, see section 3, and by inhomogeneities of the distribution of wind-produced ripples (section 4)) and interference noise (section 2), i.e.,

114

$$(\Delta I_{im})_t = I_{im} - \langle \widetilde{\overline{I}_{im}} \rangle = \Delta \overline{I}_{im} + \overline{I}_{im} \delta I_{im},$$

$$\Delta \overline{I}_{im} = \overline{I}_{im} - \langle \widetilde{\overline{I}_{im}} \rangle. \tag{28}$$

We assume that image $I_{im}(r_0)$ is subjected to spatial filtration* with the aid of an averaging window, which performs the transformation

$$I_1(r_0) = \frac{1}{(\Delta x_1 \Delta y_1)} \int\!\!\int_{-\infty}^{\infty} I_{im}(r)\,\Phi_1(r_0 - r)\,dr, \tag{29}$$

where $\Phi_1(r)$ is obtained from (8) by replacing Δx, Δy with Δx_1, Δy_1, and we find the complete dispersion of the fluctuations of the filtered image:

$$\sigma_{I_1}^2 = \langle \overline{[(\Delta I_1)_t]^2} \rangle = \overline{\langle (I_1 - \langle \widetilde{\overline{I}_1} \rangle)^2 \rangle}. \tag{30}$$

Substituting (28) into (29) we obtain

$$\sigma_{I_1}^2 = \int\!\!\int_{-\infty}^{\infty} b_{\Phi_1}(\varphi)\,B_{(\Delta I_{im})_t}(\varphi)\,d\varphi, \tag{31}$$

where $B_{(\Delta I_{im})_t}(\varphi) = \overline{\langle (\Delta I_{im}(r+\varphi))_t (\Delta I_{im}(r))_t \rangle}$, and $b_{\Phi_1}(\rho)$ coincides with (16) when $\Phi(\cdot) \to \Phi_1(\cdot)$.

If we assume $\Delta x_1 \gg \Delta x$, $\Delta y_1 \gg y$ and return to the assumption that the radar has high spatial resolution, the radius of correlation of δI_{im} [see (17)] will be small in comparison with the radius of correlation of $\overline{I}$ and with the scale of change of $b_{\Phi_1}(\rho)$. Then, using the hypothesis of the statistical independence of the function δI_{im} on the profile of a large wave and wind field, we obtain

$$\sigma_{I_1}^2 = \int\!\!\int_{-\infty}^{\infty} b_{\Phi_1}(\varphi)\,B_{\Delta \overline{I}_{im}}(\varphi)\,d\varphi + \frac{4\pi\,W_{\delta I_{im}}(0)}{\Delta x_1 \Delta y_1}\,B_{\overline{I}_{im}}(0), \tag{32}$$

where

$$B_{\Delta \overline{I}_{im}}(\varphi) = \overline{\langle \Delta \overline{I}_{im}(r+\varphi)\Delta \overline{I}_{im}(r)\rangle}, \quad B_{\overline{I}_{im}}(\varphi) = \overline{\langle \overline{I}_{im}(r+\varphi)\overline{I}_{im}(r)\rangle}.$$

---

*This procedure is used in practice (see [1], for example) for reducing the level of high-frequency (small-scale) noises in an image: they are explicit interference during observation of any large-scale surface formations.

Converting to normal functions $T = \bar{I}_{im}/[\bar{I}_{im}]_{\mu=0}^{\nu=0}$, $T_1 = I_1/[\bar{I}_1]_{\mu=0}^{\nu=0}$, $\sigma_{T_1} = $ $= \sigma_{I_1}/[\bar{I}_1]_{\mu=0}^{\nu=0}$ in (32) in consideration of the equality $[\bar{I}_1]_{\mu=0}^{\nu=0} = [\bar{I}_{im}]_{\mu=0}^{\nu=0}$ and of formulas (31), (19), we obtain

$$\sigma_T^2 \approx \sigma_T^2(\Delta x_1, \Delta y_1) = \left[\widetilde{\langle \widetilde{T} \rangle^2} + \sigma_T^2(\Delta x, \Delta y) \right] \frac{4\Delta x \, \Delta y}{9\Delta x_1 \Delta y_1 \, n_{\scriptscriptstyle\Pi}},$$

where $\sigma_T^2(\Delta x, \Delta y)$ is the dispersion of the fluctuations of the normal intensity in the original image (made by a radar system with resolution $(\Delta x, \Delta y)$, and $\sigma_T^2(\Delta x_1, \Delta y_1)$ is the analogous value for the case when the pulse area has the dimensions $(\Delta x_1, \Delta y_1)$ (the size of the hole in the transparency used for "smoothing" the distribution of $I_{im}(r_0)$). When $\Delta x_1 \to 0$, $\Delta y_1 \to 0$ the dispersion of the output fluctuations of the space filter coincides with the dispersion of the intensity fluctuations in the original image:

$$\sigma_{T_1}^2 \to \sigma_T^2 = \sigma_T^2(\Delta x, \Delta y) + \left[\widetilde{\langle \widetilde{T} \rangle^2} + \sigma_T^2(\Delta x, \Delta y) \right] \frac{1}{n_{\scriptscriptstyle\Pi}}.$$

Formulas (22), (25), (26) and Table 2 may be used for finding σ_T^2 and $\langle \widetilde{T} \rangle$.

In conclusion the authors gratefully acknowledge V. L. Veber's assistance on the numerical calculations.

BIBLIOGRAPHY

1. Brown, W. E. Jr., C. Elachi and T. W. Thompson, J. GEOPHYS. RES., Vol 81, No 15, 1976.

2. Pilon, R. O. and C. G. Purves, TRANS. IEEE, AES-9, No 5, 1973.

3. Apel, J. R., TRANS. AMERICAN GEOPHYS. UNION, Vol 57, No 9, 1976.

4. Bass, F. G. and I. M. Fuks, "Rasseyaniye Voln na Statisticheski Nerovnoy Poverkhnosti" (Scattering of Waves on Statistically Uneven Surface), izd. Nauka, Moscow, 1972.

5. Kitaygorodskiy, S. A., "Fizika Vzaimodeystviya Atmosfery i Okeana" (Physics of Interaction of Atmosphere and Ocean), Gidrometeoizdat, Moscow, 1970.

6. Leykin, I. A., I. Ye. Ostrovskiy, A. D. Rozenberg, V. G. Ruskevich and I. M. Fuks, IZV. VUZOV -- RADIOFIZIKA (News of Higher Educational Institutions -- Radio Physics), Vol 18, No 3, p 346, 1975.

FOR OFFICIAL USE ONLY

7. Zagorodnikov, A. A., RADIOTEKHNIKA I ELEKTRONIKA (Radio Engineering and Electronics), Vol 19, No 2, 1974.

8. Trunk, G. V., TRANS. IEEE, AES-8, No 2, 1972.

9. Lementa, Yu. A. and I. M. Fuks, "Kratkiye Teksty Dokladov na VII Vsosoyuznom Simpoziume po Difraktsii i Rasprostraneniyu Voln" (Condensed Text of Reports at 7th All-Union Symposium on Diffraction and Propagation of Waves), Vol 1, Moscow, 1977.

10. Yeshchenko, S. D. and A. A. Zagorodnikov, METEOROLOGIYA I GIDROLOGIYA (Meteorology and Hydrology), No 6, 1972.

11. Martsinkevich, L. M., METEOROLOGIYA I GIDROLOGIYA, No 10, 1970.

12. Pereslegin, S. V., IZV. AN SSSR, FAO (News of USSR Academy of Sciences, Physics of the Atmosphere and Ocean), Vol 11, No 5, p 6, 1975.

13. Mitsuyasu, H. and T. Honda, J. OCEANOGR. SOC. JAPAN, Vol 30, No 4, 1974.

14. Daley, J. C., J. GEOPHYS. RES., Vol 78, No 33, 1973.

15. Zel'dis, V. I., I. A. Leykin, A. D. Rozenberg and V. G. Ruskevich, AKUST. ZH. (Acoustics Journal), Vol 19, No 2, 1973.

16. "Registr SSSR, Veter i Volny v Okeanakh i Moryakh, Spravochnyye Dannyye" (The USSR Register, Wind and Waves in Oceans and Seas, Reference Data), izd. Transport, Leningrad, 1974.

7872
CSO: 1860

FOR OFFICIAL USE ONLY

SEMICONDUCTORS AND DIELECTRICS; CRYSTALS IN GENERAL

FILM ELECTRONICS AND SEMICONDUCTOR INTEGRATED CIRCUITS

[Annotation and Table of Contents from the book by Galina Ivanovna Bogdan and Mikhail Makarovich Nekrasov, Izd. Ob'yedineniye "Vishcha Shkola," 1979, 9000 copies, 208 pages]

/Text/ The text is devoted to problems of solid state physics and to the design and technology of integrated components and circuits based on thin and thick films. Schematic solutions are offered and the physical processes which enter into the electronic circuit operation are examined. The construction and principles of operation of microcircuits employing bipolar and MDP/metal-dielectric-semiconductor/ transistors are described.

This book is intended for students specializing in the fields of "Dielectrics and Semiconductors," "Electronic Devices," and "Industrial Electronics."

TABLE OF CONTENTS

FOR OFFICIAL USE ONLY

- END -

119
FOR OFFICIAL USE ONLY